New Designs for Wideband Hemispherical Helical Antennas

Hamad W. Alsawaha

Thesis submitted to the faculty of Virginia Polytechnic Institute and State University in partial fulfillment of the requirements for the degree of

Master of Science

In

Electrical Engineering

Ahmad Safaai-Jazi, Chair

William A. Davis

Wayne A. Scales

July 29, 2008

Blacksburg, Virginia

Keywords: Hemispherical Helix, Helical Antenna, Wideband Antennas

New Designs for Wideband Hemispherical Helical Antennas

Hamad W. Alsawaha

(ABSTRACT)

A unique property of spherical and hemispherical helical antennas is that they provide very broad half-power beamwdiths and circular polarization over a narrow bandwidth. In this thesis, new designs for hemispherical helical antennas are introduced that provide significant improvement in bandwidth, while maintaining the directivity and half-power beamwidth of the basic design. In the basic design, a simple wire of circular cross section is wound on the surface of a hemisphere, whereas in the proposed new designs a metallic strip forms the radiating element. Furthermore, the metallic strip may be tapered and tilted relative to the hemispherical surface, allowing wider bandwidth to be achieved. The antenna is fed by a coaxial cable with the inner conductor connected, through a matching section, to the radiating strip and its outer conductor connected to a ground plane.

Radiation properties of the proposed hemispherical helical antennas are studied both theoretically and experimentally. A commercial software, based on the method of moments, is used to perform the numerical analysis of these helices. Three-dimensional far-field patterns, axial ratio, directivity, and voltage standing-wave ratio (VSWR) are calculated for several designs. The impacts of tapering as well as tilting of the metallic strip on radiation characteristics are examined. Also, matching of the proposed hemispherical antennas to 50-ohm transmission lines is addressed. A 4.5-turn hemispherical helix with tapered radiating element and zero degree tilt angle, (metallic strip is perpendicular to the hemisphere axis of symmetry) provides the largest overall bandwidth. A nonlinearly tapered matching section is incorporated into the design in order to reduce the VSWR. For this design, an overall measured bandwidth of about 24% at a center frequency of 3.35 GHz is achieved. Over this bandwidth, the axial ratio

remains below 3 dB, the VSWR is less than 2, and the directivity is about 9 ± 1 dB. A half- power beamwidth of 70° is also obtained.

A prototype of the best design was fabricated and tested using the VT indoor antenna range. Radiation patterns, the scattering parameter S_{11}, and the axial ratio were measured. The measured and simulated results agree reasonably well. In particular, agreements between measured and calculated far-field patterns and VSWR are quite remarkable. This compact, low profile antenna might find useful applications in avionics, global positioning systems (GPS), and high data rate wireless communication systems.

Acknowledgements

First, I would like to thank my teacher and my advisor, Dr. Ahmad Safaai-Jazi, for his enormous effort on helping me in many tasks in my research. I would also like to thank Dr. William Davis for adding me as a student member of Virginia Tech Antenna Group (VTAG), and also for being a teacher and a member of my advisory committee. I also thank Dr. Wayne Scales for his services as a member of my advisory committee.

My gratitude for my friend Tae-young Yang for his advice, help in resolving many problems that I have encountered while using FEKO, his patience and appreciated effort in taking the pattern measurements. Special thanks for my friend and an expert engineer Randall Nealy, for his training on using the Network Analyzer and the facilities available at the VTAG workshop, and also for his valuable advice in the fabrication process of this research. Thanks to the members of VTAG for being supportive friends. I am also grateful to my family for their encouragement and support during my master studies and research. Last but not least, I thank the government of Saudi Arabia and King Abdullah bin Abdul Aziz Al Saud for supporting my scholarship.

Table of Contents

List of Figures

Chapter 1: Introduction

Antennas are an essential part of any wireless communication system, which facilitate the propagation of electromagnetic energy between radio systems through space as a transmission medium. Analysis and design of antennas has been an area of immense activity in the broader electromagnetic discipline. Some simple antennas may be analyzed analytically, while the majority of them have complex geometries that only numerical techniques can be used to simulate their electromagnetic behavior. Since high computational power has become available and inexpensive, numerical modeling of antennas is considered as the most cost effective approach to antenna design. The method of moments is one of the most widely used numerical techniques for solving electromagnetic problems in general and antenna design in particular. Measurement of radiation characteristics and input impedance is the most dependable technique for studying antenna performance or verifying simulation results.

Antennas are classified according to their radiation and input impedance characteristics. For example, antennas may be of resonant type which support standing waves and are usually narrowband, or of traveling-wave type on which small reflections exist and provide larger bandwidths. That is, they are capable of maintaining certain antenna characteristics over a wide range of frequencies.

Improving or tailoring the radiation characteristics of antennas has been the main objective in many antenna designs and developments. The general goal in these developments might be to increase the bandwidth, gain, specific polarization qualities, and/or to decrease the voltage standing-wave ratio. An important example is the helical antenna, first introduced by Kraus [1], which provides a largely real input impedance, high gain, and circular polarization over a wide bandwidth. The understanding of the helix and its radiation properties is essential to the research work undertaken in this thesis. A review of the helical antenna and its modifications is presented in Chapter 2.

A novel variation of the helical antenna is referred to as "spherical helix" [2], first introduced at Virginia Tech. This design offers some unique advantages, including low profile, compact size, and very broad beamwidth. A modified version of this antenna was later developed at Virginia Tech by truncating the spherical helix to half of its size; it is referred to as "hemispherical helical antenna" [3]. The hemispherical helical antenna is capable of maintaining most of the radiation characteristics of the full spherical helix but with only half the size. Further investigation of hemispherical helix at Virginia Tech lead to yet another geometry called "Multifilar hemispherical helical antenna" [4]. The investigation of this geometry has revealed some unique radiation characteristics. A detailed review of these three spherically shaped helical antennas is presented in Chapter-3.

This research extends the investigation of hemispherical helical antenna design. The aim is to maximize the bandwidth over which circular polarization is maintained and at the same time gain fluctuations remain below ± 1.5 dB, and the antenna is fairly well matched to a 50-Ω transmission line (VSWR<2). Modifications such as replacing the wire structure with a metallic strip, which may be conformal or non-conformal to the surface of hemisphere, and variable width or tapered strip are explored. Numerical analyses of hemispherical helices incorporating the above modifications are carried out, using the electromagnetic simulator FEKO suite 5.3. The FEKO suite is a widely used simulation tool for antenna analysis, design, and optimization and for solving many other applied electromagnetic problems. The FEKO suite mainly utilizes the method of moments in numerically solving radiation problems. The numerical analysis of the conformal and non-conformal hemispherical helical antennas is presented in Chapter 4. The construction and measurements of a prototype non-conformal hemispherical helical antenna are discussed in Chapter 5. The conclusion of this research, main contributions, and suggestions for further work are summarized in Chapter 6. The FEKO codes developed for simulation and numerical analyses of the proposed hemispherical helical antennas as well as computed and measured radiation characteristics that, for brevity, were not presented but referred to in Chapter 4 are given in the Appendices.

Chapter 2: Helical Antennas

The helical antenna or simply helix was invented by Kraus in 1946 [1]. Upon performing a series of experiments, Kraus found out that the helix produces a narrow beam and circular polarization along its axis. Ever since, helical antennas have been subject of extensive investigations because of their desirable radiation characteristics, including circular polarization, relatively high gain, and largely real input impedance all over a wide bandwidth.

2.1 Geometry of Helical Antenna

The helical antenna can be simply described as a wire wound over a cylindrical surface such that a constant spacing between its turns is maintained. Figure 2.1 shows the geometry and parameters of a helix. Helix parameters and their definitions are summarized in Table 2.1.

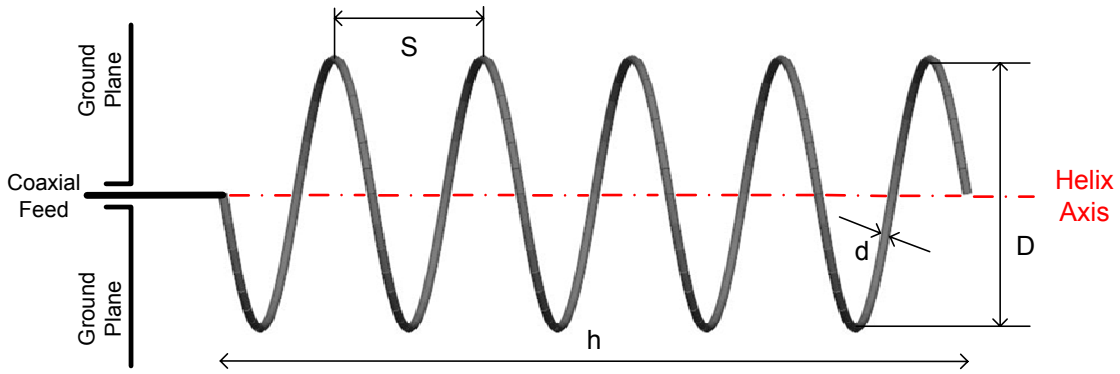

Figure 2.1: Geometry and parameters for helical antenna

Table 2.1: Helix Parameters and Their Definitions

C	Helix circumference
L	Length of a single turn
S	Turn Spacing
N	Number of turns
α	Pitch angle
D	Helix diameter
h	Height
d	Conductor diameter
l	Total length

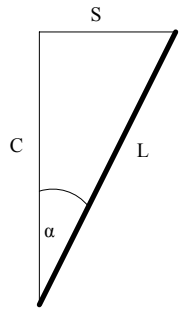

Figure 2.2: Single unfolded turn

The relationships among some of helix parameters can be easily determined by examining an unfolded turn as illustrated in Figure 2.2. Since L, C, and S form a right triangle, the following relationships are readily obtained.

$$C = \pi D \tag{2.1}$$

$$L = \sqrt{S^2 + C^2} \tag{2.2}$$

$$\alpha = \tan^{-1}\left[\frac{S}{C}\right] \tag{2.3}$$

Moreover, the number of turn, spacing between turns, and helix height are related to eachother according to

$$N = \frac{h}{S} \tag{2.4}$$

Also, it should be noted that $l = NL = NC / \cos\alpha$.

2.2 Radiation Modes of Helical Antenna

Depending upon the electrical size of the helix circumference $C_\lambda = C / \lambda$, the helix operates generally in one of two radiation modes: the normal mode and the axial mode [1, 5]. The normal mode occurs when the total length of the helix is much smaller than the wavelength of operation; that is, $l = NL << \lambda$. The axial mode, on the other hand, occurs when the diameter is nearly equal to one wavelength; $C \approx \lambda$. Approximate analytical and empirical analysis of both modes are briefly reviewed in the following subsections.

2.3 Normal Mode Helix

For the helical antenna to operate in the normal mode of radiation its total length must be small compared to the wavelength of operation; that is L << λ and D << λ. The current distribution on individual turns of a helical antenna operating in the normal mode is considered to be constant because of the small electrical size of the antenna. Based on this approximation, the electric field can be obtained analytically by considering the helix as an array of two types of small radiating elements; namely, short dipoles and small loops as shown in Figure 2.3. In the far-field region, the electric field of a single is sum of the fields of a short dipole and a small loop. That is,

$$\vec{E} = \vec{E}_D + \vec{E}_L = E_\theta \hat{a}_\theta + E_\varphi \hat{a}_\varphi \tag{2.5}$$

where,

$$E_D = j\omega\mu IS \frac{e^{-j\beta r}}{4\pi r} \sin\theta \hat{a}_\theta , \quad \text{for short dipole} \tag{2.6}$$

$$E_L = \eta\beta^2 \frac{\pi}{4} D^2 I \frac{e^{-j\beta r}}{4\pi r} \sin\theta \hat{a}_\varphi , \quad \text{for small loop} \tag{2.7}$$

As noted in (2.6) and (2.7), the phase difference between the two orthogonal components of the electric field is 90°. If the magnitudes of these orthogonal components are also equal, then the polarization of radiated field will be circular. The condition under which normal mode helix produces circular polarization is determined by setting the axial ratio as defined in (2.8) equal to unity. Doing so an expression for helix diameter in terms of spacing between the turns, S, and wavelength, λ, is obtained, as given in (2.9). Using (2.1) to (2.3) in (2.9), this condition may also be expressed in the terms of pitch angle as given in (2.10). Because its total length is much smaller than wavelength, the normal mode helix is a resonant antenna and thus narrowband. The radiation pattern of normal mode helix is defined by $\sin\theta$ which, as shown in Figure 2.4, is identical to the pattern of a short dipole.

$$AR = \frac{|E_\theta|}{|E_\varphi|} = \frac{2S\lambda}{\pi^2 D^2} \tag{2.8}$$

$$D = \frac{\sqrt{2S\lambda}}{\pi} \tag{2.9}$$

$$\alpha_{CP} = \sin^{-1}\left(\frac{-1+\sqrt{1+(L/\lambda)^2}}{L/\lambda}\right) \tag{2.10}$$

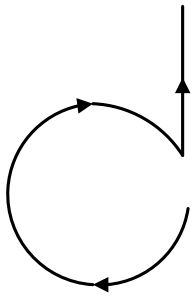

Figure 2.3: Modeling a single turn of normal mode helix as a combination of a short dipole and a small loop.

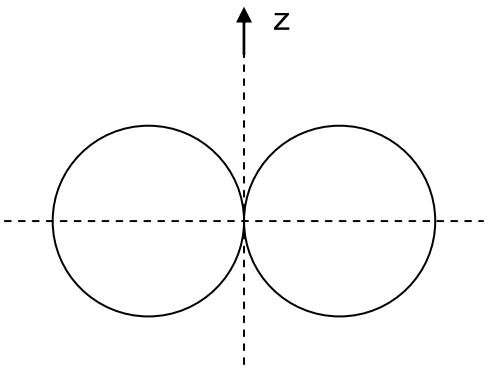

Figure 2.4: Far-field pattern of normal mode helix

2.4 Axial Mode Helix

The axial mode of radiation occurs if the helix circumference is between $3\lambda/4$ and $4\lambda/3$. Since the circumference is close to one wavelength, a single turn can be viewed as a one- wavelength loop whose far-filed pattern is described by $\cos\theta$. The entire helix is then an array of such loops. Thus, the total field of the axial-mode helix can be obtained by using the array theory. Accordingly, the total pattern of an N-turn normal mode helix is expressed as, [5]

$$F(\theta) = K\cos(\theta)\frac{\sin(N\psi/2)}{N\sin(\psi/2)} \tag{2.11}$$

where $\psi = \beta S\cos(\theta) + \alpha_h$, $K = (-1)^{N+1}N\sin(\pi/2N)$ is a normalization constant and α_h is the phase shift between the turns. A simple expression for the axial ratio of normal mode helix is given by Kraus [1],

$$AR = \frac{2N+1}{2N} \tag{2.12}$$

The input impedance of the axial mode helix is largely real due to its traveling wave behavior [5]. Figure 2.5 shows the radiation pattern of a typical axial mode helix. The main beam is directed along the helix axis and there are few side and back lobes.

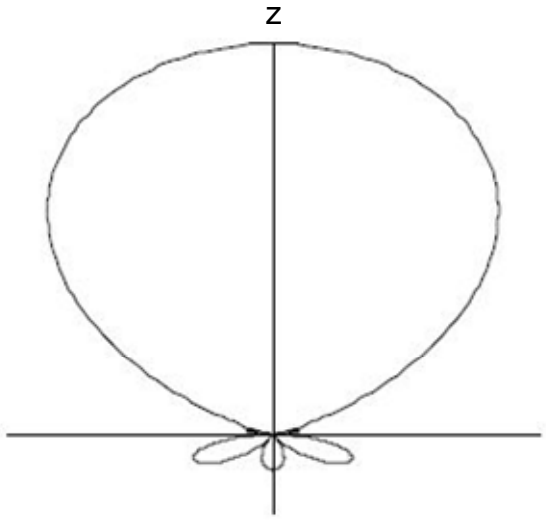

Figure 2.5: Far-field pattern of a 6-turn normal-mode helix

2.5 Modifications of Helical Antennas

Many modifications on the helical antenna geometry have been studied seeking mainly a wider bandwidth and/or size reduction. In order to appreciate the significance of modifications aimed at increasing the bandwidth, the definition of antenna bandwidth should be clarified. Balanis [6] defines the bandwidth of an antenna as "the range of frequencies within which the performance of the antenna, with respect to some characteristics, conforms to a specified standard". These characteristics are the gain or the directivity, radiation pattern, input impedance or VSWR, and axial ratio. Depending upon the size of the bandwidth, an antenna can be classified as a narrowband, wideband, or ultra wideband (UWB). The Federal Communications Commission (FCC) defines a UWB device as one that operates on a fractional bandwidth ≥ 20% or a bandwidth ≥ 500 MHz [7]. The fractional bandwidth is defined as [5],

$$B = \frac{f_U - f_L}{f_C} \times 100\% \tag{2.13}$$

where f_U, f_L and f_C are the lower, the upper, and the center frequencies, respectively.

2.5.1 Feed modifications

Feed modifications are usually performed to improve the VSWR. A VSWR value of 2 on the linear scale refers to 90% power transmission from the feed point to the antenna. Considering an antenna as a one-port network, the scattering coefficient S_{11} is the reflection coefficient, Γ. In order to achieve a 90% or higher power transmission, an S_{11} of −10 dB or less is sufficient. The corresponding value of VSWR for $|S_{11}|=|\Gamma|=$-10 dB is calculated as follows,

$$|\Gamma| = 10^{-1/2},$$

$$VSWR = \frac{1+|\Gamma|}{1-|\Gamma|} = \frac{1+\sqrt{10}}{1-\sqrt{10}} \approx 1.93$$

An interesting technique for matching the normal mode helical antenna to a 50-Ω reference impedance has been introduced by Kraus [8]. He achieved matching by increasing the helical conductor size at the feed point close to the ground plane. The helical geometry itself can be used as a matching element for other antenna designs. In [9] a helical wire with a certain pitch angle and diameter is used to match a spiral antenna to a 50-Ω reference impedance.

2.5.2 Tapering

Tapering of the helical radiating element can bring about some improvements in bandwidth. For example, a tapered printed quadrifilar helix provides a VSWR bandwidth larger than that with a constant strip width [10]. Tapering may also be implemented on the helical structure by gradually increasing or decreasing its radius. An example of a tapered helix is the conical helix studied by Nakano [11]. This design has exhibits an axial ratio of less than 3-dB over a wide bandwidth. Kraus [1] has also examined the effect of gradual variations of the parameters of helix individually while keeping the others constant. A different type of tapering was introduced by Wong, el al. [12] which consisted of winding a wire over a nonuniformly tapered cylinder. The latter design has shown improvements on the axial ratio, gain and VSWR over the conventional helix. Variations of pitch angle has also studied and optimized using genetic algorithms by Lovestead [13]. This design provides higher gain, lower axial ratio and a wider

bandwidth over the conventional helix. A recent study was carried out by exponentially tapering the core of the helix, and it was shown that by varying the pitch angle and the helix height, S_{11} and cross polarization rejection can be controlled [14].

2.5.3 Other Modifications

Other types of modifications have also been examined with the aim of improving the radiation characteristics or reducing the antenna size. Examples are the spiro-helical antenna by Ghoreishian [15] and the stub loaded helix by Barts, et al. [16]. The first design largely maintains the characteristics of the conventional helix with a significantly reduced size. The stub loaded helix is constructed by bending the helical wire periodically to shape small stubs that extend into the core of the helix. This design has offered significant reduction in the size, maintains the gain performance, but has a reduced axial ratio bandwidth.

Chapter 3: The Spherical Helix and Its Modifications

3.1 Full Spherical Helix

The spherical helical antenna was first proposed by Safaai-Jazi in 1991 and was studied by Cardoso and Safaai-Jazi [17, 18]. The antenna was constructed by winding a thin wire over a spherical surface backed by a metallic disc serving as ground plane and fed by a coaxial cable with its inner conductor connected to the helix while the outer conductor connected to the ground plane, as shown in figure 3.1. The spacing between the turns is kept constant, but the length of individual turns and the pitch angle vary as the wire is wound around the spherical surface. An interesting feature of this antenna is that it provides circular polarization over a broad beamwidth, around 120°. The broad beamwidth and compact size of this antenna are its main advantages over the conventional helix, which provides circular polarization only over a narrow angular region about its axis.

3.1.1 Geometry of full spherical helix

The geometry of spherical helix can be conveniently described in the spherical coordinate system (r,θ,ϕ). The path of the helix wire, as any curve in the three-dimensional space, can be viewed as the intersection of two surfaces, which are determined as follows. Clearly, all points on the helix have the same radial coordinate that is equal to the radius of the spherical surface on which the helix is wound; that is, $r = a$. The other surface is determined based on the property that turns are of equal spacing. This, in other words, implies that for every 2π increase in the coordinate ϕ, corresponding to a single full turn, the axial coordinate z should increase by a constant amount equal to the spacing between two successive turns. For a spherical surface of radius a and N turns, the spacing between turns is $2a/N$. Based on these considerations, the equations describing the geometry of a full spherical helix are summarized as:

$$r = a \tag{3.1}$$

$$z = a\left(\frac{\phi}{2N\pi} - 1\right), 0 \le \phi \le 2N\pi \tag{3.2}$$

Equation (3.2) may be expressed in terms of the coordinate θ as given below, but it is emphasized that it is not independent of (3.1) and (3.2).

$$\theta = \cos^{-1}\left(\frac{\phi}{2N\pi} - 1\right) \tag{3.3}$$

One can notice that the geometry of a spherical helix can be fully described by its radius and the number of turns. For numerical computations, coordinates in the Cartesian system are more desirable. The coordinate z is already expressed in Cartesian form in (3.2), and the coordinates x and y are readily obtained from the following equations.

$$\mathrm{x} = r\sin\theta\cos\phi \tag{3.4a}$$

$$\mathrm{y} = r\sin\theta\sin\phi \tag{3.4b}$$

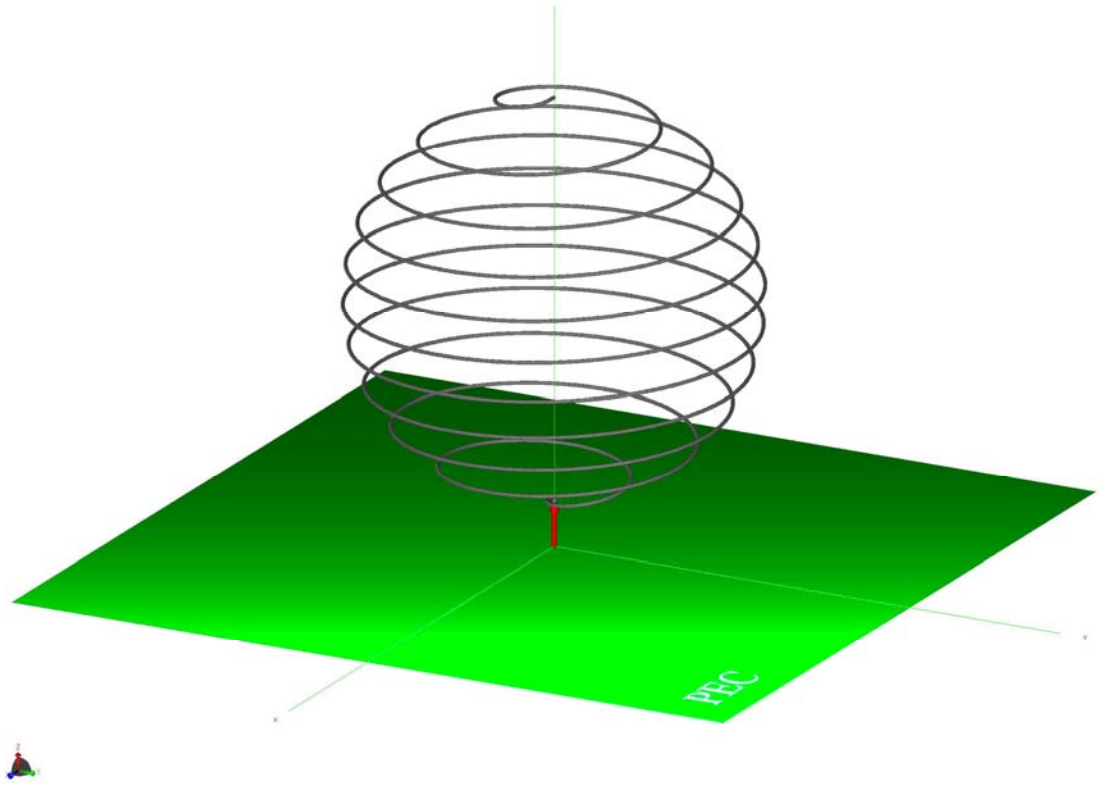

Figure 3.1: A 10-turn spherical helical antenna

3.1.2 Radiation Characteristics of full spherical helix

The study of spherical helix by Safaai-Jazi, et al. [18] revealed that its directivity remains around 9 dB over a wide bandwidth. Two distinct radiation patterns were observed as the frequency was increased. They were called the axial and the axial-null modes, as shown in figures 3.2 and 3.3, respectively. From figure 3.3 it can be noticed that a dip of about 10 dB occurs on the axis at higher frequencies, and is maintained over a very wide bandwidth. It should be noted that the frequencies shown in these figures are in terms of the normalized spherical circumference with respect to the wavelength of operation. Although circular polarization was maintained over a wide beamwidth, but the bandwidth over which this polarization was present was narrow. Moreover, no attempts were made to match the input impedance of the antenna to the transmission line at the feed point, largely because the software used at the time for the numerical analysis of the spherical helix was believed not to provide accurate input impedance results. A recent study by Hui, et al. [19] shows that the length of the feed wire segment above the ground plane and the number of turns have significant impact on the impedance. It was shown that with a longer feed wire segment the real part of the input impedance increases and also with less number of turns its fluctuations reduces.

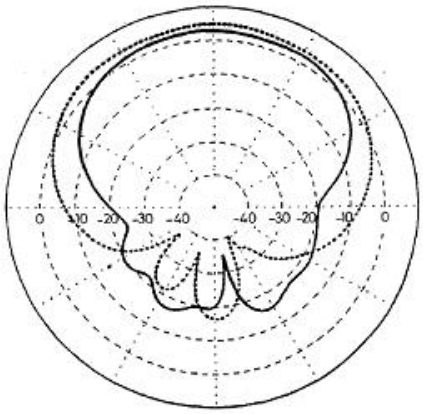

Figure 3.2: Computed far-field patterns in xz-plane for a 7-turn spherical helix with a circumference of 1.308λ,——G_θ , - - - G_ϕ in dB, [2].

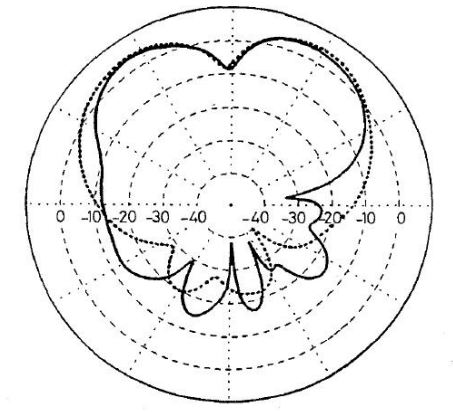

Figure 3.3: Computed far-field patterns in xz-plane for a 7-turn spherical helix with a circumference of 2.077λ, ——G_θ, - - -G_ϕ in dB, [2].

3.2 Hemispherical Helix

The main goal of this design, as mentioned by Weeratumanoon and Safaai-Jazi [20, 21], was to study the reduction of the physical size of the full spherical helix. This was realized by truncating the sphere to half of its original size, which makes it a hemispherical helix. With this modification, the antenna becomes more compact and mechanically more stable.

3.2.1 The hemispherical helix geometry

Equations (3.1) and (3.2) can still be used to describe the geometry of a hemispherical helix, but the range of ϕ will be limited to $0 \le \phi \le N\pi$, as half the number of turns is considered for the hemispherical design. Figure 3.4 illustrates a hemispherical helix with 4.5 turns.

3.2.2 Radiation characteristics of hemispherical helical antenna

The idea of hemispherical helix was not only useful in providing a smaller size than the full spherical design, but also was found to yield circular polarization over a wider bandwidth. Approximately the same directivity of 9 dB, as for the full spherical design, was achieved over the same bandwidth. The number of turns was optimized in order to achieve the desired radiation characteristics over the bandwidth of interest.

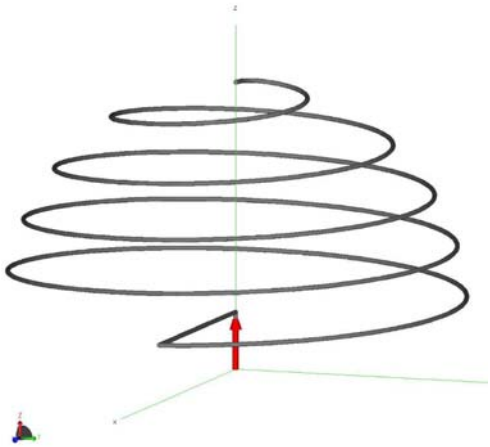

Figure 3.4: 4.5-turn hemispherical helical antenna

The main characteristics considered in optimizing the number of turns were directivity and axial ratio. Figure 3.5 and Figure 3.6 show the directivity and the axial ratio, respectively, for several hemispherical antennas of the same radius but different number of turns over the same frequency range. It is noted that the design with 4.5 turns generally provides the highest directivity as well as the widest bandwidth over which the axial ratio remains less than 3 dB.

This antenna geometry was also investigated by Hui, et al. [22]. The antenna was fed by a coaxial cable on the side of the hemispherical helix, with the inner conductor of the cable extending vertically slightly above the ground plane. Through measurements carried out in this study, it was found that the height of the vertical feed wire above the ground plane does not affect the impedance significantly. The design was further investigated by Chan, et al. [23] with a 3-turn hemispherical helix fed from the center of the hemisphere. This design is very close to the one studied by Weeratumanoon, et al. [20], which consisted of a 4.5 turn hemispherical helix. Improvements over the side-fed antenna on axial ratio and input impedance were observed in the study by Chan, et al. [23]. The likely reason for the improvement in the impedance is that the horizontal part of the feed wire above the ground plane, as shown in figure 3.4, acts as a matching element.

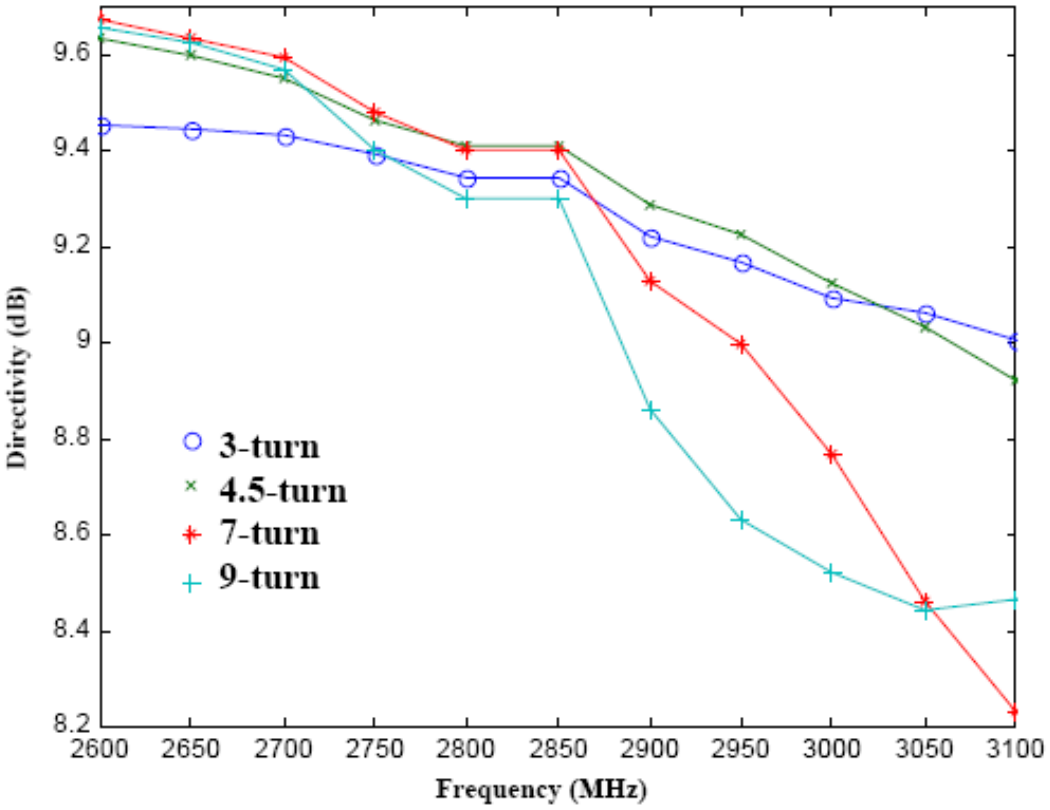

Figure 3.5: Directivity of several hemispherical helical antennas with different number of turns and a radius of 2 cm, [3].

However, the deterioration of circular polarization, evidenced by an increase in the axial ratio, indicates that the horizontal feed section is radiating. The noticeable impact of the feed section on radiation characteristics of the antenna suggests that the feed section is not close enough to the ground plane. This design was again revised by Hui, et al. [24] through examining the current distribution along the helix. It was noted in this latter study that at some frequencies a reflected wave emerges at the open end of the antenna that disturbs its circular polarization. Yet another study by Chen, et al. [25] shows a technique for impedance matching to a 50Ω reference by adding a copper strip with specific dimensions to the design presented by Chan, et al. [23]. It was found that this modification does not affect the radiation pattern or the axial ratio of the antenna.

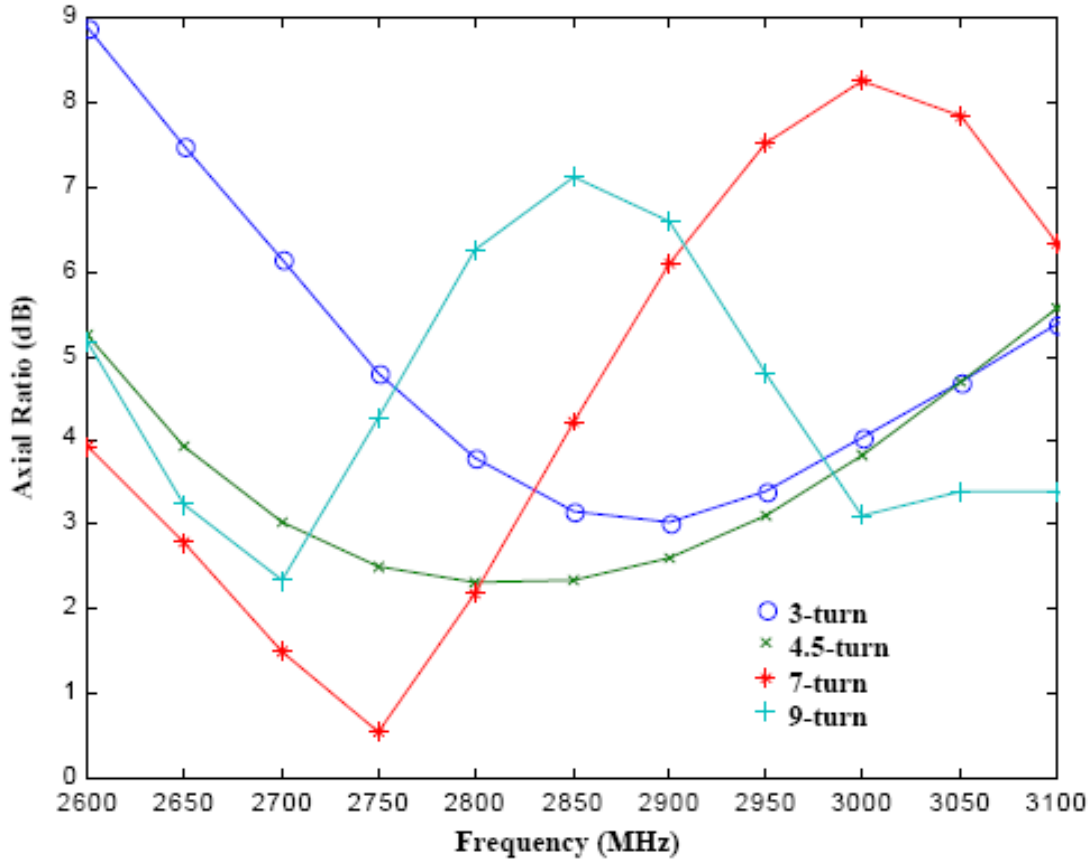

Figure 3.6: Axial ratio versus frequency for several hemispherical helical antennas with different number of turns and a radius of 2 cm, [3].

An interesting study was presented in [26] involved the inclusion of a dielectric material in the core of hemispherical helix. It was found that as the relative permittivity of the dielectric increases and the frequency decreases the antenna continues to provide circular polarization over a wide beamwidth. This result suggests that the size of hemispherical helix can be reduced by filling the helix core with a dielectric material.

3.3 Multifilar Hemispherical Helical Antenna

The multifilar hemispherical helix was investigated by Best [27] as an electrically small antenna. In that study, it was found that the multifilar helix performed as a resonance antenna with linear polarization at the resonance frequency. Similar

modification of the hemispherical helix was studied by Clark et al. [28] where the antenna was fed from the top. Particularly a bifilar three-turn hemispherical antenna was proposed and examined in this study.

3.3.1 The bifilar hemispherical helical antenna

One can think of this geometry as a hemispherical helix with an additional identical arm or radiating element rotated 180° around the z-axis or the normal to the ground plane. The arms are shorted at the bottom of the hemisphere by attaching them to the ground plane. The antenna is fed from the top of the hemisphere where the two arms meet. The feeding element, which extends vertically from the ground plane to the top of the hemisphere, is assumed to have negligible effect on the radiation properties of the antenna. Figures 3.7 and 3.8 illustrate two views of the geometry of a bifilar hemispherical helical antenna.

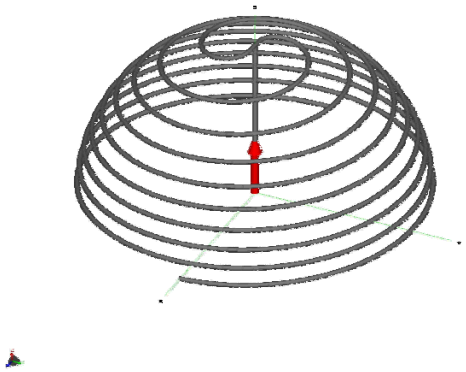

Figure 3.7: Side view of a bifilar hemispherical helical antenna

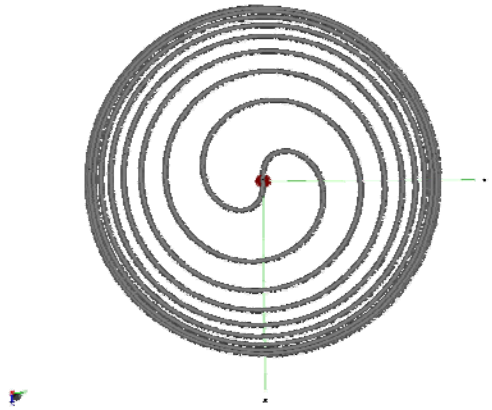

Figure 3.8: Top view of a bifilar hemispherical helical antenna

3.3.2 Radiation characteristics of bifilar hemispherical helix

This design exhibits a very interesting behavior by presenting an axial null pattern over the whole bandwidth of interest. The polarization is elliptical in general and circular over a narrow beamwidth over some frequencies. VSWR was relatively high over the bandwidth of interest, but its variation was rather slow which makes this design highly qualified for impedance matching. Figure 3.9 shows an example of the radiation pattern of a bifilar hemispherical helix and figure 3.10 shows the VSWR over the bandwidth of interest. It is emphasized that this figure shows the frequency information in the form of the normalized spherical circumference with respect to the wavelength of operation.

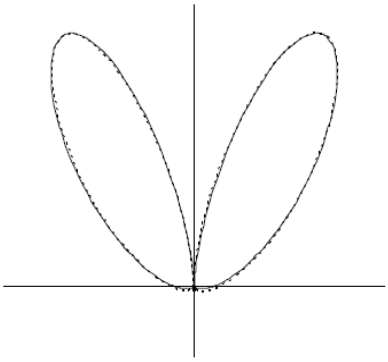

Figure 3.9: Far field radiation pattern of a bifilar hemispherical helical antenna, [4].

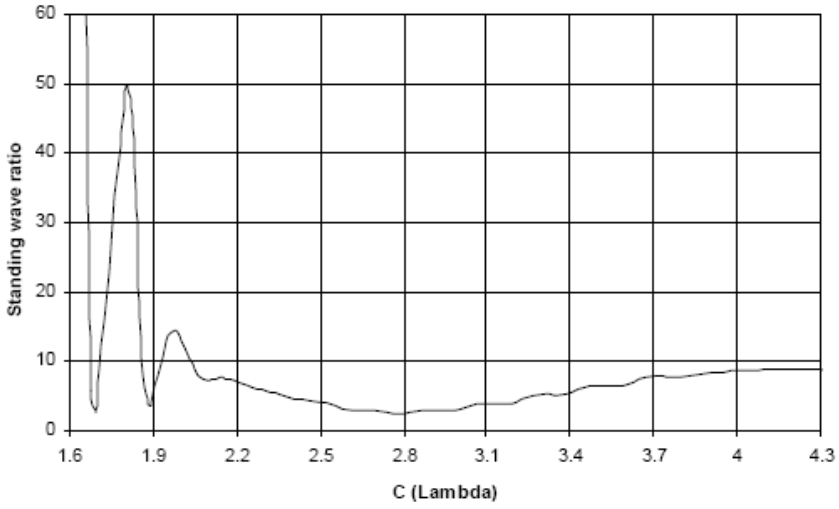

Figure 3.10: VSWR of the bifilar hemispherical helical antenna, [4].

Chapter 4: Numerical Analysis of Conformal and Non- Conformal Hemispherical Helical Antennas

In this chapter modifications of hemispherical helical antennas and their numerical analysis are presented. The main goal of these investigations is to improve the overall bandwidth of the hemispherical helix. The antenna characteristics that are examined to achieve this improvement include axial ratio, VSWR, and directivity. The use of numerical techniques to investigate the radiation characteristics of a complicated geometry such as the hemispherical helix is inevitable as analytical methods are very difficult if not impossible. A commercial simulator called FEKO is used to perform the numerical analysis. In this chapter the geometries as well as numerical analyses of several modifications of the hemispherical helix are discussed.

4.1 Simulation program FEKO

FEKO is a commercial software package that provides simulation tools and electromagnetic field analysis for several electromagnetic problems [29]. FEKO is an abbreviation in German and stands for field computations involving bodies of arbitrary shape. For calculating the components of the far field, the program generally employs the method of moments (MoM). By setting up the output data format, several antenna characteristics such as directivity, axial ratio, and input impedance, can be calculated. Physical optics is also used in the FEKO suite to solve electrically large structures. There is a 256 MB memory limitation if the floating license is used, but unlimited memory allocation is possible by using hardware based key that can be connected through a universal serial bus.

The command user interface of the FEKO suite is used to describe the geometry of the conformal and the non-conformal designs. This interface, called EDITFEKO, allows the use of mathematical functions of multiple variables to describe the geometry. The use of loops in the script of EDITFEKO and variable mathematical functions provides a great deal of convenience and simplicity in introducing the antenna geometry for the solver of

FEKO suite. Meshing the geometry can be controlled by presetting the dimensions of wire mesh segments and the triangle edges of surface meshes. It is recommended in the FEKO user's manual [29] that the segment lengths and the mesh triangle edges be less than or equal to $\lambda_o/10$, while the length of a wire segment should be greater than or equal to four times its radius. The FEKO suite offers the option of setting variable meshing, which makes the simulator effective in terms of memory cost and processing power, especially when simulation of finite ground planes of antennas is required. A more effective option that is available is the simulation of infinite ground planes by simply using the image theory, but back lobes cannot be observed below the infinite ground plane. It must be kept in mind that in continuous meshing, identical edge length for adjacent meshing triangles and wire segments positioned at vertices of meshing triangles, are necessary for the consistency of simulation results.

There are basically two processing levels that FEKO performs to solve a problem, the pre-processing and the post-processing levels. In general, the pre-processing level shows warnings related to the geometry flaws, meshing, and syntax errors in the geometry script. The pre-processing level is useful because it requires significantly less memory and processing power than the post-processing level in which the electromagnetic problem is solved numerically. After the post-processing, the output data are generated and stored in a text file (*.out) with a certain format. The formatted output data are then processed in the data interpretation utility of the FEKO suite, POSTFEKO, and are used to generate 2D and 3D graphs for several antenna characteristics along with views of the meshed geometry. It is emphasized that to obtain the required output data certain commands must first be set in the script in EDITFEKO to instruct the solver on how to calculate the parameters of interest.

4.2 Calculation of Directivity and Axial Ratio

Both far-field components, E_θ and E_ϕ, are used to calculate the directivity and axial ratio for each design. This section explains the mechanism used by FEKO to calculate these two antenna characteristics.

4.2.1 Calculation of Directivity

With both far-field components calculated, the directivity of the antenna can be obtained from the following equation [29],

$$D = \frac{2\pi}{Z_{FO}} . \frac{|E_\theta|^2 + |E_\phi|^2}{P_r} \tag{4.1}$$

$$P_r = P_t - P_v \tag{4.2}$$

where Z_{FO} is the wave impedance of the surrounding medium; it is air in the case of this design. Also, P_t is the source input power, P_v is the ohmic power loss in the radiating structure and P_r is the radiated power. In the designs investigated here the ohmic loss is considered to be negligible, that is all parts of the antenna structure are assumed to be perfect conductor. Following the discussion of directivity concept in [5], *D* as defined in (4.1) is the maximum directivity of the antenna along a direction that the normalized power pattern function, $|F(\theta,\phi)|^2$, is unity.

4.2.2 Calculation of Axial Ratio

The polarization ellipse, shown in Figure 4.1, is used to calculate the axial ratio in FEKO suite. This technique depends on the complex amplitudes of field components as discussed below.

Starting with the phasor forms of the field components, E_θ and E_ϕ, the minimum and maximum field magnitudes on the polarization ellipse can be found using the following equations.

$$\begin{aligned} E_\theta &= Ae^{j\alpha} \\ E_\phi &= Be^{j\beta} \end{aligned} \tag{4.3}$$

$$\vec{E}(r,t) = \frac{A}{r} . \cos(\omega t + \alpha - k_0 r)\hat{e}_\theta + \frac{B}{r} . \cos(\omega t + \beta - k_0 r)\hat{e}_\varphi \tag{4.4}$$

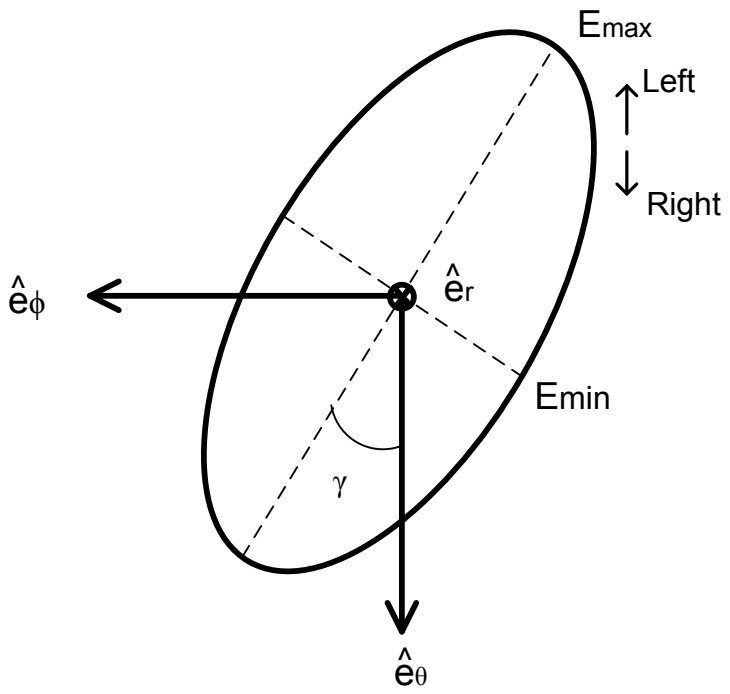

Figure 4.1: The polarization ellipse

where $\vec{E}(r,t)$ is the total electric field vector in the time domain along the direction (θ,ϕ) at distances far from the antenna and $k_0 = 2\pi/\lambda$ is the free-space propagation constant. If $\tau_1 = \omega t_1$ is considered as the time constant at which the field magnitude is maximum and $\tau_2 = \omega t_2 = \tau_1 + \frac{\pi}{2}$ the time constant at which the field amplitude is minimum, then by differentiating the magnitude of the right-hand-side of (4.4) and equating the first derivative at τ_1 to zero, the following result is obtained:

$$\tau_1 = -\frac{1}{2}\tan^{-1}\left[\frac{A^2\sin(2\alpha - 2k_0 r) + B^2\sin(2\beta - 2k_0 r)}{A^2\cos(2\alpha - 2k_0 r) + B^2\cos(2\beta - 2k_0 r)}\right] \tag{4.5}$$

Now, letting $|\vec{E}|_{\max} = |\vec{E}(\tau_1)|$ and $|\vec{E}|_{\min} = |\vec{E}(\tau_2)|$ the axial ratio is determined as

$$AR = \frac{|\vec{E}|_{\min}}{|\vec{E}|_{\max}} \tag{4.6}$$

$$\text{Axial Ratio [dB]} = 20\log_{10}(AR) \tag{4.7}$$

The concept of the polarization ellipse is also explained in [30] but in a slightly different manner. In [30], Stutzam defines the axial ratio as $|\vec{E}|_{\max} \big/ |\vec{E}|_{\min}$ such that it varies in the range $0 < AR < \infty$. The axial ratio defined in the FEKO suite, based on equation (4.6), varies in the range $0 < AR < 1$. The absolute value of axial ratio in dB will be the same using either of the above two definitions. The simulation results for the axial ratio in this thesis are presented as the absolute value of the dB-based axial ratio. Also, from (4.4) and Figure 4.1,

$$E_{\theta\max}\cos(\gamma) = \frac{A}{r}\cos(\tau_1 + \alpha - k_0 r)$$

$$E_{\phi\max}\sin(\gamma) = \frac{B}{r}\cos(\tau_1 + \beta - k_0 r)$$

By dividing the above two equations

$$\gamma = \tan^{-1}\left[\frac{B\cos(\tau_1 + \beta - k_0 r)}{A\cos(\tau_1 + \alpha - k_0 r)}\right] \tag{4.8}$$

where γ is the polarization angle defined as the angle between the major axis of the polarization ellipse and the unit vector $\hat{e}_\theta$.

4.3 Bandwidth Improvements for Hemispherical Helical Antennas

As it was indicated in the previous chapter, the hemispherical helical antenna has become a subject of extensive research in recent years because of its geometrical advantages such as compact size and low profile as well as its desirable radiation characteristics. This research continues to further investigate the hemispherical helical antenna with the aim of improving its performance in terms of overall bandwidth. That is, novel modifications of the basic hemispherical helix geometry are sought such that the antenna provides desired gain, axial ratio, input impedance, and beamwidth simultaneously over a certain frequency range regarded as overall bandwidth.

The guidelines for designing broadband antennas are stated in [5] as below:

1. **Emphasis on angles rather than lengths:** as in helical and spiral antennas in which the radiating element length follows an angular function rather than fixed lengths. Equations (3.2) and (3.3) illustrate this property.
2. **Self-complementary structures:** The spiral as well as the dipole and the slot antenna are good examples of complementary structures.
3. **Tapered radiating element:** for example the bowtie antenna can be viewed as a dipole with a tapered radiating element.

It is also mentioned in [5] that an antenna could be broadband without strictly following the above guidelines. In this thesis, having these guidelines in mind, bandwidth improvements on the hemispherical helical antenna will be sought.

4.4 Conformal Strip Hemispherical Helical Antenna

As noted in chapter 3, Weeratumanoon and Safaai-Jazi [20] found that the optimal number of turns for a wire hemispherical helix that yields maximum axial ratio bandwidth is about four and half. The first modification is realized by replacing the helical wire with a metal strip that conforms to the surface of the hemisphere on which the wire was wound. The metal strip may be printed on the hemispherical surface, thus the name conformal or printed hemispherical helical antenna. This modification allows for width adjustment of the radiating element and also might offer some advantages such as structural rigidity and stability. This idea was examined in [31], with a five-turn helix linked to the source by a matching section attached to the side of the helix above the ground plane, as shown in Figure 4.2. The antenna in [31] was found to have an input impedance bandwidth of 6% and a 3-dB axial ratio bandwidth of 7%. The gain is about 9 dB and the return loss, S_{11}, is less than -20 dB at the center frequency. Figure 4.3 illustrates variations of the gain and the axial ratio versus frequency, while Figure 4.4 shows the return loss for this antenna. The drawback of this design is that the matching section with its fixed lengths makes the hemispherical helix to behave as a resonant antenna as axial ratio and S_{11} curves in Figures 4.3 and 4.4 clearly indicate.

(a) (b)

Figure 4.2: Printed hemispherical helical antenna with 2 mm strip width, (a) top view, (b) side view

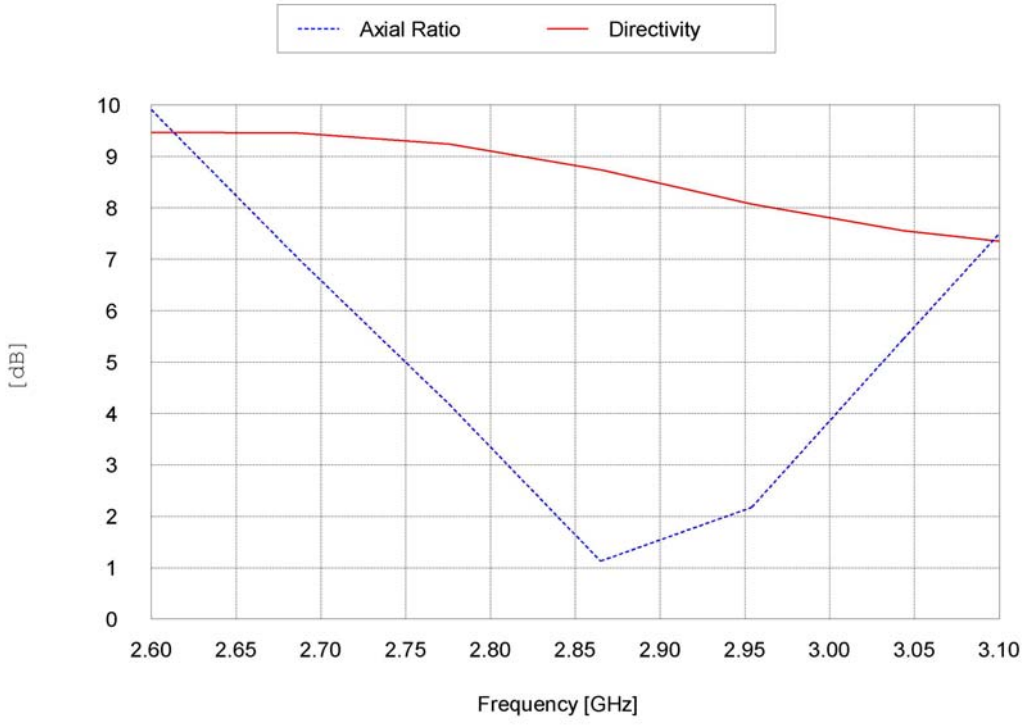

Figure 4.3: Calculated axial ratio and gain versus frequency for the hemispherical helix of Fig, 4.2

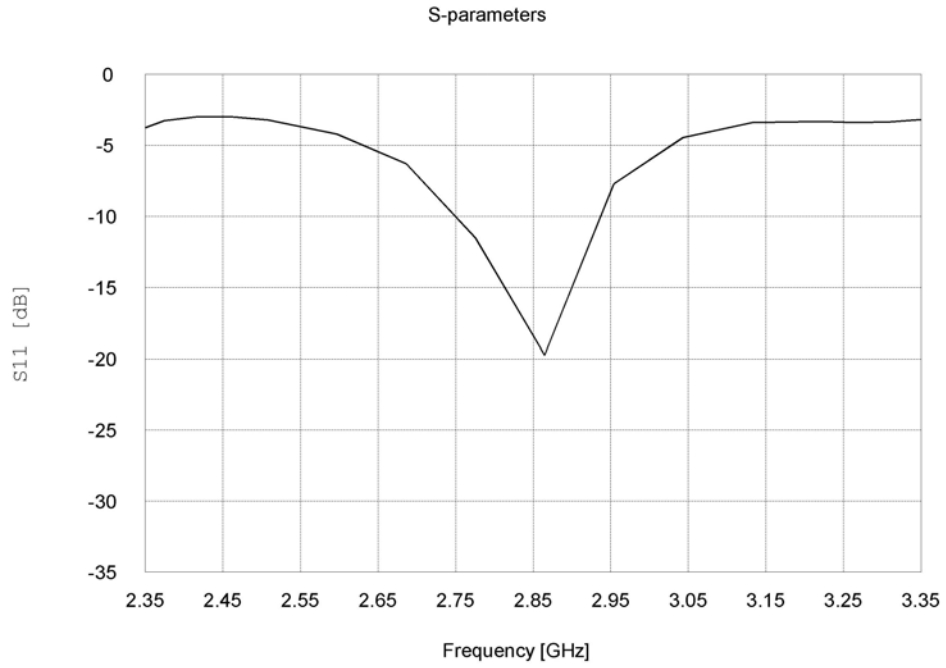

Figure 4.4: Calculated return loss versus frequency for the hemispherical helix of Fig. 4.2

4.4.1 Geometry of Conformal Hemispherical Helical Antenna

In order to define the geometry of the conformal hemispherical helix, it is assumed that the central line of the metal strip follows the same path as the wire helix described by (3.2) to (3.4). For operation in the frequency range 2 to 4 GHz, a width of 2 mm for the metal strip over a hemisphere of radius a=20 mm is reasonable to maintain sufficient spacing between the turns of the helix. The upper and lower edge points of the metal strip conforming to the hemispherical surface of radius a are merely the same points as the wire design but shifted up and down following the constant radius of the hemisphere. To facilitate the calculation of the shift in the coordinates of the central line points, an angle θ' as shown in Figure 4.5 is defined. Since the width of strip is much smaller than the radius of hemisphere; i.e. $w << a$, the angle θ' measured in radians is determined as

$$\theta' = \frac{w}{2a} \text{ (radians)} \tag{4.9}$$

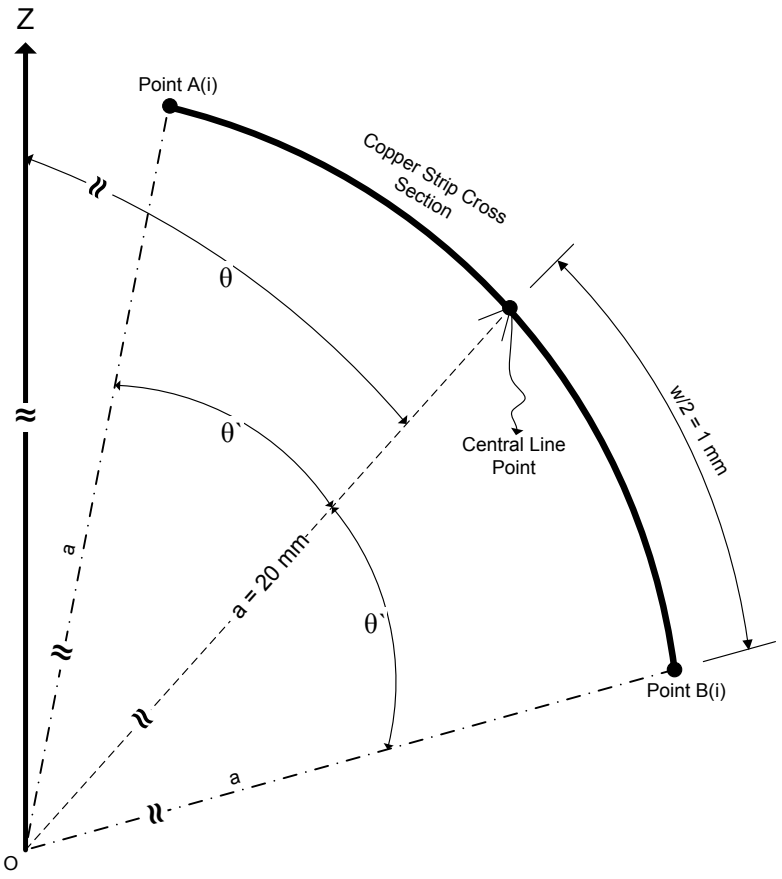

Figure 4.5: Geometry, coordinates, and cross sectional view of a sample conformal strip

As shown in Figure 4.5, the points A(i) and B(i) are the up-shift and down-shift of the central line point, respectively. The coordinates of the points A(i) and B(i) are obtained from (3.2) to (3.4) in which θ is replaced with θ_A and θ_B, respectively. Here, θ_A and θ_B are defined as

$$\theta_A = \cos^{-1}\left(\frac{\phi}{N\pi} - 1\right) - \theta' \tag{4.10}$$

$$\theta_B = \cos^{-1}\left(\frac{\phi}{N\pi} - 1\right) + \theta' \tag{4.11}$$

with $0 \le \phi \le N\pi$.

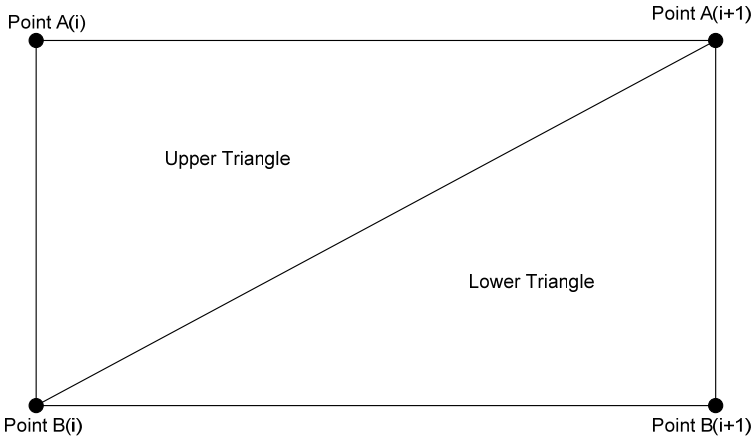

Figure 4.6: Dividing a strip segment into two triangles

Using (4.9) to (4.11) in conjunction with (3.2) to (3.4), the calculation of coordinates for points A and B for the entire conformal strip hemispherical helix is now a recursive process. Each segment on the strip is divided into two triangles referred to as upper and lower triangles, as shown in Figure 4.6. The script by which the geometry of the conformal hemispherical helix is introduced to the command-based interface of the FEKO suite, EDITFEKO, is given in appendix A.1.1.

4.4.2 Numerical Analysis of Conformal Hemispherical Helical Antenna

Figure 4.7 shows the geometry of a conformal hemispherical helix above an infinite conducting ground plane. The antenna is fed from the side by a wire segment 5 mm long above the ground plane. For comparison purposes, this length is kept equal to that of the feed wire used for the hemispherical helix studied in [20]. Examination of simulation results reveals that purer circular polarization can be obtained by using the conformal strip as a modification to the design presented in [20]. Figure 4.8 shows the axial ratio of the conformal strip design. Comparison of results in Figures 3.6 and 4.8 indicates that the axial ratio values for the conformal design are smaller over the same bandwidth, implying purer circular polarization.

The VSWR of the conformal design was also examined and it was found that the input impedance is not matched to the source reference impedance ($50\ \Omega$). Thus, in

order to achieve a VSWR of less than 2 in linear scale over the bandwidth of interest, modifications to the feed element need to be considered. With regard to other radiation characteristics, the antenna provides a half-power beamwidth of about 70° with a symmetrical radiation pattern and a directivity of 9 dB with less than 1 dB variations over a wide bandwidth including the bandwidth in which circular polarization is maintained. Figures 4.9 and 4.10 show the radiation pattern and the directivity along the axis of the helix, respectively. The effect of variation of number of turns, form 3 to 5 in steps of 0.5 turns, on radiation characteristics was also investigated. All designs with different number of turns exhibited mostly the same behavior in terms of axial ratio, directivity and radiation patterns, except that the 5-turn design provided a higher axial ratio bandwidth compared to the others. Appendix B.1.1 shows the radiation characteristics of the antenna with different number of turns as well as the radiation pattern of the 4.5-turn antenna at different frequencies.

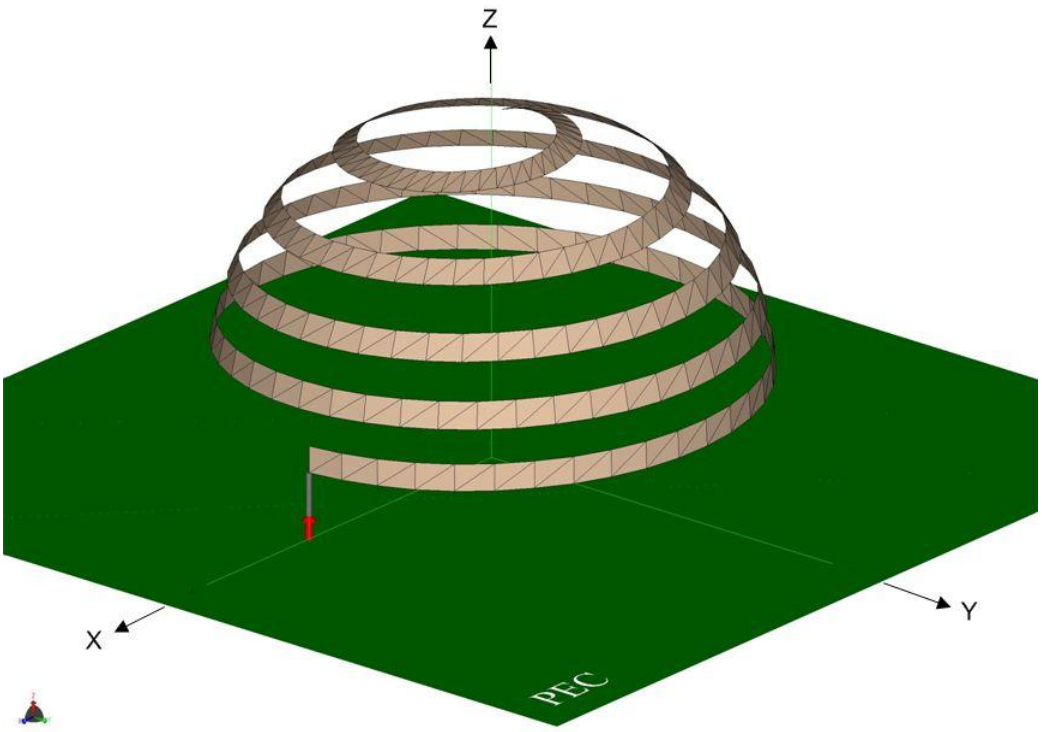

Figure 4.7: Geometry of 4.5-turn conformal hemispherical helical antenna with radius a=20 mm, strip width w=2 mm, side fed by a 5 mm vertical short wire, and backed by infinite ground plane

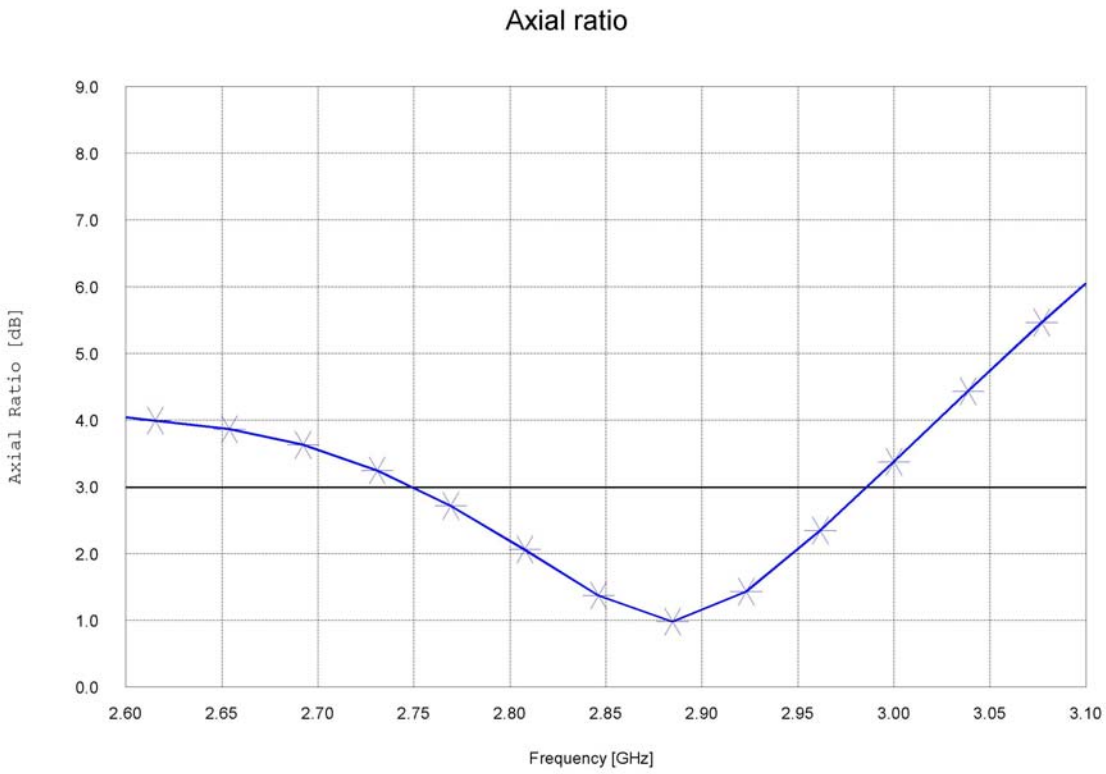

Figure 4.8: Variations of axial ratio versus frequency for the hemispherical helix of Fig. 4.7

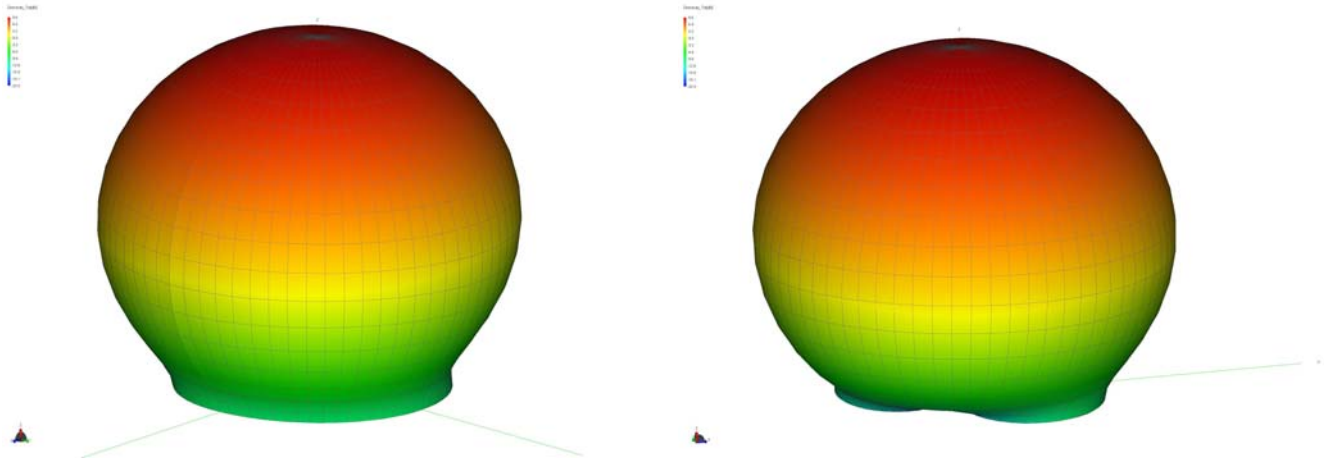

(a) (b)

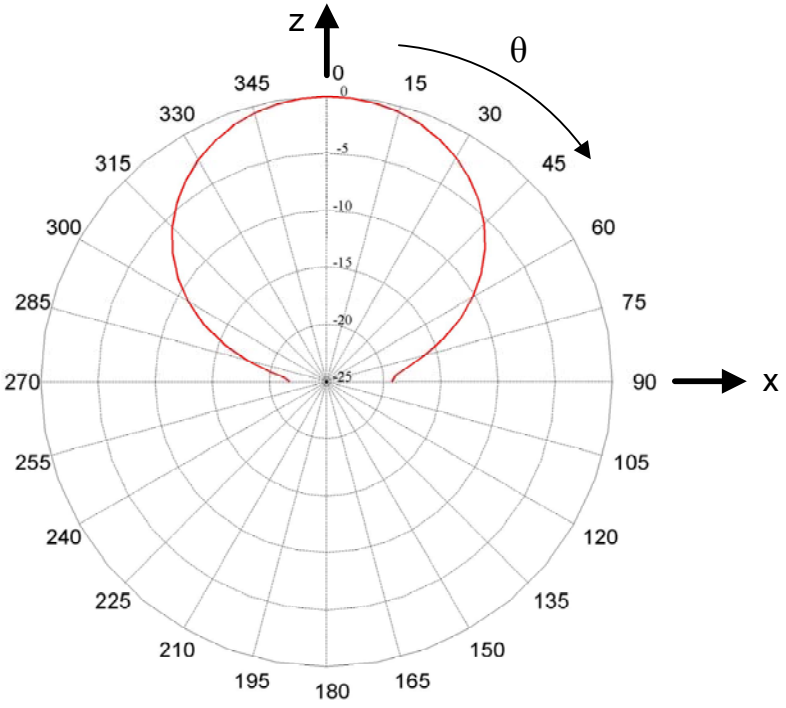

(c)

Figure 4.9: Radiation patterns for the hemispherical helix of Fig. 4.7 at *f*= 2.692 GHz. (a) and (b) are two views of the 3-D radiation pattern, (c) normalized 2-D radiation pattern in the xz-plane ($\phi = 0$ *and* $\phi = \pi$) on dB scale.

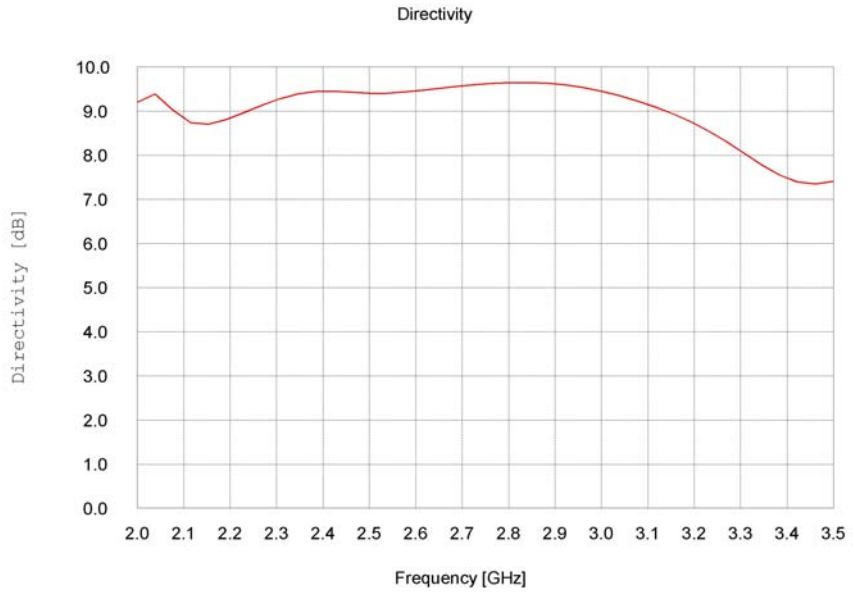

Figure 4.10: Variations of directivity versus frequency for the hemispherical helix of Fig. 4.7

4.4.3 Impedance Matching of Conformal Hemispherical Helical Antenna

It was pointed out in section 3.2.2 that the horizontal feed wire between the center of the hemisphere and the starting point of the helical conductor might affect the radiation characteristics of the antenna. Among these characteristics the input impedance is the one affected most, while the directivity, axial ratio, and radiation pattern remain largely unchanged. The feed wire and the ground plane together form a transmission line which can transform the input impedance of the hemispherical helix. On the other hand, if the horizontal feed wire is sufficiently close to the ground plane, due to its opposite image current in the ground plane, will have negligible contribution to radiated fields and thus very little impact on axial ratio and directivity.

One may take advantage of the above mentioned impedance transformation property and try to match the antenna to the coaxial cable that brings power to it. However, it is desirable that the impedance matching occurs over a wide bandwidth. Tapered transmission lines are known to be capable of wideband impedance transformation. The idea of matching the impedance of a conventional helix to a 50Ω

reference impedance was first presented in [8]. The theoretical analysis of the tapered transmission lines can be found in [32].

Accordingly, the horizontal feed wire in the design shown in Figure 3.4 is replaced with a tapered microstrip that increases linearly in width from the center of the hemispherical helix to the point it is connected to the helical strip as shown in Figure 4.11. The spacing between the microstrip matching element and the ground plane varies from 1 mm at the center hemisphere to 5 mm at the point of connection to the helix. Thus, the microstrip matching element is in fact a doubly tapered transmission line. The maximum width of the matching element is varied with the number of segments on the helical strip conductor that are attached to it. Figures 4.11b, c, and d show microstrip matching elements with three maximum width sizes, referred to as width 1, width 2, and width 3, respectively.

Figure 4.12 shows the axial ratio and VSWR for the 4.5-turn conformal strip hemispherical antenna with three matching sections of different widths. It is noted that all three different widths of the matching section provide essentially the same axial ratio bandwidth but the matching sections of width 1 and width 2 provide wider VSWR (input impedance) bandwidths. The effects of variations in the number of turns on radiation characteristics were also examined and the corresponding simulation results are presented in Appendix B.1.2.

The overall bandwidth is defined as the frequency range over which an axial ratio of less than or equal to 3 dB, a VSWR of less than or equal to 2 on a linear scale, and a directivity/gain fluctuation of less than 3 dB are simultaneously maintained. Based on this definition, the overall bandwidth of the 4.5 turn matched conformal hemispherical helical antenna is 13% relative to a center frequency of 2.76 GHz. Individual bandwidths can also be of interest, for instance the 3-dB axial ratio bandwidth is 14% at 2.78 GHz center frequency, the VSWR bandwidth is 17% at a center frequency of 2.69 GHz, and the bandwidth in which the directivity along the axis of the helix is 9±1.5 dB is more than 50% at 2.65 GHz center frequency.

The bandwidth performance of this 4.5-turn conformal hemispherical helix surpasses that of the basic wire-based design presented in [20]. It provides a purer circular polarization and at the same time the input impedance is matched to a 50Ω source over the bandwidth that circular polarization (AR<3 dB) exists. The directivity is about 9 dB with less than 1 dB variations over a much wider bandwidth.

Since tapering of the feed element provides significant improvements on the VSWR bandwidth of the antenna, it is expected that tapering the radiating element would further increase the VSWR bandwidth. Figure 4.13 illustrates a 4.5-turn hemispherical helix with a tapered radiating element whose width at the start and end points are 1 mm and 3 mm, respectively. Although not shown in Figure 4.13, the hemispherical helix is, as usual, backed by an infinite conducting ground plane. Examination of the radiation characteristics of the hemispherical helix with tapered radiating element, presented in Figure 4.13, indicates that a small improvement, about 50 MHz, on the VSWR bandwidth and a reduction in the 3-dB axial ratio bandwidth occur. The matching/feed section for this deign is that of width 1. The input code of the FEKO suite for the tapered helix geometry is given in Appendix A.1.3. To further investigate the effect of tapering the radiating element, the feed element is replaced by a 5 mm vertical short wire, similar to the design in Figure 4.7. Simulation results for the tapered helix with short wire feed revealed no noticeable improvements in axial ratio or VSWR bandwidth.

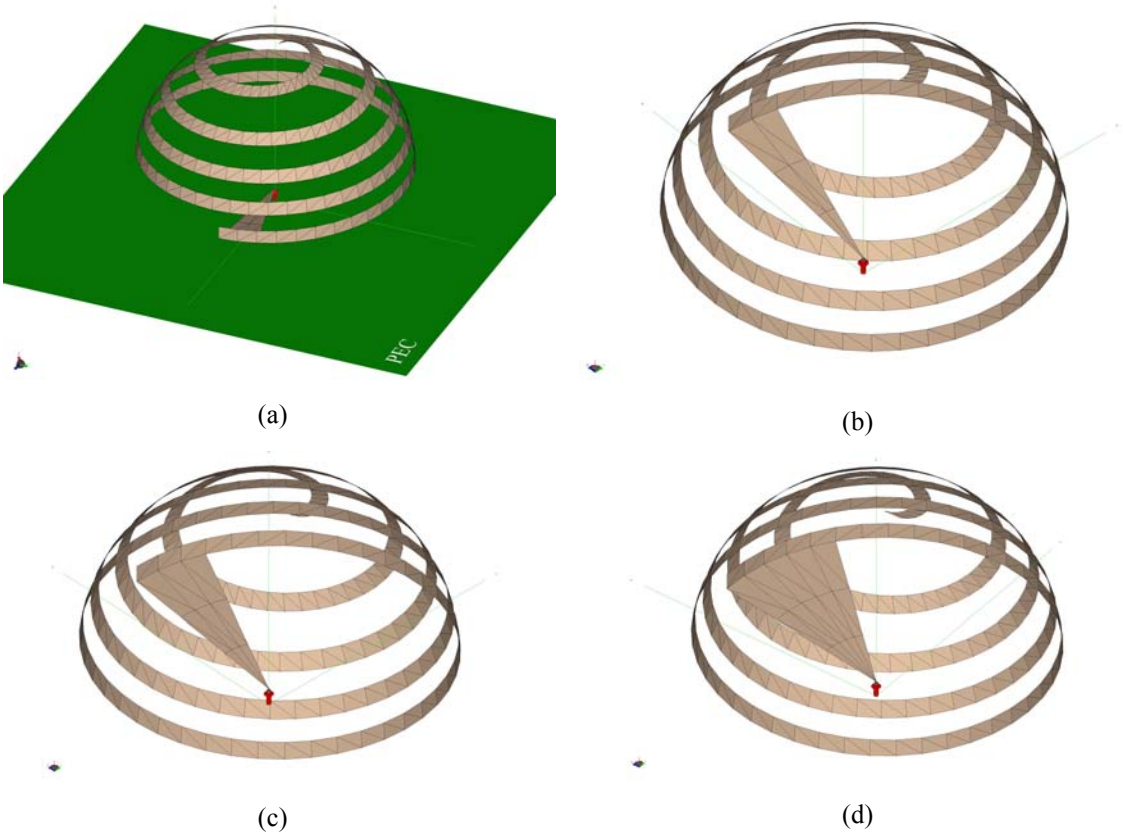

Figure 4.11: Geometry of 4.5-turn conformal hemispherical helical antenna with radius a=20 mm, strip width w=2 mm and center-fed by a tapered matching section, (a) width 1 top view, (b) width 1 bottom view, (c) width 2 bottom view, (d) width 3 bottom view

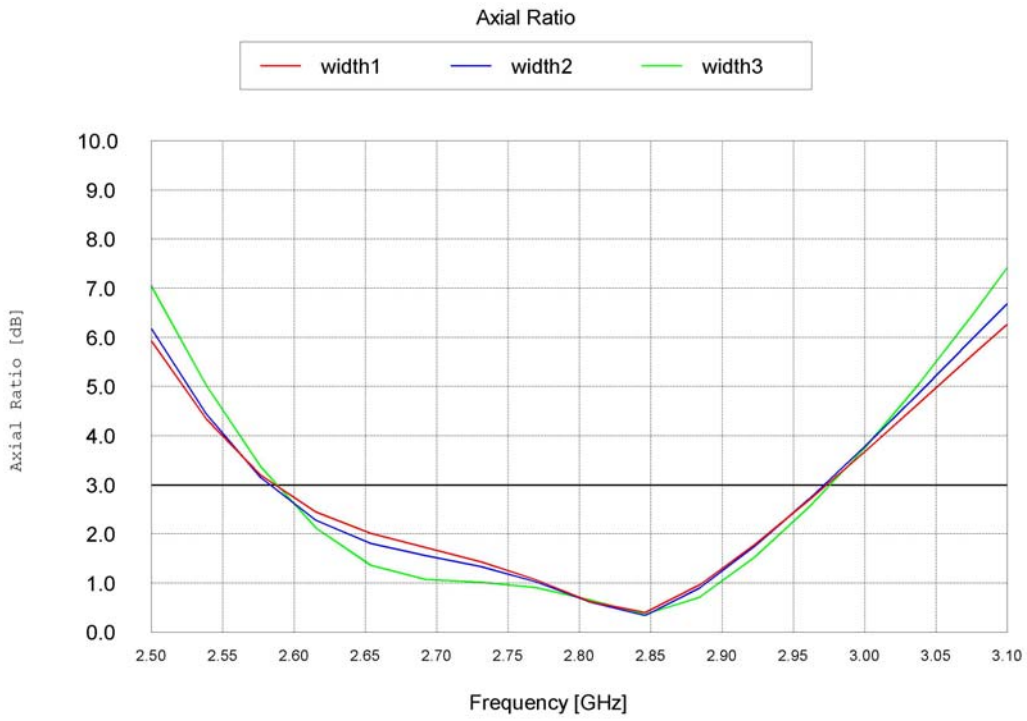

(a)

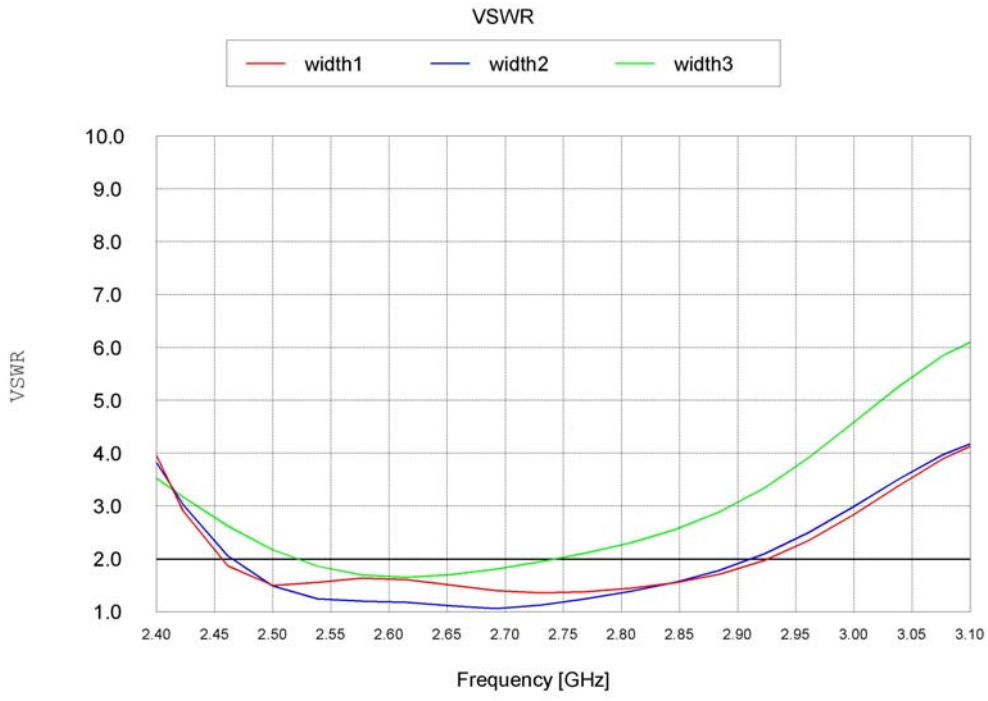

(b)

Figure 4.12: Variations of (a) axial ratio and (b) VSWR versus frequency for the hemispherical helix of Fig. 4.11.

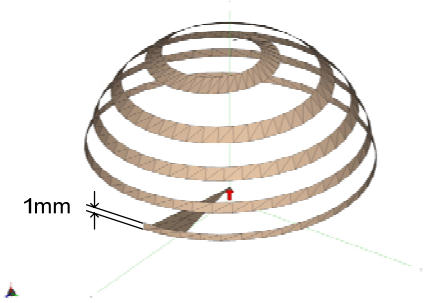

(a)

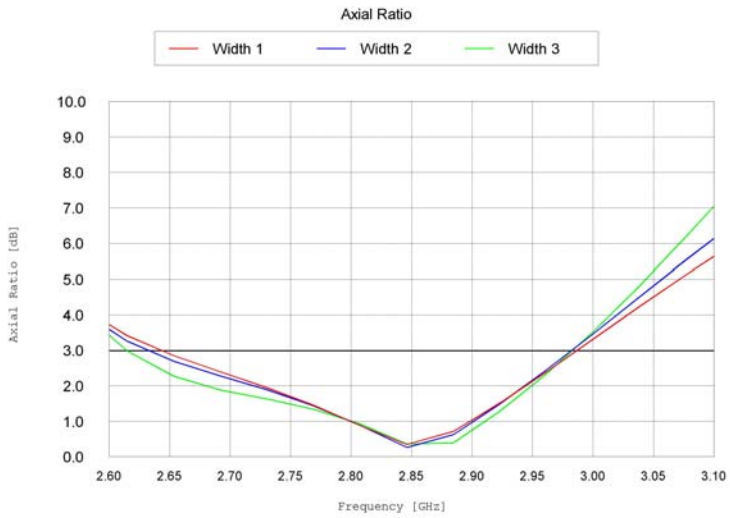

(b)

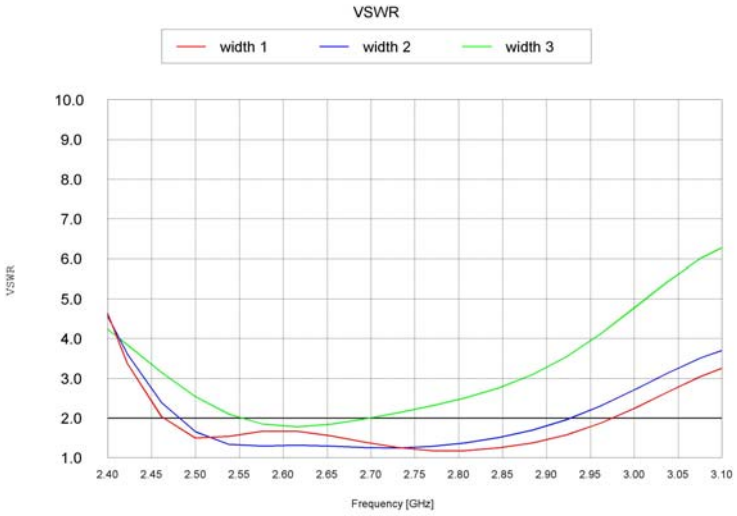

(c)

Figure 4.13: (a) Geometry of 4.5-turn tapered hemispherical helix with tapered radiating element. Variations of (b) axial ratio and (c) VSWR versus frequency for the geometry of part (a)

4.5 Non Conformal Strip Hemispherical Helical Antenna

Radiating elements conformal to the hemispherical surface limit the spacing between the turns, and with wider strip width the hemispherical helix becomes more of a resonant structure. This observation gave rise to the idea of the non-conformal radiating element. By non-conformal it is meant that the strip radiating element does not conform to the hemispherical surface. A literature search revealed that this idea has never been investigated before, thus non-conformal hemispherical helical antennas discussed hereafter are novel designs.

4.5.1 Geometry of Non-Conformal Hemispherical Helical Antenna

Other than radiating element not conforming to the hemispherical surface, all other geometrical features of this antenna are the same as those of the conformal design discussed in section 4.4. Figure 4.14 shows the geometry of a 4.5-turn non-conformal hemispherical helical antenna fed by a vertical short wire. For clarity, the ground plane is not shown in the figures pertaining to non-conformal geometry, but is accounted for in the simulations and numerical analyses.

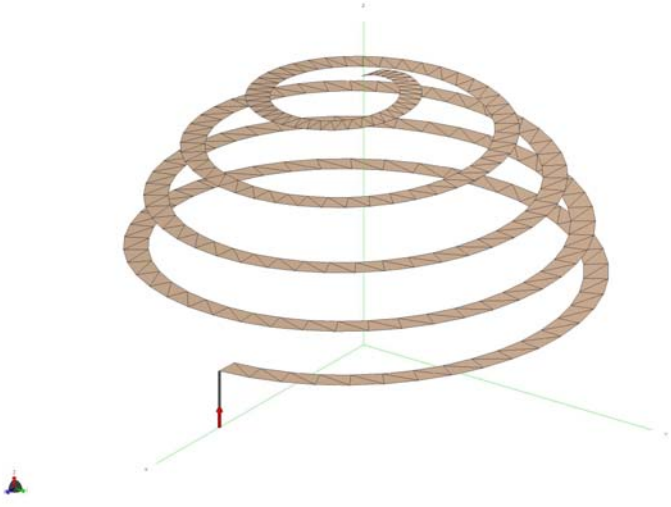

Figure 4.14: Geometry of 4.5-turn non-conformal hemispherical helical antenna

In non-conformal hemispherical helical designs, the slope of the strip element can be varied with respect to the xy-plane or the ground plane. This slope may be regarded as a new design parameter that can be adjusted for optimum performance. Variations of the slope of radiating element might be accounted for by defining an angle, Ψ, referred to as tilt angle; see Figure 4.15(a). Three values of the tilt angle, $\Psi = 0^\circ, 45^\circ, 135^\circ$, were considered in simulation of this antenna. To simplify the definition of the non-conformal strip geometry, it is assumed that the outer edge of the strip follows the same path as the wire hemispherical helix. Accordingly, the coordinates of points on the outer edge can be obtained from (3.2) to (3.4). The outer edge points are denoted as A(i) as shown in Figure 4.15(a). The coordinates of the points B(i) on the inner edge of the strip are obtained from the following equations:

$$x_B = \left[a.\sin\theta - W.\cos\Psi\right].\cos\phi \tag{4.12}$$

$$y_B = \left[a.\sin\theta - W.\cos\Psi\right].\sin\phi \tag{4.13}$$

$$z_B = z_A - W\sin\Psi \tag{4.14}$$

4.5.2 Numerical Analysis of Non-Conformal Hemispherical Helical Antenna

Simulation results for 4.5-turn non-conformal hemispherical helical antennas are presented here. For such antennas with other number of turns, the results are presented in Appendix B.2.1. The code describing the antenna geometry to the FEKO suite is given in Appendix A.2.1. First, 4.5-turn hemispherical helices with a vertical short wire feed and different tilt angles, as shown in Figure 4.16, are examined. Variations of axial ratio versus frequency for tilt angles $\Psi = 0^\circ, 45^\circ, 135^\circ$ are depicted in Figure 4.17. Examination of these results indicates that non-conformal designs with tilt angles 0° and 45° indeed increase the axial ratio bandwidth. For example, the non conformal helix with a tilt angle of 0° provides a 3-dB axial ratio bandwidth of 18% relative to a center frequency of 3.078GHz. Furthermore, comparison of axial ratio curves for tilt angles 0° and 45° reveals an interesting phenomenon; namely, a left shift in the bandwidth associated with the

larger tilt angles as seen in Figure 4.17. This phenomenon might be useful in fine tuning the antenna to a desired frequency range.

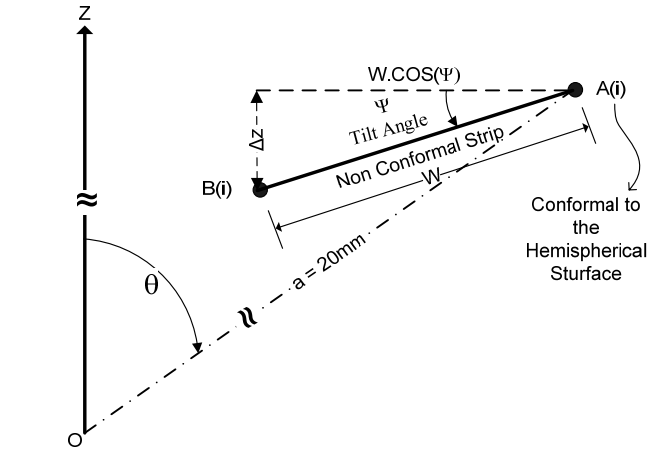

(a)

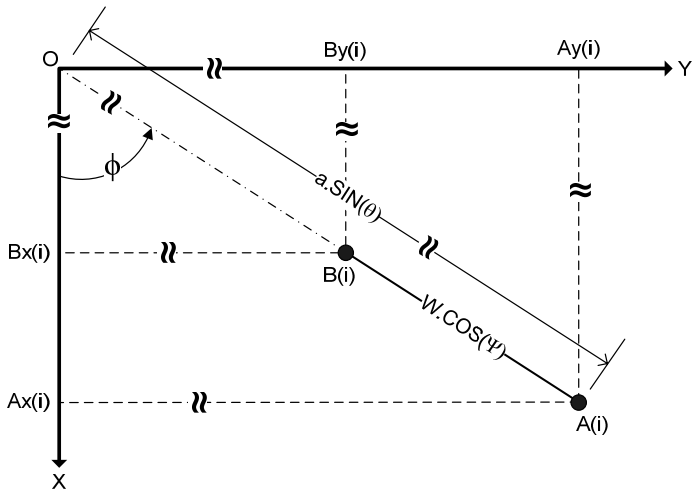

(b)

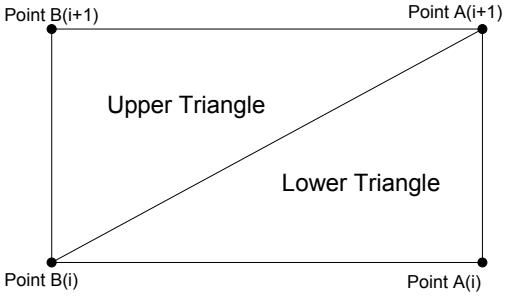

(c)

Figure 4.15: Geometry, coordinates, and cross sectional view of non-conformal strip. (a) cross sectional view, (b) projection on the ground plane, (c) top view of a strip segment

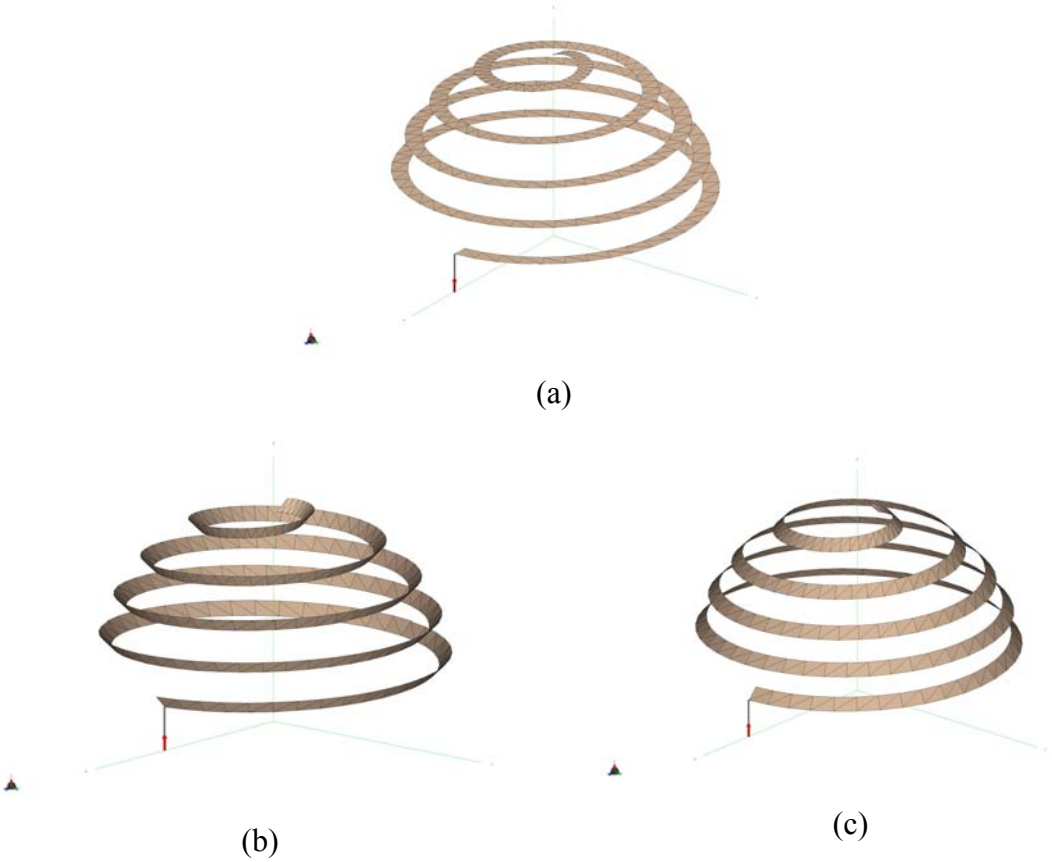

Figure 4.16: 4.5-turn non-conformal hemispherical helical antennas with constant width, fed by a short vertical wire, and tilt angle of (a) 0°, (b) 45°, (c) 135°

Next, tapering of the non-conformal strip is considered. The tapering is expected to yield a smooth decay in the current magnitude from the feed to the end of the radiating element, thus minimizing current reflections from the open end of the strip and allowing the hemispherical helix to behave as a traveling wave antenna. This concept is also discussed in [33] which presents general properties of antennas that provide circular polarization.

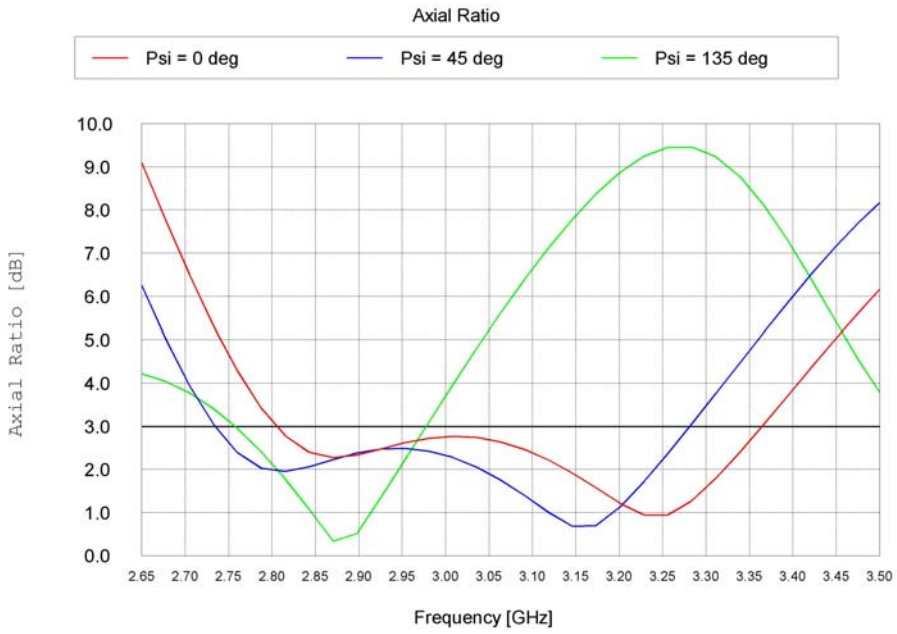

Figure 4.17: Variations of axial ratio versus frequency for 4.5-turn non-conformal hemispherical helical antenna with radius of 20 mm, constant strip width of 2 mm, fed by a 5 mm short wire, and tilt angle of (a) 0°, (b) 45°, (c) 135°

The process of tapering the radiating element is carried out by linearly increasing the width of the strip, in a manner similar to that in the case of conformal hemispherical helix. The code that describes the geometry as an input to the FEKO suite is given in Appendix A.2.2. Also, as in the case of conformal design, the width of the tapered strip for the non-conformal design is 1 mm at the feed point and 3 mm at the end point at the top of the helix. Figure 4.18 illustrates the geometry of the tapered non-conformal helix for tilt angles of 0° and 45°. The corresponding axial ratio results are shown in Figure 4.19. It is noted that tapering of radiating element has increased the 3-dB axial ratio. For example, the 3-dB axial ratio bandwidth for the tapered 4.5-turn non-conformal helix with 0° tilt angle is about 20% relative to the center frequency of 3.275GHz, while that of the 4.5-turn non-conformal design with constant width and 0° tilt angle is 18%. The modification of tapering the helical structure has not contributed to the matching of the input impedance of the antenna to the source reference. Further adjustments to the design with the aim of achieving a VSWR value of 2 or less in linear scale are discussed in the following section.

4.5.3 Impedance Matching of Non-Conformal Hemispherical Helical Antenna

After examining the VSWR of non-conformal hemispherical helices fed by a short wire as in Figure 4.18, it was found out that these antennas are highly mismatched to 50Ω over the 3-dB axial ratio bandwidth. In a first attempt to match the antenna input impedance to 50Ω, the technique based on tapered microstrip that was used in conformal designs is employed. Figure 4.20 illustrates the geometry of non-conformal hemispherical helices with two different tilt angles and fed by tapered microstrip elements. Examination of calculated radiation characteristics for helices with such feed elements indicates dramatic reductions in the 3-dB axial ratio bandwidth as noted in Figure 4.21. Despite the deteriorating impact on axial ratio, the tapered microstrip feed improves the VSWR as seen in Figure 4.22. From Figure 4.21, a 3-dB axial ratio bandwidth of about 7% relative to the center frequency 3.045 GHz for the case of 0° tilt angle is obtained. Over this bandwidth, VSWR remains below 2. In summary, tapered feed elements improve matching of the antenna, but at the expense of reducing the overall bandwidth.

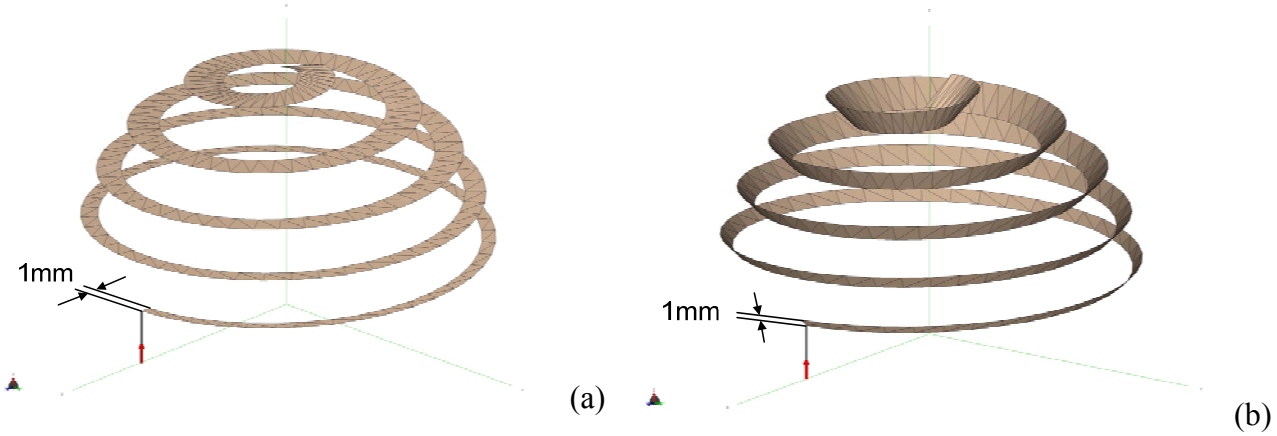

Figure 4.18: 4.5-turn non-conformal hemispherical helical antenna fed by vertical short wire, tapered strip and with a tilt angle of (a) 0°, (b) 45°

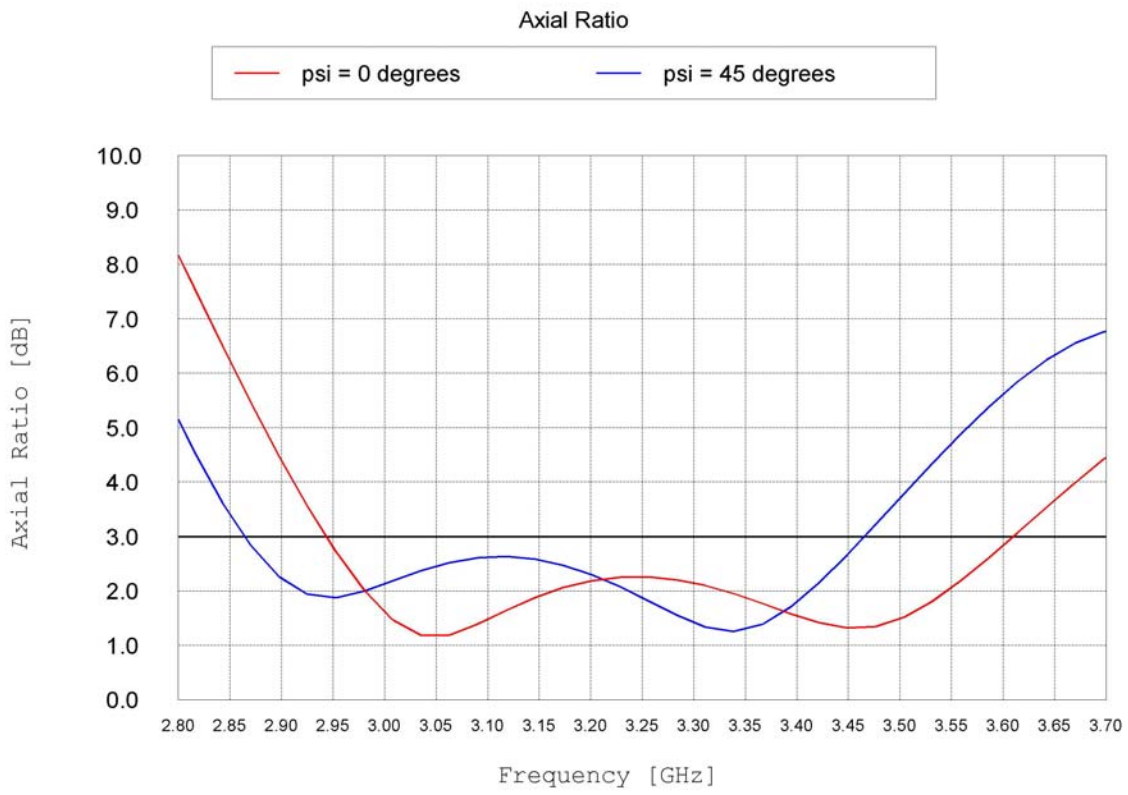

Figure 4.19: Variations of axial ratio versus frequency for 4.5-turn non-conformal hemispherical helical antenna fed by a 5 mm vertical short wire and with a tilt angle of (a) 0°, (b) 45°

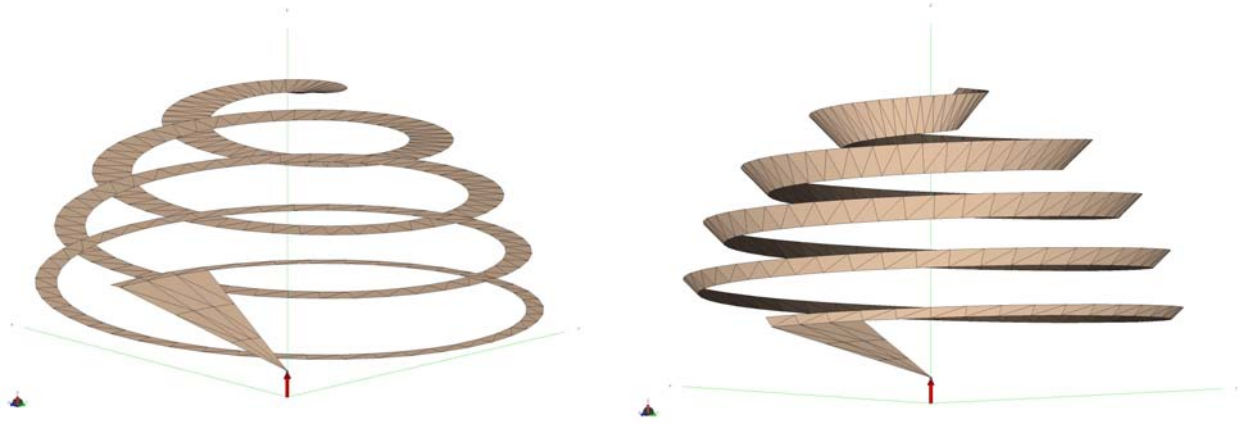

(a) (b)

Figure 4.20: 4.5- turn non-conformal hemispherical helical antenna fed by a tapered microstrip segment and with a tilt angle of (a) 0°, (b) 45°

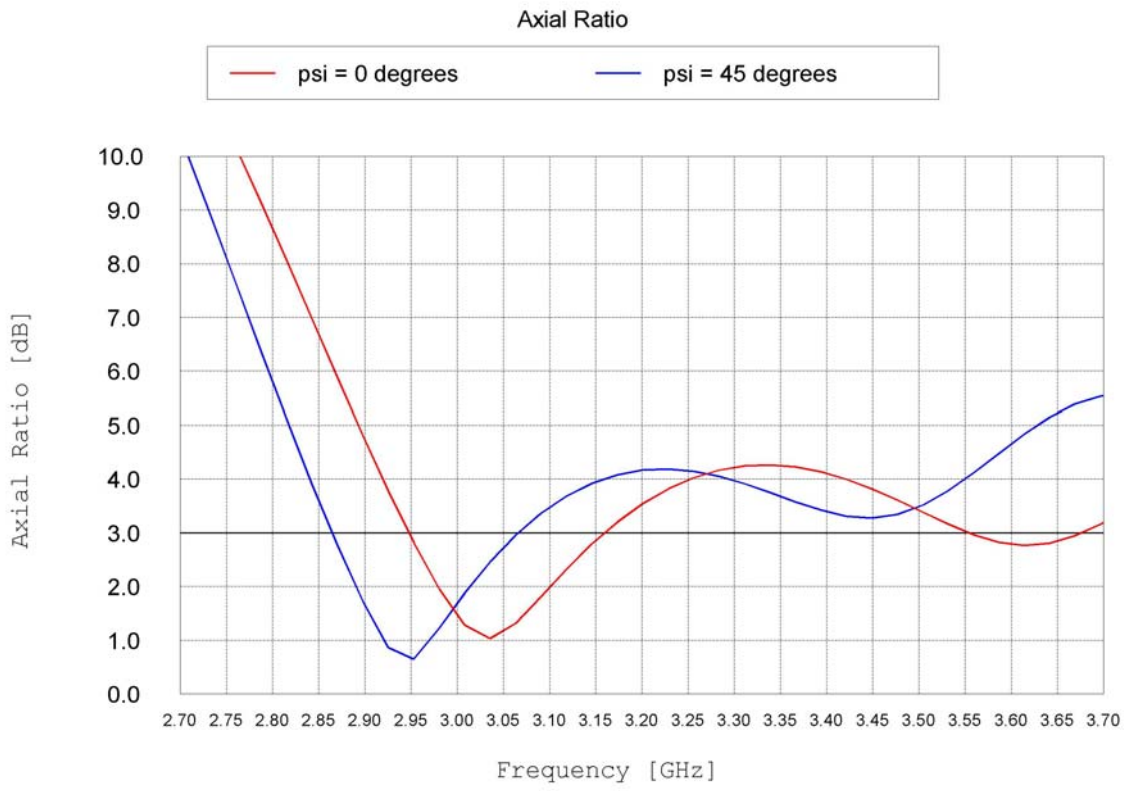

Figure 4.21: Variations of axial ratio versus frequency for 4.5-turn non-conformal hemispherical helical antenna fed by a tapered microstrip segment and with a tilt angle of (a) 0°, (b) 45°

Since the tapered matching element discussed above does not yield desirable increases in axial ratio bandwidth, believed to be due to radiation by the matching element, a logical next modification is to think of a matching section that is closer to the ground plane and its start point is at the side instead of the center of hemispherical helix. One way to implement this modification is to vary the height of the matching element nonlinearly rather than linearly. This way, a major part of the matching section will remain closer to the ground plane. Furthermore, instead of varying the width of matching section linearly, which leads to abrupt discontinuity or sharp angles at the point of connection to the helix, the width is varied such that connection to the radiating element occurs smoothly, as shown in Figures 4.23a and b. The width of this matching section is varied following a half-wave sinusoidal function. It is forced to be zero at the start point and 1 mm at the end point

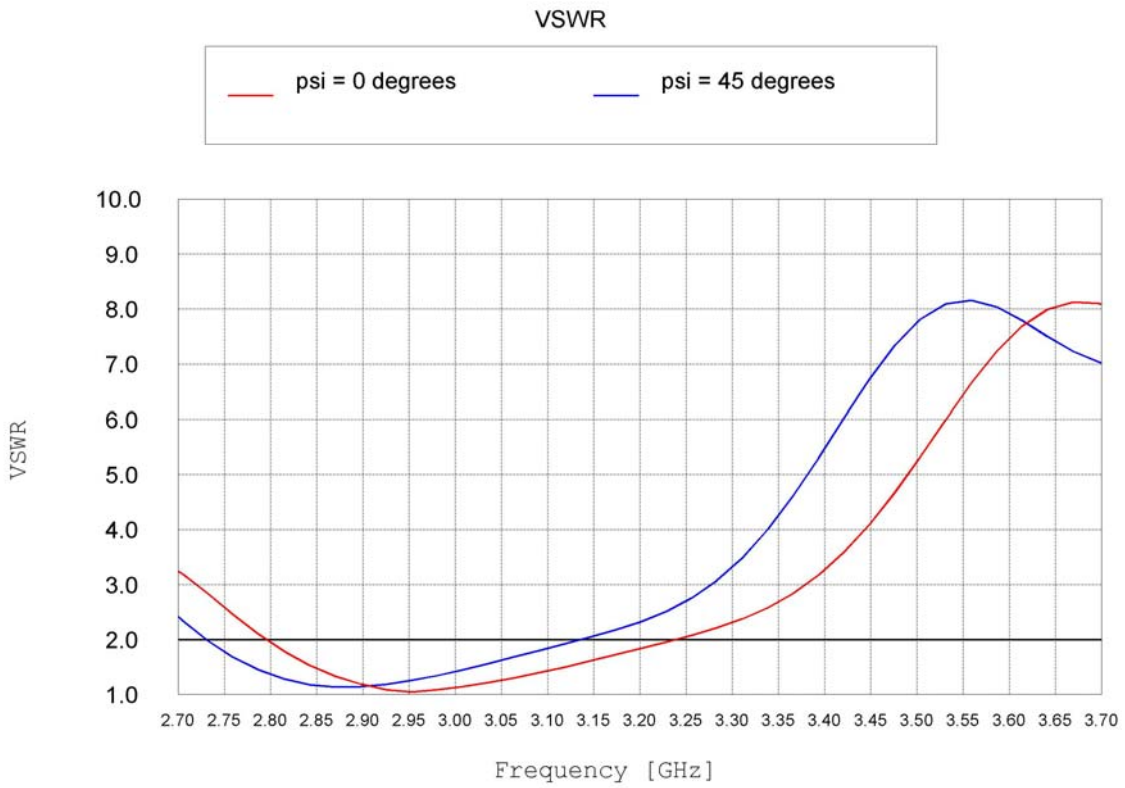

Figure 4.22: Variations of VSWR versus frequency for 4.5-turn non-conformal hemispherical helical antenna fed by a tapered microstrip segment and with a tilt angle of (a) 0°, (b) 45°

which is equal to the starting width of the tapered helical structure. Also, the median curve that divides the width of the matching section in half is forced to lie on the hemisphere surface near its base, as shown in Figure 4.23c. The height of the tapered matching section is 1 mm at the start point and 5 mm at the end point; see Figure 4.23b. Details of the functions that define the matching section are given in Appendix A.2.3.

The axial ratio and VSWR results for the 4.5-turn non-conformal hemispherical helix, side fed with a nonlinearly tapered matching element, are shown in Figure 4.24. From Figure 4.24a, the 3-dB axial ratio bandwidth is about 18% relative to the center frequency 3.26 GHz, while from Figure 4.24b a VSWR bandwidth of more than 46% relative to the center frequency 3.7 GHz is obtained. Thus, the overall bandwidth, over which AR<3 dB and VSWR<2 are maintained, is 18%. Over this bandwidth, the

directivity is 9±1 dB. Figure 4.25 illustrates radiation patterns, while Figure 4.26 shows variation of the directivity at $\theta = 0$ versus frequency. It is also interesting to examine the current distribution on the helix, which helps one to better understand the traveling-wave nature of the antenna and its very wide VSWR bandwidth. Figure 4.27 shows the magnitude of the current distribution on the helix. At the top of the helix the current magnitude is more than 40 dB below that at the start of the helix. Figure 4.28 shows the instantaneous current distribution in vector form at different times.

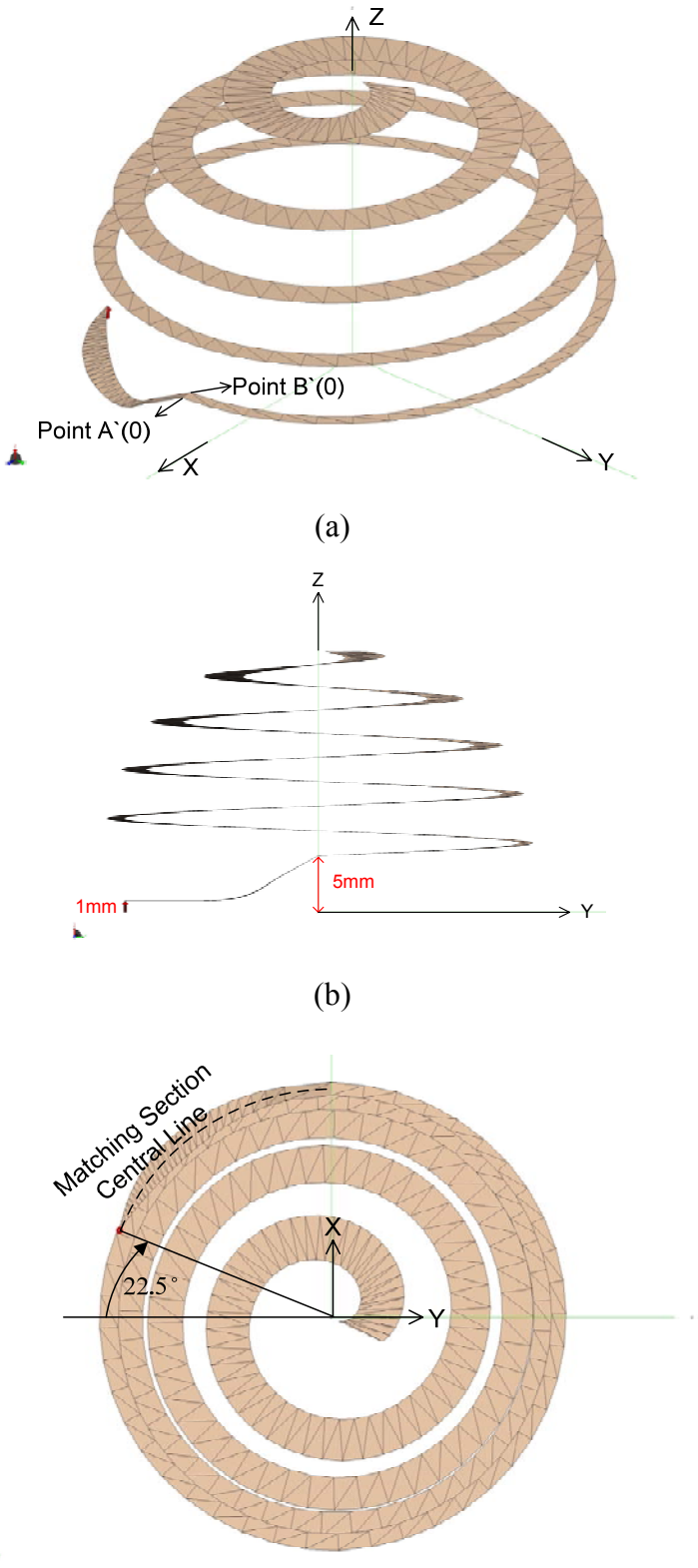

Figure 4.23: Geometry of 4.5-turn non-conformal hemispherical helix with tapered element and side-fed by a nonlinearly tapered matching element. (a) 3-D view, (b) front view, (c) bottom view

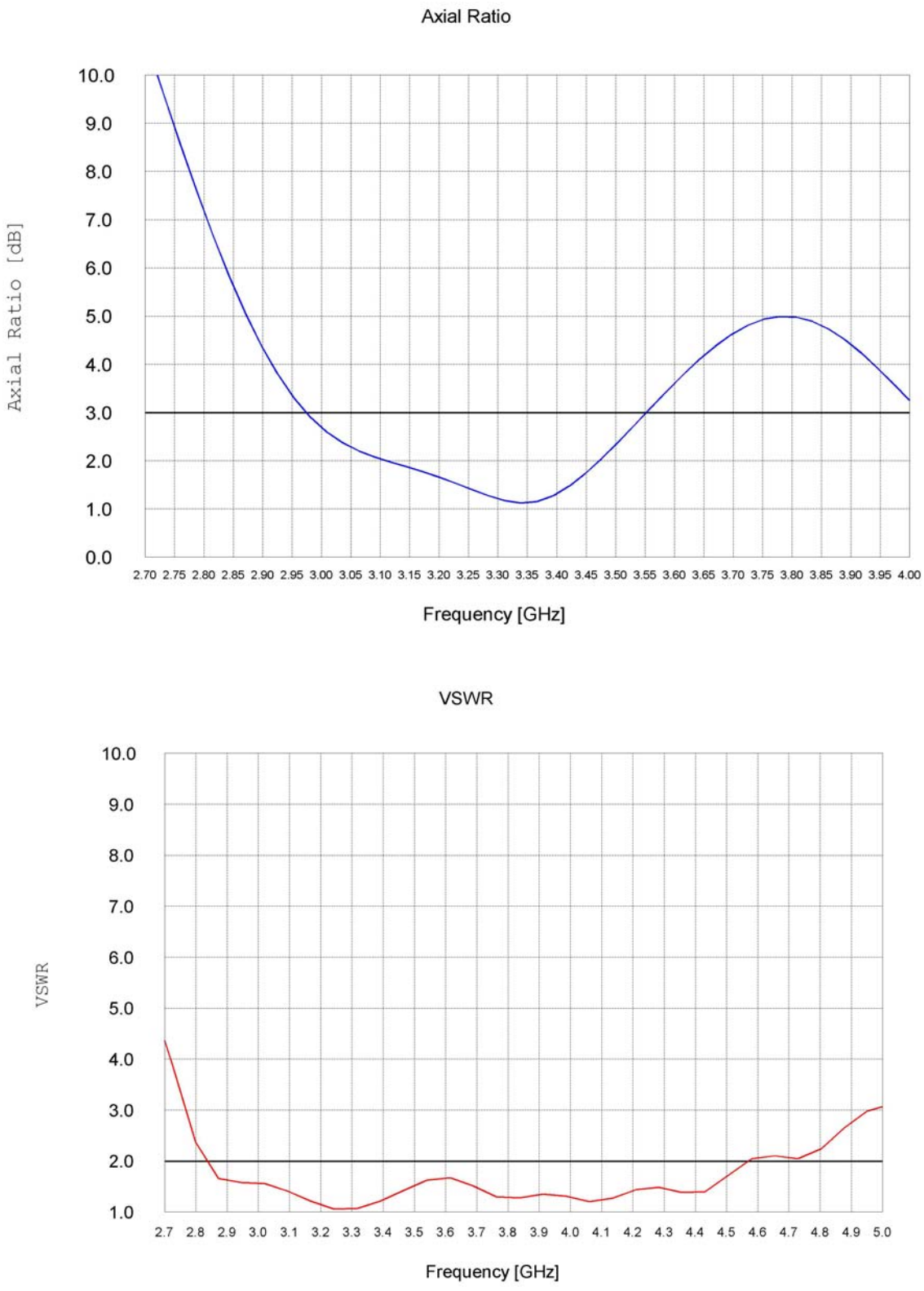

Figure 4.24: Variations of (a) axial ration and (b) VSWR versus frequency for the hemispherical helix of Fig. 4.23.

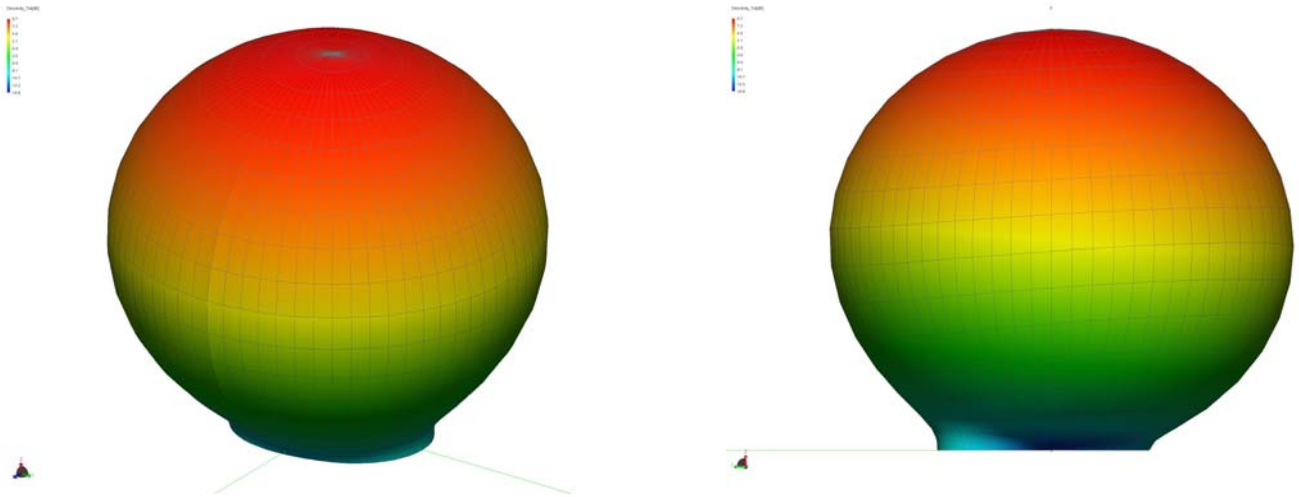

(a) (b)

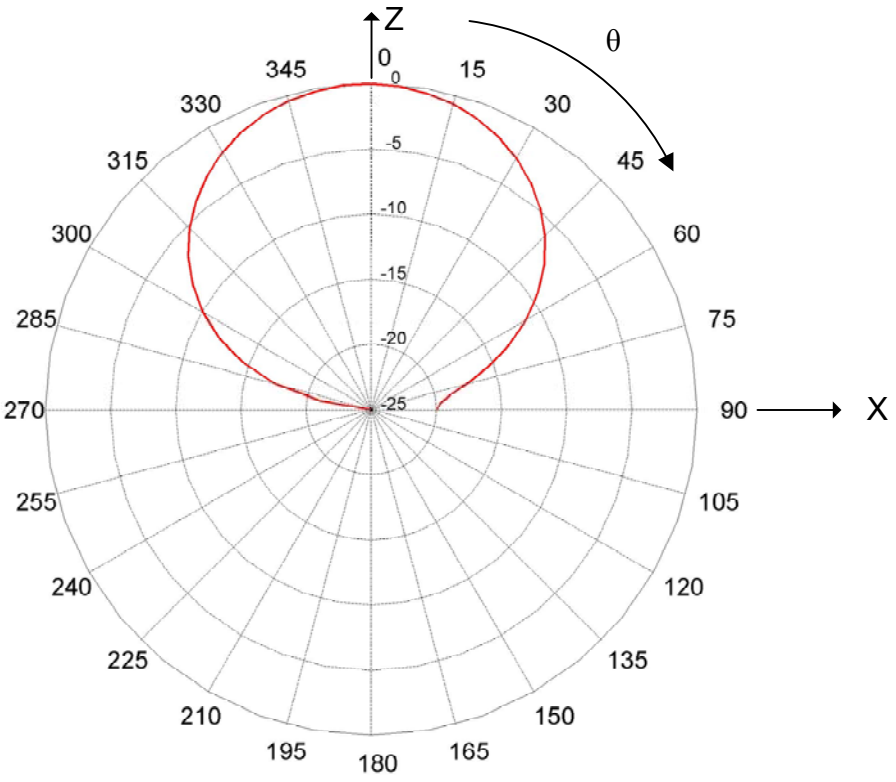

(c)

Figure 4.25: Radiation patterns at 3.256 GHz for the hemispherical helix of Fig. 4.23, (a) and (b) two different 3-D views, (c) normalized 2-D pattern in the xz-plane.

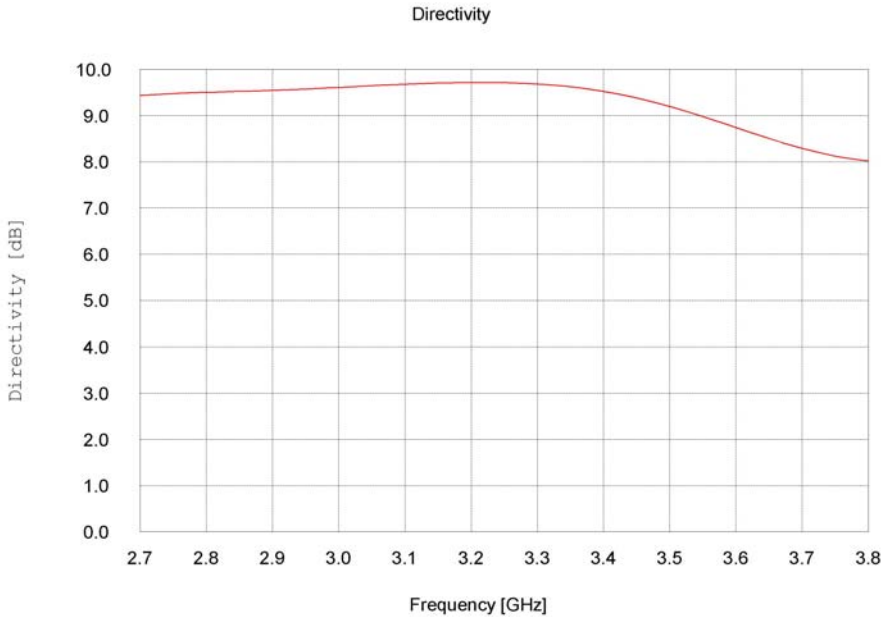

Figure 4.26: Variations of directivity versus frequency for the hemispherical helix of Fig. 4.23

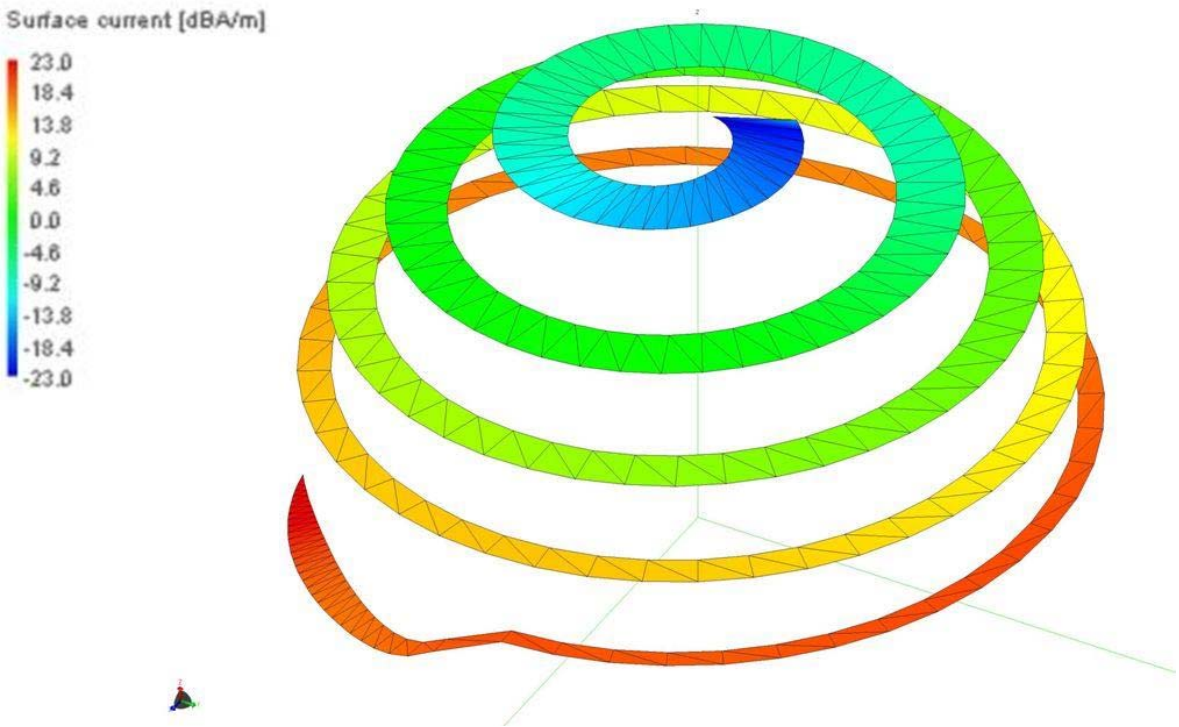

Figure 4.27: Spatial distribution of current magnitude on the radiating element of the hemispherical helix of Fig. 4.23 at 3.256 GHz

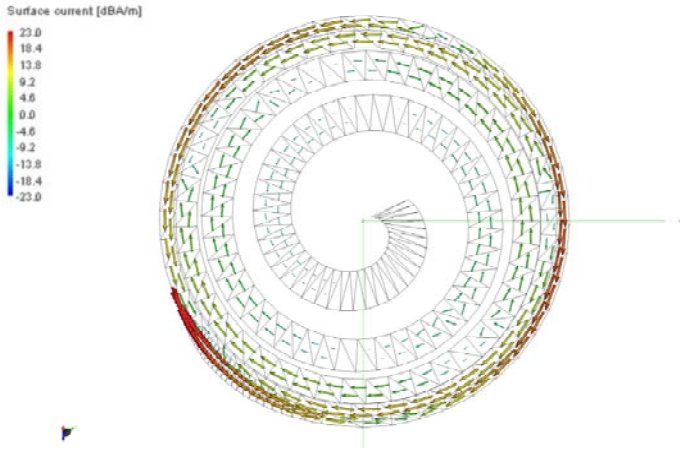

(a)

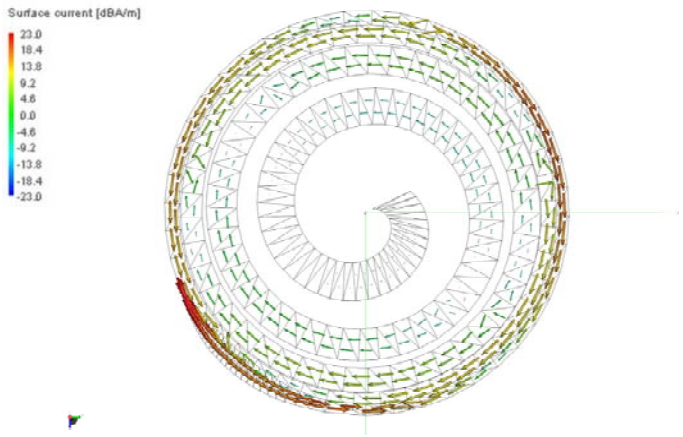

(b)

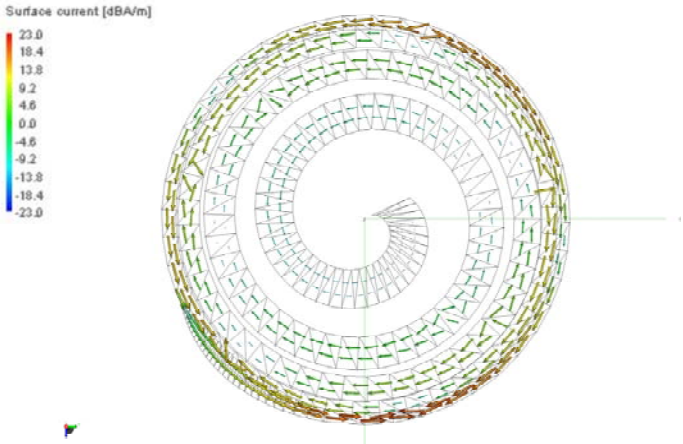

(c)

Figure 4.28: Instantaneous current distribution for the hemispherical helix of Fig. 4.23 at (a) $\omega t = 0$, (b) $\omega t = 45^{\circ}$, and (c) $\omega t = 90^{\circ}$

4.5.4 Simulation of Finite Ground Plane

So far, the ground plane has been assumed to be infinite in size. While this assumption is adequate for ground planes with characteristic dimensions on the order of one wavelength, it would be desirable to simulate the actual shape and size of the ground plane used. In the experimental part of this research, a 14" diameter circular steel pizza pan is used as ground plane. This finite ground plane is simulated as a perfectly conducting thin circular disk. The CAD tool, the graphical user interface, of the FEKO suite is used for providing continuously variable meshing. The variation of the size of the meshing triangles allows efficient use of memory and processing power. In areas where the current magnitude is expected to be weakest, for example near the edges of the ground plane, it is reasonable to increase the size of the meshing elements. On the other hand, in areas where stronger current magnitudes are expected, for example the antenna structure itself and areas on the ground plane close to it, fine meshing should be considered. It is also important to make sure that the feed wires are always located on the vertices of the meshing triangles. Figure 4.29 shows the view of a meshed antenna with a finite ground plane. The simulation of this geometry required a peak memory of about 900 MB and lasted around 9 hours on a workstation equipped with Intel Xeon processor with a clock speed of 3.60 GHz. Radiation characteristics at 50 frequencies in the range 2.65 GHz to 4.00 GHz were obtained.

Compared to the infinite ground plane, the directivity increased slightly and the radiation patterns above the ground plane remained essentially unchanged. The advantage of simulating a finite ground plane is in assessing radiation level in rear directions. A back-lobe, about 25 dB lower than the main beam, was noticed in the simulation results of the design with finite ground plane. Figure 4.30 shows the polar graph of the directivity for the design with finite ground plane, while Figure 4.31 shows variations of the directivity versus frequency of that design.

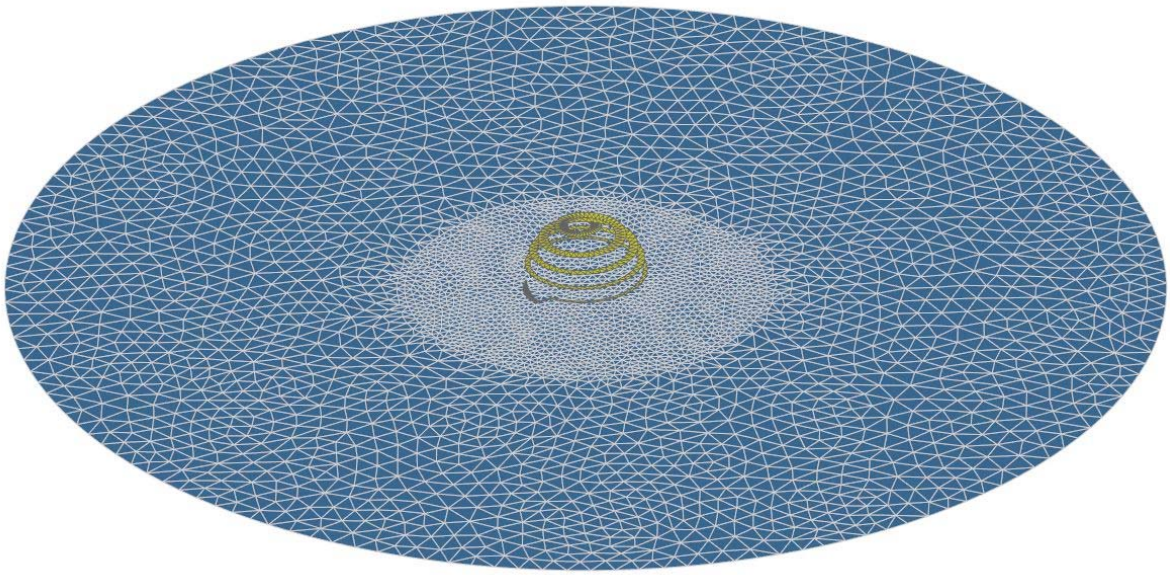

Figure 4.29: Meshed 4.5-turn non-conformal hemispherical helical antenna above a finite ground plane

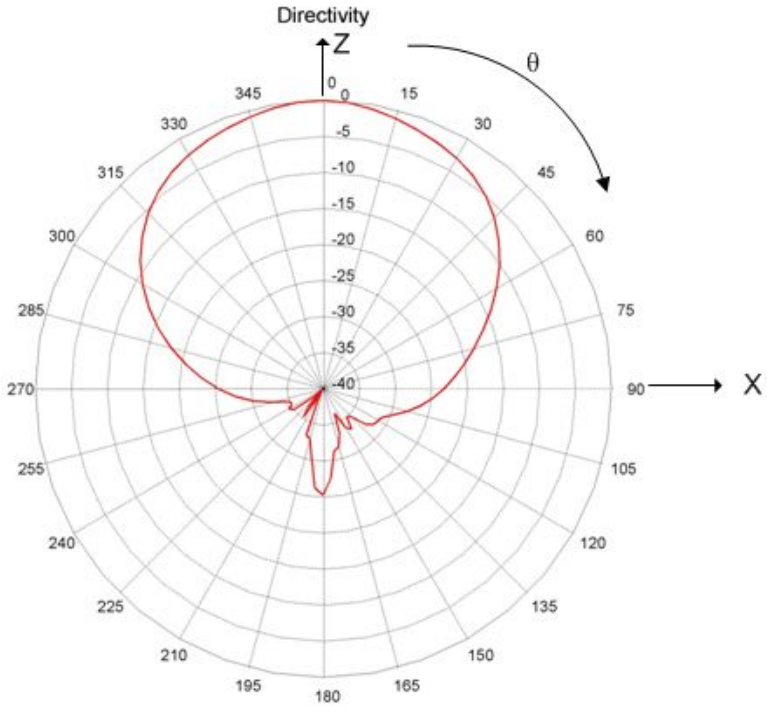

Figure 4.30: Normalized 2-D radiation pattern in the xz-plane on dB scale for the 4.5-turn non-conformal hemispherical helical antenna above a finite ground plane at 3.256 GHz.

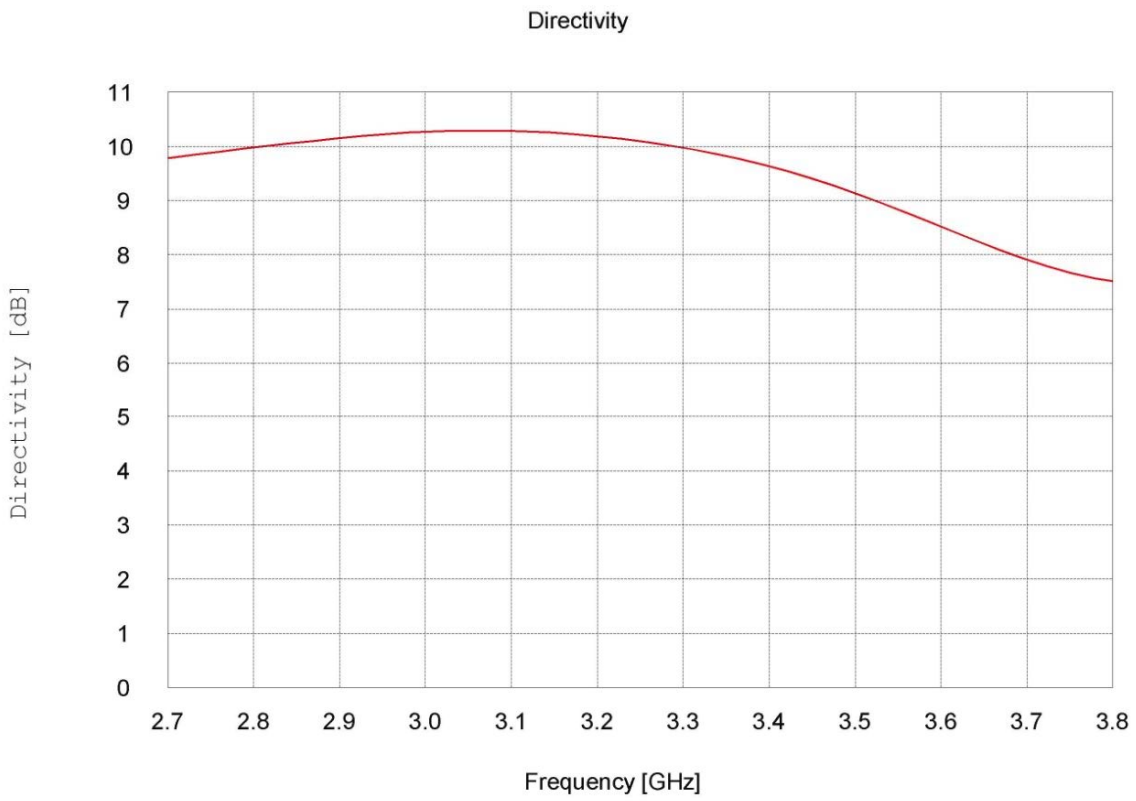

Figure 4.31: Variations of directivity versus frequency of the 4.5-turn non-conformal hemispherical helical antenna above a finite ground plane.

Chapter 5: Fabrication and Measurements of Non-Conformal Hemispherical Helical Antenna

Simulation results for various modifications to the basic wire hemispherical helix presented in Chapter 4 indicate that a hemispherical helical antenna with a tapered radiating element of zero tilt angle and side fed by a nonlinearly tapered matching section is the best design. This design provides the largest overall bandwidth. A prototype of this design is fabricated and measured. Measurement results for far-field patterns, axial ratio, VSWR, and directivity are presented and compared with the corresponding simulation results in this chapter.

5.1 Antenna Fabrication

Since the metallic strip used as the radiating element is very thin, a support structure, on which the helix will be mounted, is required in the construction of the prototype antenna. Balsa wood is chosen for this purpose because it is light weight and can be shaped easily. The dielectric properties of Balsa wood do not have considerable effect on the antenna radiation characteristics. It has a relative permittivity of 1.2 [34], and has also been used by others for the same purpose [13].

5.1.1 Construction of Support Structure

The support structure consists of two half disks made of 1/4" thick Balsa wood. The radius of each disk is chosen to be about 2 mm more than the radius of the hemisphere, so that all of the helical structure can be embedded firmly into the support structure. The 3D drawing of the two half disks together with the helical structure is obtained using AUTOCAD, in order to determine the intersection points of the helical structure and half disks as shown in Figure 5.1. The sides of each half disk are printed to scale on a paper with adhesive on one side and attached to a piece of Balsa wood. Then, the desired shape is cut out of the wood. Figure 5.2 shows the sides of each disk, not to scale. Balsa wood is very soft to cut through but should be handled delicately. A razor and a small fine filer

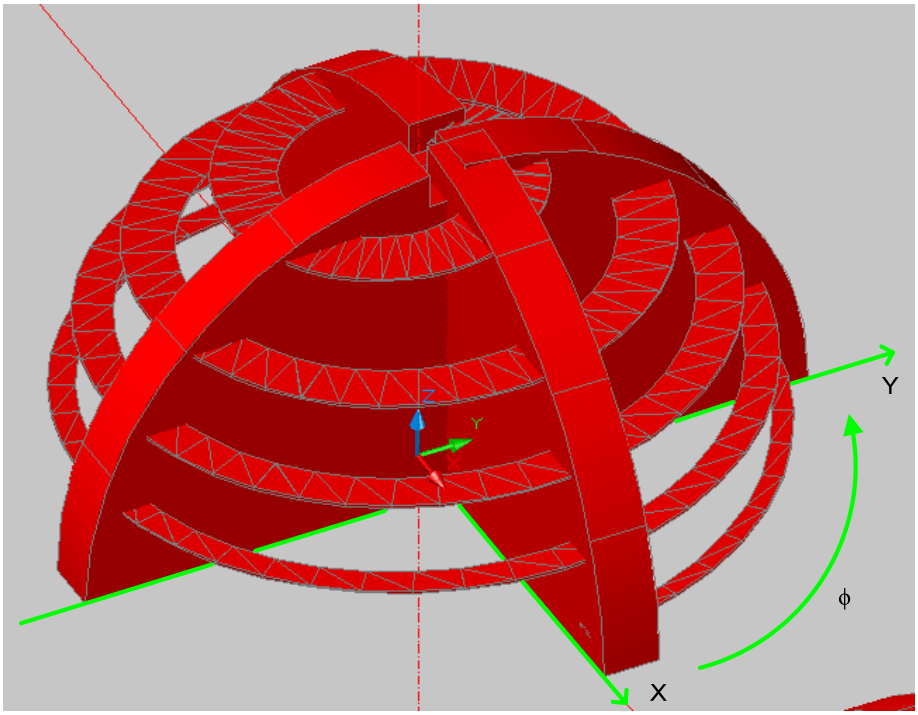

Figure 5.1: Support structure for a 4.5-turn non-conformal hemispherical helical antenna

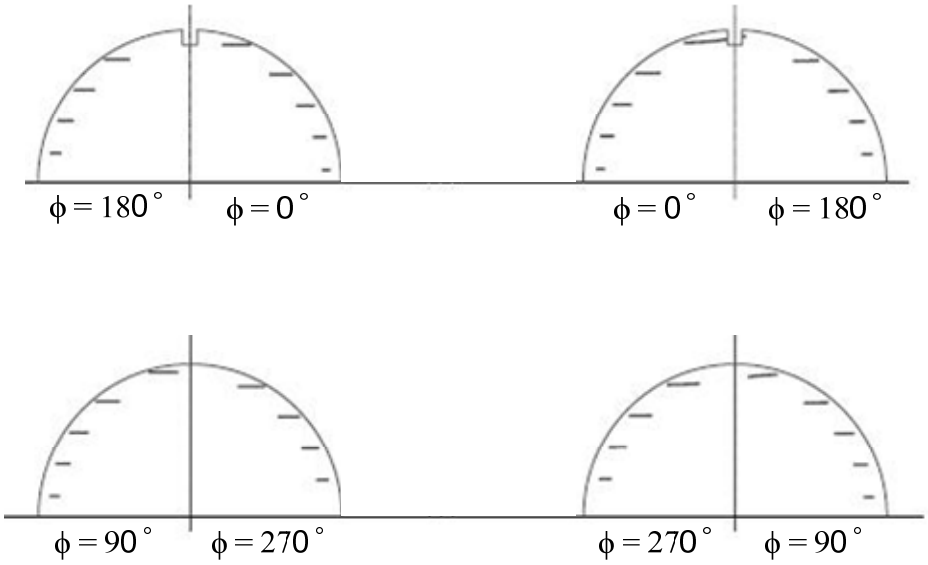

Figure 5.2: Intersections of strip helix and support structure. Narrow slots are carved at these intersections to embed the helix

are used to cut the wood and shape the round edges. Also, as shown in Figure 5.2, narrow slots are carved out at the intersection lines of half disks and the support structure. The radiating strip is inserted into these slots to be held in place firmly.

A support structure for the feed element is also desirable in order to maintain the shape of its nonlinear taper accurately. To construct this part, a base is drawn in 3D by AUTOCAD as shown in Figure 5.3. The support base fills the space beneath the matching/feed section. The 2D projections of the base are printed to scale on the same kind of paper used in the construction of half disks. Then, the base is cut out of Balsa wood and one side of it is shaped so that it coincides with the matching element surface.

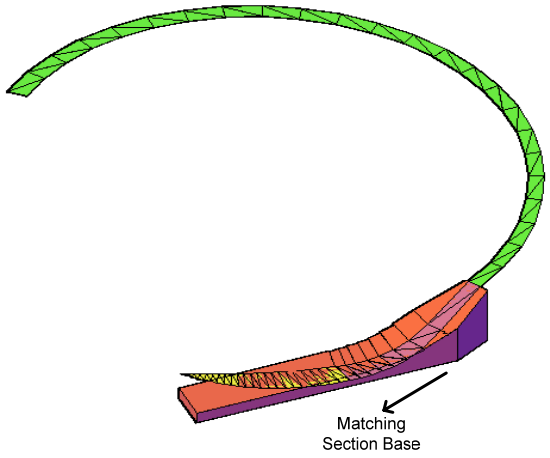

Figure 5.3: Support base for matching section, not to scale

5.1.2 Construction of Helical Metallic Strip and Matching Section

A 0.05" thick copper sheet is used to construct the helical radiating element. This metal has sufficient rigidity and yet can be cut by hand with regular scissors. Since cutting the entire helix out of the copper sheet manually is a very difficult task, the helix is divided into four parts, as shown in Figure 5.4, and each part is made separately. Then, the four segments are soldered to one another and mounted on the support structure. Cutting the individual segments out of the copper sheet should be handled with extreme care since the minimum width of the strip is as small as1mm. To facilitate the accurate construction of helical segments, each segment is first collapsed onto the xy-plane

(ground plane) to form a 2D structure. The coordinates of points on the collapsed structure are calculated from the actual coordinates of points on the 3D helix by means of a MATLAB code developed for this purpose. The 2D images of the four parts with collapsed geometries are printed to scale on a paper with adhesive on one side and attached to the copper sheet. Then, the helical parts are carefully cut out of the copper sheet by hand.

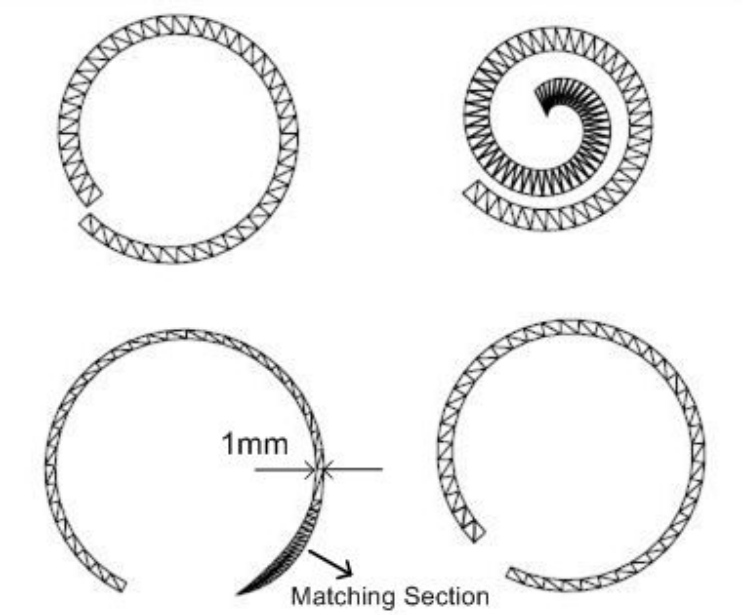

Figure 5.4: Individual helix segments in collapsed form for a 4.5-turn hemispherical helical antenna

The assembly of helical strip on support structure and the matching element is mounted on a circular metallic disk (actually a pizza pan) of 14"diameter which serves as ground plane. This size for a ground plane is a good approximation for an infinite ground plane as its diameter is more than 7 times larger than wavelength at a center band frequency of 3.26GHz. Finally, a 50 Ω SMA coaxial connector is attached to the ground plane at the start point of the matching element. The inner and outer conductors of the SMA connecter are soldered to the matching element and ground plane, respectively. Several views of the completed prototype are shown in Figure 5.5. The intended

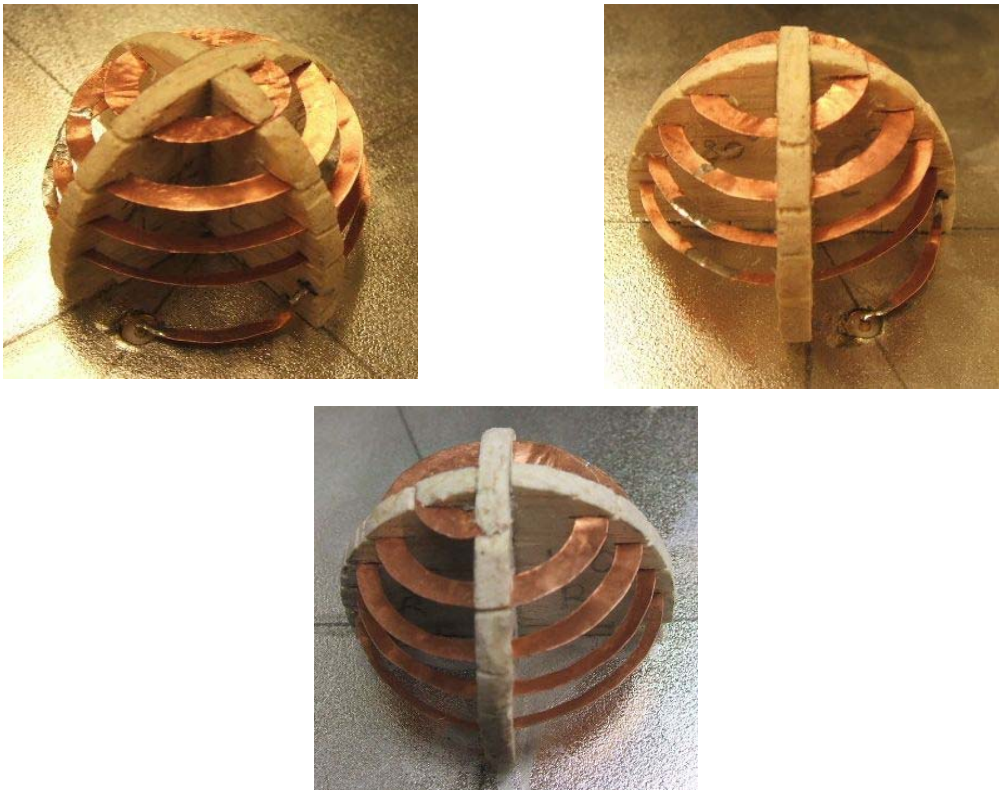

Figure 5.5: Different views of a constructed 4.5-turn non-conformal hemispherical helical antenna with tapered radiating element

dimensions for the fabricated antenna were: a=20 mm (radius of the hemisphere), $w_1 = 1$ mm (width of the radiating element at the starting point), $w_2 = 3$ mm (width of the radiating element at the end point), z_1 =1 mm (distance of the starting point of the matching element from ground plane), and z_2 =5 mm (distance of the end point of the matching element from ground plane). Of course, the actual dimensions of the constructed antenna differ slightly (estimated to be $\leq 5\%$) from the intended sizes. The only dimension that ended up being more than 5% different from the intended size is w_2 which is 4 mm instead of 3 mm.

5.2 Measurements of Fabricated Antenna

5.2.1 VSWR Measurement

VSWR measurements were performed using a HP 8510 network analyzer. Figure 5.6 shows the measured VSWR and compares it with the corresponding simulated results. Examination of these results indicates that measured and calculated VSWRs are in reasonably good agreement. The bandwidth over which the VSWR of the fabricated antenna remains below 2 is about 50% with a center frequency of 3.975GHz. Of course, the overall bandwidth, as will be seen below, is limited by the axial ratio bandwidth and is much less than 50%.

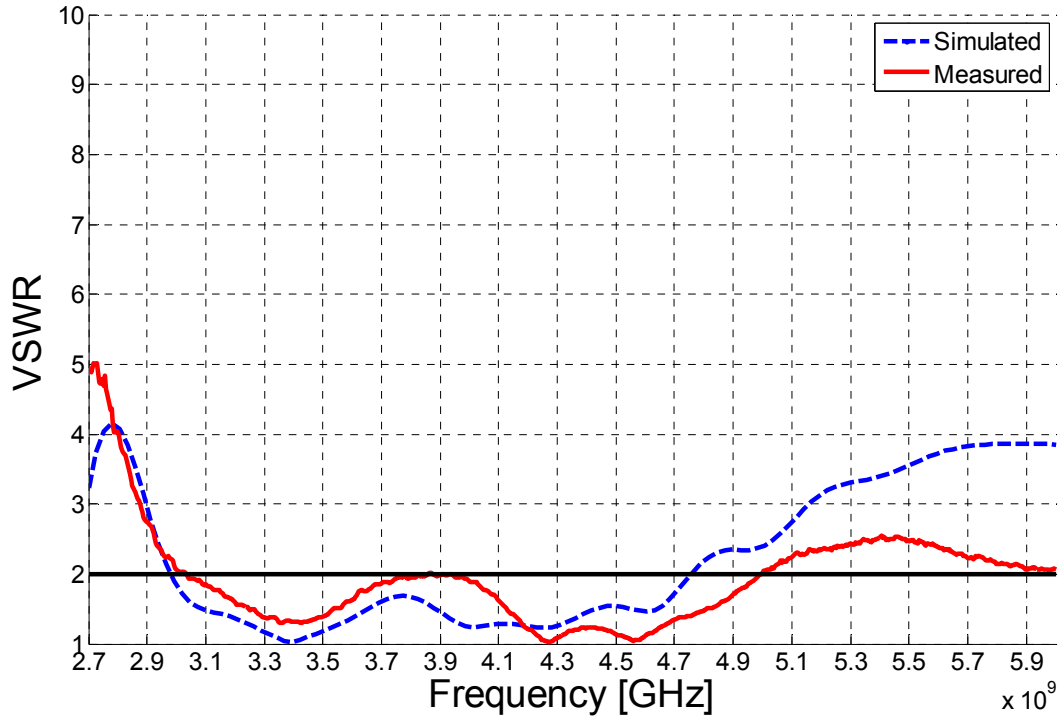

Figure 5.6: Comparison of measured and simulated VSWRs for the fabricated antenna

5.2.2 Pattern and Axial Ratio Measurements

Far-field pattern measurements were carried out using the indoor antenna range facility of VTAG (Virginia Tech Antenna Group). Figure 5.7 illustrates the setup for pattern measurements.

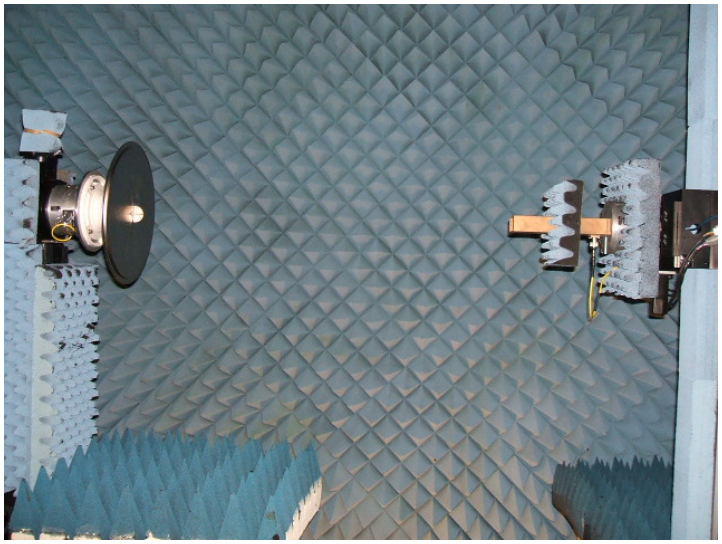

Figure 5.7: Pattern measurement setup with the fabricated hemispherical helical antenna seen on the left side

Figures 5.8 and 5.9 show the measured polar plots of far-field radiation pattern and axial ratio at a frequency of 3.25 GHz, respectively. Co-polarization measurements were taken for a right hand circularly polarized wave. Comparison of Figures 4.30 and 5.8 indicates that simulated and measured far-field patterns are in very good agreement. The half-power beamwidth obtained from either pattern is about 70 degrees. Measured patterns at several other frequencies are given in Appendix C.

Figures 5.10 and 5.11 shows the measured axial ratio and directivity (in the $\theta = 0^{\circ}$ direction) versus frequency, respectively. For comparison, the corresponding simulated results are also provided on the same figures. From Figure 5.10, the measured 3-dB axial ratio bandwidth is determined to be about 24% with a center frequency of 3.35 GHz. This bandwidth is somewhat larger than the theoretical axial ratio bandwidth which is about 20%. Clearly, the measured axial ratio bandwidth falls within the measured VSWR bandwidth, thus the overall measured bandwidth of the antenna is 24%. Also, it is noted that the simulated data are shifted to the right by approximately 130MHz compared to the measured data. This shift is attributed to the difference between the intended and actual dimensions of the fabricated hemispherical helix. Examination of results in Figure 5.11

indicates excellent agreement between the measured and calculated directivities. It is further noted from this figure that the 3-dB directivity bandwidth is more than 50%.

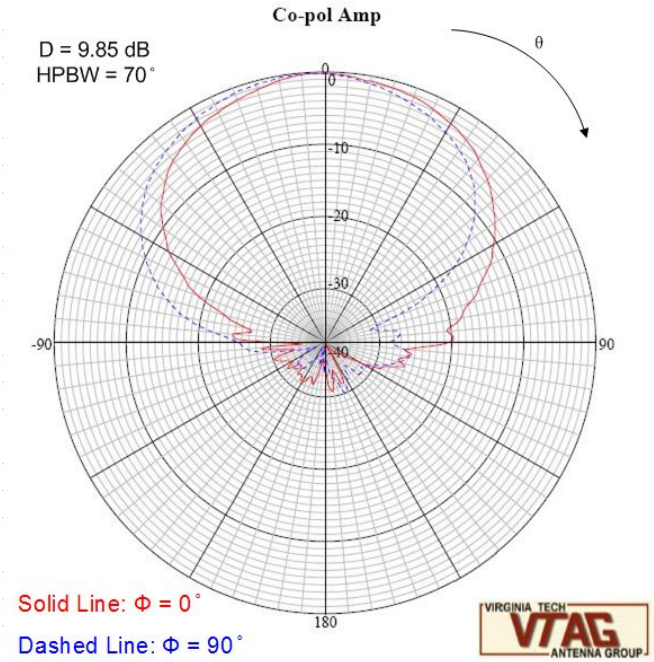

Figure 5.8: Measured far-field radiation pattern for the fabricated antenna at *f*=3.25 GHz

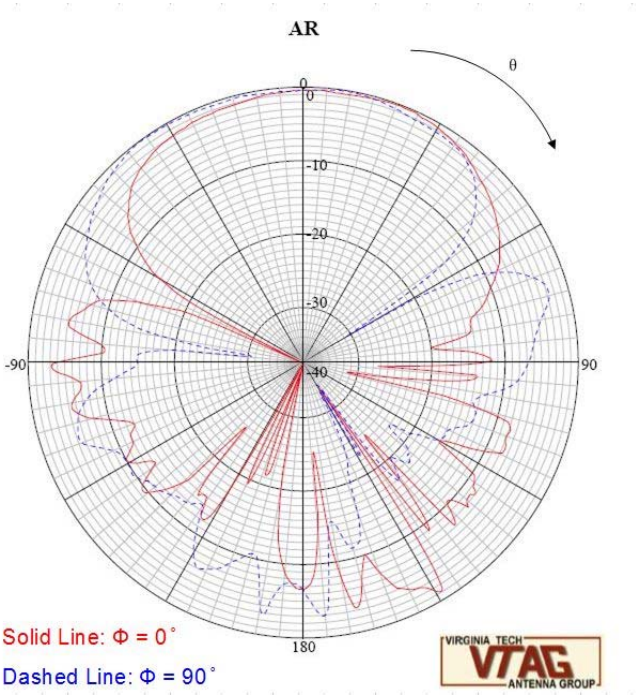

Figure 5.9: Measured axial ratio pattern for the fabricated antenna at *f*=3.25 GHz

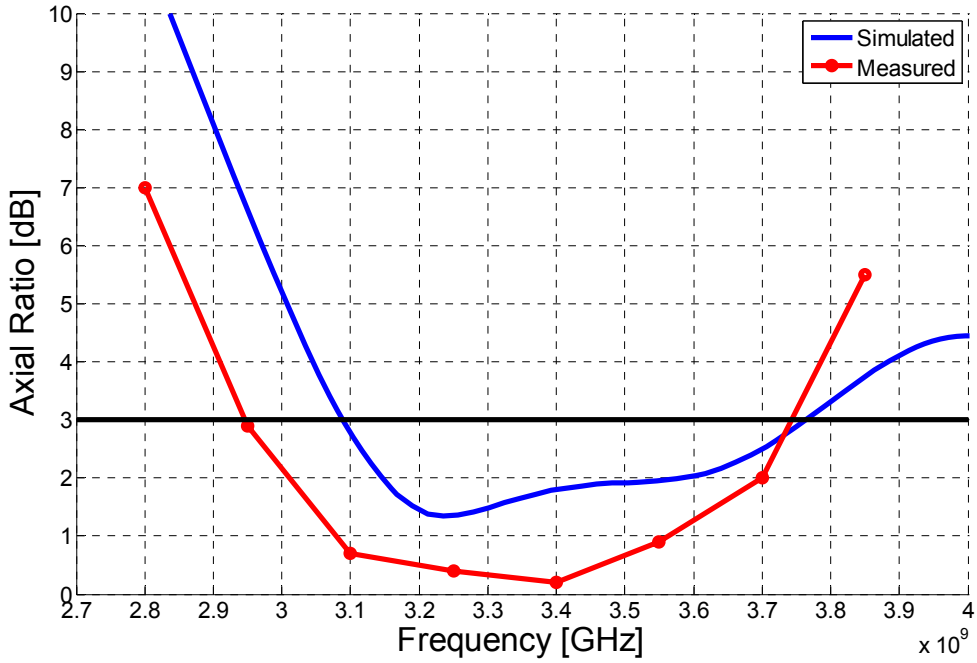

Figure 5.10: Comparison of measured and simulated axial ratios for the fabricated antenna

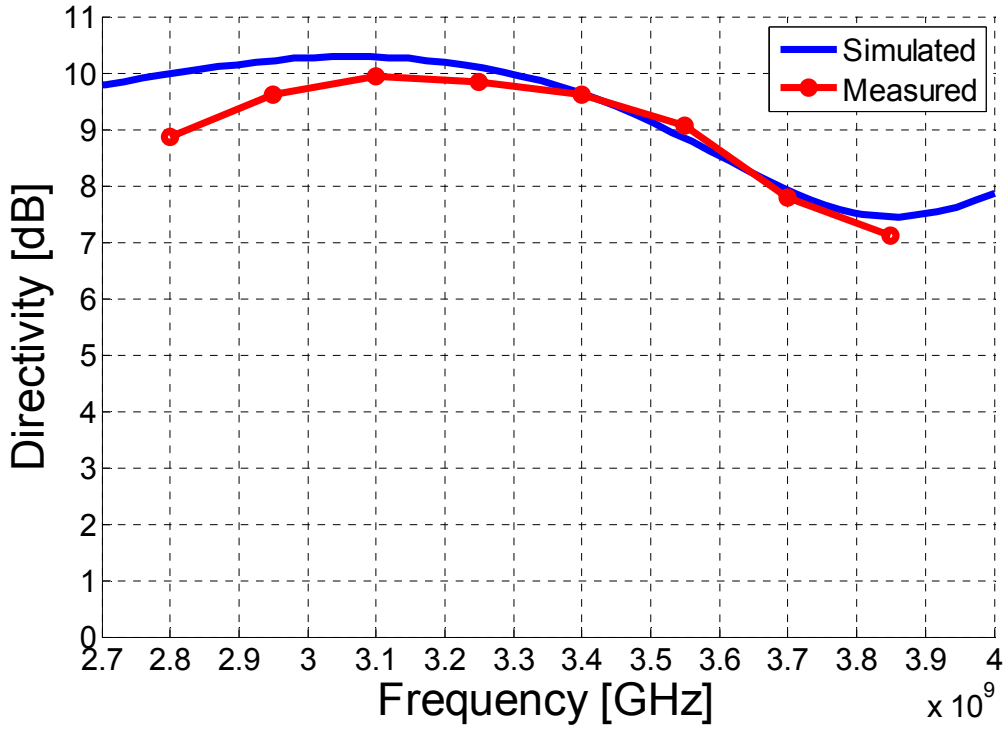

Figure 5.11: Comparison of measured and simulated directivities for the fabricated antenna

Chapter 6: Conclusions and Suggestions for Future Work

Several modifications to the wire hemispherical helical antenna have been introduced and studied in detail. The objectives of these modifications have been to maximize the bandwidth over which circular polarization is maintained and the input impedance is closely matched to 50 Ω, while fluctuations in directivity and half-power beamwidth are kept small. Modifications were applied to both the radiating element and the feed segment of the hemispherical helix. A summary of these modifications and their impacts on radiation characteristics is presented below. The main contributions of this research are pointed out and suggestions for further investigations are offered.

6.1 Summary of Results and Contributions

6.1.1 Modification of Radiating Element

Two new modifications on the radiating element of hemispherical helix were introduced, including the replacement of helical wire with (i) tapered metallic strip conformal to the surface of hemisphere and (ii) non-conformal metallic strip with constant or varying width (tapered). Hemispherical helices with such radiating elements were analyzed numerically and their far-field pattern, directivity, axial ratio, and input impedance (or VSWR relative to 50 Ω) were calculated and compared with those of a wire hemispherical helix of the same radius. These comparisons revealed that the axial ratio is the only characteristic whose bandwidth is increased significantly. The impacts of these modifications on radiation pattern and directivity are small and essentially no improvement on the VSWR bandwidth is achieved. Furthermore, the non-conformal tapered radiating element with zero degree tilt angle yields the largest increase in axial ratio bandwidth, while the conformal radiating element increases this bandwidth only moderately.

6.1.2 Modification of Feed Element

Two new feed elements that match the hemispherical helix to $50\,\Omega$ over a broad frequency range were introduced. These include: (i) a linearly and doubly tapered microstrip connecting the radiating element to the center of helix (center fed), and (ii) a nonlinearly tapered microstrip connecting the radiating element to a point on the ground plane while its median curve coincides on the hemispherical surface (side fed). Conformal and non-conformal hemispherical helices with such feed elements were analyzed numerically and their radiation characteristics were calculated and compared with those of a hemispherical helix of the same radius and fed by a short vertical wire on the side. These comparisons revealed that the input impedance (or VSWR) is the only characteristic whose bandwidth is increased significantly. The impacts of these feed elements on radiation pattern and directivity are negligible and little or no improvement on the axial ratio bandwidth is achieved. Furthermore, side-fed helices with nonlinearly tapered feed elements provide significantly larger VSWR bandwidths than center-fed helices with linearly tapered feed elements.

6.1.3 Optimum Design

Combining the most effective modifications on radiating element and feed, an optimum design is obtained which provides the largest overall bandwidth. This design is a hemispherical helical antenna with a tapered radiating element of zero tilt angle and side fed by a nonlinearly tapered matching segment. Simulation, fabrication, and measurement of a 4.5-turn optimally designed hemispherical helix were carried out. Predicted bandwidths for this optimum design are: 20% for axial ratio, 46% for VSWR, and 36% for directivity. Thus, the overall theoretical bandwidth is 20%. Also, over the latter bandwidth a directivity of 9 ± 1 dB and a half-power beamwidth of more than 70 degrees are provided. A prototype of the optimum design was fabricated and measured. The measured bandwidths are: 24% for axial ratio and 50% for VSWR, thus the overall bandwidth is 24%. Over this bandwidth a directivity of 9 ± 1 dB and a half-power beamwidth of more than 70 degrees are maintained. It is noted that reasonably good agreement exists between theoretical and experimental result.

In summary, novel hemispherical helical antennas have been proposed and evaluated both theoretically and experimentally. These antennas provide significantly larger overall bandwidth than the basic wire hemispherical helix. Over a nearly 20% bandwidth, axial ratio <3 dB, VSWR<2, directivity=9 ± 1 dB, and HPBW$\approx 70^{\circ}$ are achieved.

6.2 Suggestions for Future Work

Nonuniform tapering of radiating element:

The radiating elements examined in this work have either a constant width or are tapered in such a manner that their widths increase linearly. Nonuniform tapering might results in interesting features with potentially useful applications.

Hemispherical helices with variable spacing between turns:

Nearly all investigations on hemispherical helical antennas have been limited to geometries with constant spacing between turns. Variable spacing between turns will undoubtedly impact the radiation characteristics, but the question is how much and in what manner. Further investigation of hemispherical helices with variable spacing is worth pursuing.

Arrays of Hemispherical Helices:

Arrays of hemispherical helices for the purpose increasing the gain, coverage area, etc. might find useful applications in wireless communication systems and avionics. With radiation properties of single unit hemispherical helix understood quite well, extending the research to arrays of these helices is the next logical step.

References

[1] J. D. Kraus and R. J. Marhefka, *Antennas*, Third ed., McGraw-Hill, 2002

[2] J. C. Cardoso, "The Spherical Helical Antenna," Master of Science Thesis, Bradley Department of Electrical and Computer Engineering, Virginia Polytechnic Institute and State University, 1992

[3] E. Weeratumanoon, "Helical Antennas with Truncated Spherical Geometry," Master of Science Thesis, Bradley Department of Electrical and Computer Engineering, Virginia Polytechnic Institute and State University, 2000

[4] J. R. Clark, "Multifilar Hemispherical Helical Antennas," Master of Science Thesis, Bradley Department of Electrical and Computer Engineering, Virginia Polytechnic Institute and State University, 2003

[5] W. L. Stutzman and G. Z. Thiele, *Antenna Theory and Design*, Second Edition ed., John Wiley and Sons, Inc., 1998

[6] C. A. Balanis, *Antenna Theory*, Second ed., John Wiley and Sons, Inc., 1997

[7] "IEEE Standard for Ultrawideband Radar Definitions," *IEEE Std 1672-2006,* pp. c1-9, 2007.

[8] J. Kraus, "A 50-ohm input impedance for helical beam antennas," *Antennas and Propagation, IEEE Transactions on [legacy, pre - 1988],* vol. 25, pp. 913-913, 1977.

[9] H. Nakano, Y. Okabe, H. Mimaki, and J. Yamauchi, "A monofilar spiral antenna excited through a helical wire," *Antennas and Propagation, IEEE Transactions on,* vol. 51, pp. 661-664, 2003.

[10] J. C. Louvigne and A. Sharaiha, "Broadband tapered printed quadrifilar helical antenna," *Electronics Letters,* vol. 37, pp. 932-933, 2001.

[11] H. Nakano, *Helical and Spiral Antennas*, Research Studies Press Ltd., 1987

[12] J. Wong and H. King, "Broadband quasi-taper helical antennas," *Antennas and Propagation, IEEE Transactions on [legacy, pre - 1988],* vol. 27, pp. 72-78, 1979.

[13] R. L. Lovestead, "Helical Antenna Optimization Using Genetic Algorithms," Master of Science Thesis, Bradley Department of Electrical and Computer Engineering, Virginia Polytechnic Institute and State University, 1999

[14] V. G. Kononov and C. A. Balanis, "Exponentially tapered helical antennas," in *Antennas and Propagation International Symposium, 2007 IEEE*, 2007, pp. 2985-2988.

[15] I. Ghoreishian, "The Spiro-Helical Antenna," Master Of Science, Electrical and Computer Engineering, Virginia Polytechnic Institute and State University, 1999

[16] R. M. Barts and W. L. Stutzman, "A reduced size helical antenna," in *Antennas and Propagation Society International Symposium, 1997. IEEE., 1997 Digest*, 1997, pp. 1588-1591 vol.3.

[17] J. C. Cardoso and A. Safaai-Jazi, "Spherical helical antenna with circular polarisation over a broad beam," *Electronics Letters,* vol. 29, pp. 325-326, 1993.

[18] A. Safaai-Jazi and J. C. Cardoso, "Radiation characteristics of a spherical helical antenna," *Microwaves, Antennas and Propagation, IEE Proceedings -,* vol. 143, pp. 7-12, 1996.

[19] H. T. Hui, K. Y. Chan, and E. K. N. Yung, "The input impedance and the antenna gain of the spherical helical antenna," *Antennas and Propagation, IEEE Transactions on,* vol. 49, pp. 1235-1237, 2001.

[20] E. Weeratumanoon and A. Safaai-Jazi, "Truncated spherical helical antennas," *Electronics Letters,* vol. 36, pp. 607-609, 2000.

[21] A. Safaai-Jazi and E. Weeratumanoon, "Hemispherical Helical Antenna," in *IEEE International Symposium on Antennas and Propagation and USNC/URSI National Radio Science Meeting* Orlando, Florida: URSI Digest, July 1999, p. 325.

[22] H. T. Hui, K. Y. Chen, E. K. N. Yung, and X. Q. Shing, "Coaxial-feed axial mode hemispherical helical antenna," *Electronics Letters,* vol. 35, pp. 1982-1983, 1999.

[23] K. Y. Chan, H. T. Hui, and E. K. N. Yung, "Central-fed hemispherical helical antenna," in *Antennas and Propagation Society International Symposium, 2001. IEEE*, 2001, pp. 545-548 vol.4.

[24] H. T. Hui, K. Y. Chan, and E. K. N. Yung, "The low-profile hemispherical helical antenna with circular polarization radiation over a wide angular range," *Antennas and Propagation, IEEE Transactions on,* vol. 51, pp. 1415-1418, 2003.

[25] C. H. Chen, B. J. Hu, Z. H. Wu, and E. K. N. Yung, "A Self-matching Hemispherical Helical Antenna," in *Antennas and Propagation Society International Symposium 2006, IEEE*, 2006, pp. 4709-4712.

[26] D. X. Wang, E. K. N. Yung, and R. S. Chen, "Theoretical study of hemispherical helical antenna loaded with dielectric resonator," in *Antennas and Propagation Society International Symposium, 2005 IEEE*, 2005, pp. 499-502 vol. 2B.

[27] S. R. Best, "The performance properties of an electrically small folded spherical helix antenna," in *Antennas and Propagation Society International Symposium, 2002. IEEE*, 2002, pp. 18-21 vol.4.

[28] J. Clark and A. Safaai-Jazi, "Multifilar hemispherical helical antennas," in *Antennas and Propagation Society International Symposium, 2004. IEEE*, 2004, pp. 3333-3336 Vol.3.

[29] "FEKO User's Manual Suite 5.3," July 2007.

[30] W. L. Stutzman, *Polarization in electromagnetic systems* Artech House, 1993

[31] Z. Yingbo and H. T. Hui, "A printed hemispherical helical antenna for GPS receivers," *Microwave and Wireless Components Letters, IEEE,* vol. 15, pp. 10-12, 2005.

[32] D. M. Pozar, *Microwave Engineering*, 3rd ed., John Wiley & Sons Inc., 2005

[33] H. Nakano, S. Okuzawa, K. Ohishi, H. Mimaki, and J. Yamauchi, "A curl antenna," *Antennas and Propagation, IEEE Transactions on,* vol. 41, pp. 1570-1575, 1993.

[34] C. Jung-Hwan, M. Jung-Ick, and P. Seong-Ook, "Measurement of the modulated scattering microwave fields using dual-phase lock-in amplifier," *Antennas and Wireless Propagation Letters, IEEE,* vol. 3, pp. 340-343, 2004.

Appendix A: Input codes to EDITFEKO and MATLAB

A.1: Conformal hemispherical helical antenna geometry

A.1.1: 4.5-turn conformal hemispherical helical antenna with a strip of constant width and a vertical short wire feed

```
**setting the overall unit
SF   1                    1e-3
#a=20 ** Spherical radius
#n=9 **no. of turns of a full sphere
#w= 2 ** strip width
#thetap=(#w/2)/#a **theta prime
#plates=200 **number of strip segments
#dz=#a/#plates ** divisions on the z-axis
** Segment Dimensions
IP                        .2       9        2
** Defining the geometry
#z[0]=0
#theta[0]=ARCCOS(#z[0]/#a)
#x[0]=#a
#y[0]=0
#zp[0]=#a*COS(#theta[0]-#thetap)
#xp[0]=#a*SIN(ARCCOS(#zp[0]/#a))*COS(#n*#pi*#z[0]/#a)
#yp[0]=#a*SIN(ARCCOS(#zp[0]/#a))*SIN(#n*#pi*#z[0]/#a)
#zpp[0]=#a*COS(#theta[0]+#thetap)
#xpp[0]=#a*SIN(ARCCOS(#zpp[0]/#a))*COS(#n*#pi*#z[0]/#a)
#ypp[0]=#a*SIN(ARCCOS(#zpp[0]/#a))*SIN(#n*#pi*#z[0]/#a)
**Defining the intial points
#Ax[0]=#xp[0]
#Ay[0]=#yp[0]
#Az[0]=#zp[0]
#Bx[0]=#xpp[0]
#By[0]=#ypp[0]
#Bz[0]=#zpp[0]
!!for #i = 1 to #plates step 1
#z[#i]=(#i)*#dz
#x[#i]=#a*SIN(ARCCOS(#z[#i]/#a))*COS(#n*#pi*#z[#i]/#a)
#y[#i]=#a*SIN(ARCCOS(#z[#i]/#a))*SIN(#n*#pi*#z[#i]/#a)
#zp[#i]=#a*COS(ARCCOS(#z[#i]/#a)-#thetap)
#xp[#i]=#a*SIN(ARCCOS(#zp[#i]/#a))*COS(#n*#pi*#z[#i]/#a)
#yp[#i]=#a*SIN(ARCCOS(#zp[#i]/#a))*SIN(#n*#pi*#z[#i]/#a)
#zpp[#i]=#a*COS(ARCCOS(#z[#i]/#a)+#thetap)
#xpp[#i]=#a*SIN(ARCCOS(#zpp[#i]/#a))*COS(#n*#pi*#z[#i]/#a)
#ypp[#i]=#a*SIN(ARCCOS(#zpp[#i]/#a))*SIN(#n*#pi*#z[#i]/#a)
#Ax[#i]=#xp[#i]
#Ay[#i]=#yp[#i]
#Az[#i]=#zp[#i]
#Bx[#i]=#xpp[#i]
#By[#i]=#ypp[#i]
#Bz[#i]=#zpp[#i]
!!next
** ***constructing the strip segments***
**now building the triangular plates
```

```
!!for #i = 1 to #plates step 1
DP   P2#i                #Bx[#i]   #By[#i]   #Bz[#i]
DP   P3#i                #Ax[#i]   #Ay[#i]   #Az[#i]
DP   P4#i                #Ax[#i-1] #Ay[#i-1] #Az[#i-1]
DP   P1#i                #Bx[#i-1] #By[#i-1] #Bz[#i-1]
** Upper triangle
BT   P3#i P1#i P4#i
** Lower triangle
BT   P2#i P1#i P3#i
!!next
*********************************************
***Now defining the feeding section***
**Long wire
DP: Feed0p :  :  :  :  : #Bx[0] : #By[0] : #Bz[0]-3
DP: Feed1p :  :  :  :  : #Bx[0] : #By[0] : #Bz[0]
BL: Feed0p : Feed1p
 ** small wire as a source
DP   Feed0               #Bx[0]    #By[0]    #Bz[0]-5
DP   Feed1               #Bx[0]    #By[0]    #Bz[0]-3
LA   wire1
BL   Feed0Feed1
***Shifting the Geometry and making a room for the feeding wire
TG:  : -1 : -1 :  : 0 :  :  :  :  :  : abs(#Bz[0])+5
EG   1    0    0        0                                                    1 1
**Setting an infinite ground plane
BO   2 **Infinite GND Plane
** Set frequency
FR   40   0              2e9             3.5e9
** Sources
A1   0    wire1          1        0                          50
** S-parameters: SParameter1
SP   1    1  ** SParameter1
** Total source power
** use defaults
PW   0    0
** Far fields: FarField1
OF   1    0              0        0        0
FF   1    19   73   1        0        0        5        5  ** FarField1
**Request output file
DA   0    0    0    0    0    0        0
** End of file
EN
```

A.1.2: 4.5-turn conformal hemispherical helical antenna with a strip of constant width and a center fed matching section of width #2

```
*** Defining the feeding and the matching sections ***
DP: S11 : : : : : #Bx[1] : #By[1] : #Bz[1]+abs(#Bz[0])+5
DP: S13 : : : : : #Bx[0] : #By[0] : #Bz[0]+abs(#Bz[0])+5
DP   S12                  0        0        2
DP: S21 : : : : : #Bx[2] : #By[2] : #Bz[2]+abs(#Bz[0])+5
DP: S31 : : : : : #Bx[3] : #By[3] : #Bz[3]+abs(#Bz[0])+5
BT   S11  S12  S13
BT   S21  S12  S11
BT   S31  S12  S21
** small side wire
DP   Feed0                0        0        0
DP   Feed1                0        0        2
LA   wire1
BL   Feed0Feed1
EG   1    0    0        0                                                  1 1
```

A.1.3: 4.5-turn conformal hemispherical helical antenna with a strip of tapered width and a center fed matching section of width #2

```
**setting the overall unit
SF   1                    1e-3
#a=20
#n=9 **no. of turns on a full sphere
#ws= 1 ** strip width at the start
#we1= 3 ** strip width at the top
#we=#we1-#ws
#plates=200 ** number of strip segments
#dz=#a/#plates ** number of divisions on the z-axis
** Segment Dimensions
IP                        .2       9        2
** Defining the geometry
#z[0]=0
#theta[0]=ARCCOS(#z[0]/#a)
#x[0]=#a
#y[0]=0
#q=(#we+#ws)/2
#t[0]=((#q-#ws/2)/#a)*(#z[0])+#ws/2
#thetap[0]=(#t[0])/#a
#zp[0]=#a*COS(#theta[0]-#thetap[0])
#xp[0]=#a*SIN(ARCCOS(#zp[0]/#a))*COS(#n*#pi*#z[0]/#a)
#yp[0]=#a*SIN(ARCCOS(#zp[0]/#a))*SIN(#n*#pi*#z[0]/#a)
#zpp[0]=#a*COS(#theta[0]+#thetap[0])
#xpp[0]=#a*SIN(ARCCOS(#zpp[0]/#a))*COS(#n*#pi*#z[0]/#a)
#ypp[0]=#a*SIN(ARCCOS(#zpp[0]/#a))*SIN(#n*#pi*#z[0]/#a)
**Defining the intial points
**** here they are the same ****
#Ax[0]=#xp[0]
#Ay[0]=#yp[0]
#Az[0]=#zp[0]
#Bx[0]=#xpp[0]
```

```
#By[0]=#ypp[0]
#Bz[0]=#zpp[0]
!!for #i = 1 to #plates step 1
#z[#i]=(#i)*#dz
#x[#i]=#a*SIN(ARCCOS(#z[#i]/#a))*COS(#n*#pi*#z[#i]/#a)
#y[#i]=#a*SIN(ARCCOS(#z[#i]/#a))*SIN(#n*#pi*#z[#i]/#a)
#t[#i]=((#q-#ws/2)/#a)*(#z[#i])+#ws/2
#thetap[#i]=(#t[#i])/#a
#zp[#i]=#a*COS(ARCCOS(#z[#i]/#a)-#thetap[#i])
#xp[#i]=#a*SIN(ARCCOS(#zp[#i]/#a))*COS(#n*#pi*#z[#i]/#a)
#yp[#i]=#a*SIN(ARCCOS(#zp[#i]/#a))*SIN(#n*#pi*#z[#i]/#a)
#zpp[#i]=#a*COS(ARCCOS(#z[#i]/#a)+#thetap[#i])
#xpp[#i]=#a*SIN(ARCCOS(#zpp[#i]/#a))*COS(#n*#pi*#z[#i]/#a)
#ypp[#i]=#a*SIN(ARCCOS(#zpp[#i]/#a))*SIN(#n*#pi*#z[#i]/#a)
#Ax[#i]=#xp[#i]
#Ay[#i]=#yp[#i]
#Az[#i]=#zp[#i]
#Bx[#i]=#xpp[#i]
#By[#i]=#ypp[#i]
#Bz[#i]=#zpp[#i]
!!next
** ***constructing the plates***
** **The first triangle from the bottom
** DP   S2                  #Ax[0]   #Ay[0]   #Az[0]
** DP   S3                  #Ax[1]   #Ay[1]   #Az[1]
** DP   S1                  #Bx[1]   #By[1]   #Bz[1]
** BT   S1   S2   S3
**now building the triangular plates
!!for #i = 1 to #plates-1 step 1 **#plates-1 because it gets crazy at the top
DP   P2#i                #Bx[#i]   #By[#i]   #Bz[#i]
DP   P3#i                #Ax[#i]   #Ay[#i]   #Az[#i]
DP   P4#i                #Ax[#i-1] #Ay[#i-1] #Az[#i-1]
DP   P1#i                #Bx[#i-1] #By[#i-1] #Bz[#i-1]
** Upper triangle
BT   P3#i P1#i P4#i
** Lower triangle
BT   P2#i P1#i P3#i
!!next
***Shifting the Geometry and making a room for the feeding wire
TG:  : -1 : -1 :  : 0 :  :  :  :  :  : abs(#Bz[0])+5
***Now defining the feeding section***
DP: S11 :  :  :  :  : #Bx[1] : #By[1] : #Bz[1]+abs(#Bz[0])+5
DP: S13 :  :  :  :  : #Bx[0] : #By[0] : #Bz[0]+abs(#Bz[0])+5
DP   S12                 0        0        2
DP: S21 :  :  :  :  : #Bx[2] : #By[2] : #Bz[2]+abs(#Bz[0])+5
DP: S31 :  :  :  :  : #Bx[3] : #By[3] : #Bz[3]+abs(#Bz[0])+5
BT   S11  S12  S13
BT   S21  S12  S11
BT   S31  S12  S21
** small side wire
DP   Feed0               0        0        0
DP   Feed1               0        0        2
LA   wire1
BL   Feed0Feed1
EG   1    0    0        0
```

A.2: Non-Conformal hemispherical helical antenna geometry

A.2.1: 4.5-turn non-conformal hemispherical helical antenna with a strip of constant width and a vertical short wire feed

```
**setting the overall unit
SF   1                    1e-3
#a=20
#n=9 **no. of turns on a full sphere
#w= 2 ** strip width
#thetap=(#w/2)/#a
#ps=0 **tilt angle
#ddz=#w*sin(#ps) **the difference in z between Az and Bz
#plates=200 ** number of strip segments
#dz=#a/#plates
** Segment Dimensions
IP                    .1      9       2
**************************
** Defining the geometry **
**************************
**Defining the Central Line
#z[0]=0
#theta[0]=ARCCOS(#z[0]/#a)
#x[0]=#a
#y[0]=0
#zp[0]=#a*COS(#theta[0]-#thetap)
#xp[0]=#a*SIN(ARCCOS(#zp[0]/#a))*COS(#n*#pi*#z[0]/#a) ** Keeping the same Phi of the originl wire
#yp[0]=#a*SIN(ARCCOS(#zp[0]/#a))*SIN(#n*#pi*#z[0]/#a) **Keeping the same Phi of the originl wire
#zpp[0]=#zp[0]-#ddz
#xpp[0]=(#a*SIN(ARCCOS(#zp[0]/#a))-#w*COS(#ps))*COS(#n*#pi*#z[0]/#a) **Keeping the same Phi of the originl wire
#ypp[0]=(#a*SIN(ARCCOS(#zp[0]/#a))-#w*COS(#ps))*SIN(#n*#pi*#z[0]/#a) **Keeping the same Phi of the originl wire
**Defining the intial points
#Ax[0]=#xp[0]
#Ay[0]=#yp[0]
#Az[0]=#zp[0]
#Bx[0]=#xpp[0]
#By[0]=#ypp[0]
#Bz[0]=#zpp[0]
!!for #i = 1 to #plates step 1
#z[#i]=(#i)*#dz
#x[#i]=#a*SIN(ARCCOS(#z[#i]/#a))*COS(#n*#pi*#z[#i]/#a)
#y[#i]=#a*SIN(ARCCOS(#z[#i]/#a))*SIN(#n*#pi*#z[#i]/#a)
#zp[#i]=#a*COS(ARCCOS(#z[#i]/#a)-#thetap)
#xp[#i]=#a*SIN(ARCCOS(#zp[#i]/#a))*COS(#n*#pi*#z[#i]/#a)
#yp[#i]=#a*SIN(ARCCOS(#zp[#i]/#a))*SIN(#n*#pi*#z[#i]/#a)
#zpp[#i]=#zp[#i]-#ddz
#xpp[#i]=(#a*SIN(ARCCOS(#zp[#i]/#a))-#w*cos(#ps))*COS(#n*#pi*#z[#i]/#a) **Keeping the same Phi of the originl wire
#ypp[#i]=(#a*SIN(ARCCOS(#zp[#i]/#a))-#w*cos(#ps))*SIN(#n*#pi*#z[#i]/#a) **Keeping the same Phi of the originl wire
#Ax[#i]=#xp[#i]
#Ay[#i]=#yp[#i]
#Az[#i]=#zp[#i]
```

```
#Bx[#i]=#xpp[#i]
#By[#i]=#ypp[#i]
#Bz[#i]=#zpp[#i]
!!next
**now building the triangular plates
!!for #i = 1 to #plates step 1
DP   S12#i              #Bx[#i]   #By[#i]   #Bz[#i]
DP   S22#i              #Bx[#i-1] #By[#i-1] #Bz[#i-1]
DP   S32#i              #Ax[#i]   #Ay[#i]   #Az[#i]
DP   S31#i              #Ax[#i-1] #Ay[#i-1] #Az[#i-1]
** Upper Triangle
BT   S12#iS22#iS32#i
!!next
!!for #i = 1 to #plates step 1
** Lower Triangle
BT   S32#iS22#iS31#i
!!next
*********************************************
***Now defining the feeding section***
**Long side wire
DP: Feed0p :  :  :  :  : #Ax[0] : #Ay[0] : #Az[0]-3
DP: Feed1p :  :  :  :  : #Ax[0] : #Ay[0] : #Az[0]
BL: Feed0p : Feed1p
** small side wire
DP   Feed0              #Ax[0]    #Ay[0]    #Az[0]-5
DP   Feed1              #Ax[0]    #Ay[0]    #Az[0]-3
LA   wire1
BL   Feed0Feed1
** shifting the whole geometry to make a space for the feeding wire
TG       -1   -1       0                                    5-#Az[0]
EG   1    0    0       0                                              1 1
**Setting an infinite ground plane
BO   2 **Infinite GND Plane
** Set frequency
FR   50   0             2.65e9          4e9
** Sources
A1   0    wire1          1       0                          50
** S-parameters: SParameter1
SP   1    1  ** SParameter1
** Total source power
** use defaults
PW   0    0
** Far fields: FarField1
OF   1    0             0       0       0
FF   1    19   73   1       0       0       5       5  ** FarField1
**Request output file
DA   0    0    0    0    0    0       0
** End of file
EN
```

A.2.2: 4.5-turn non-conformal hemispherical helical antenna with a strip of tapered width and a vertical short wire feed

```
**setting the overall unit
SF   1                    1e-3
#a=20
#n=9 **no. of turns on a full sphere
#w= 3 ** strip width
#thetap=(#w/2)/#a
#ps=0  **tilt angle
#plates=200 ** number of strip segments
#dz=#a/#plates
** Segment Dimensions
IP                    .1       9        2
**************************
** Defining the geometry **
**************************
**Defining the Central Line
#z[0]=0
#theta[0]=ARCCOS(#z[0]/#a)
#x[0]=#a
#y[0]=0
#zp[0]=#a*COS(#theta[0]-#thetap)
#xp[0]=#a*SIN(ARCCOS(#zp[0]/#a))*COS(#n*#pi*#z[0]/#a)
#yp[0]=#a*SIN(ARCCOS(#zp[0]/#a))*SIN(#n*#pi*#z[0]/#a)
** Increased thickness as going to the top
#t[0]=((#w/2-0.5)/#a)*(#z[0])+0.5
#ddz=#t[0]*sin(#ps) **the difference in z between Apz and Bpz
#zpp[0]=#zp[0]-#ddz
#xpp[0]=(#a*SIN(ARCCOS(#zp[0]/#a))-#w/2*COS(#ps))*COS(#n*#pi*#z[0]/#a)
#ypp[0]=(#a*SIN(ARCCOS(#zp[0]/#a))-#w/2*COS(#ps))*SIN(#n*#pi*#z[0]/#a)
**Defining the intial points
#Ax[0]=#xp[0]
#Ay[0]=#yp[0]
#Az[0]=#zp[0]
#Cx[0]=#xpp[0]
#Cy[0]=#ypp[0]
#Cz[0]=#zpp[0]
#Apz[0]=#Cz[0]+#ddz
#Apx[0]=(#a*SIN(ARCCOS(#zp[0]/#a))-#w/2*COS(#ps)+#t[0]*COS(#ps))*COS(#n*#pi*#z[0]/#a)
#Apy[0]=(#a*SIN(ARCCOS(#zp[0]/#a))-#w/2*COS(#ps)+#t[0]*COS(#ps))*SIN(#n*#pi*#z[0]/#a)
#Bpz[0]=#Cz[0]-#ddz
#Bpx[0]=(#a*SIN(ARCCOS(#zp[0]/#a))-#w/2*COS(#ps)-#t[0]*COS(#ps))*COS(#n*#pi*#z[0]/#a)
#Bpy[0]=(#a*SIN(ARCCOS(#zp[0]/#a))-#w/2*COS(#ps)-#t[0]*COS(#ps))*SIN(#n*#pi*#z[0]/#a)
!!for #i = 1 to #plates step 1
#z[#i]=(#i)*#dz
#x[#i]=#a*SIN(ARCCOS(#z[#i]/#a))*COS(#n*#pi*#z[#i]/#a)
#y[#i]=#a*SIN(ARCCOS(#z[#i]/#a))*SIN(#n*#pi*#z[#i]/#a)
#zp[#i]=#a*COS(ARCCOS(#z[#i]/#a)-#thetap)
#xp[#i]=#a*SIN(ARCCOS(#zp[#i]/#a))*COS(#n*#pi*#z[#i]/#a)
#yp[#i]=#a*SIN(ARCCOS(#zp[#i]/#a))*SIN(#n*#pi*#z[#i]/#a)
** Increased thickness as going to the top
#t[#i]=((#w/2-0.5)/#a)*(#z[#i])+0.5
#ddz=#t[#i]*sin(#ps) **the difference in z between Apz and Bpz
#zpp[#i]=#zp[#i]-#ddz
```

```
#xpp[#i]=(#a*SIN(ARCCOS(#zp[#i]/#a))-#w*cos(#ps))*COS(#n*#pi*#z[#i]/#a)
#ypp[#i]=(#a*SIN(ARCCOS(#zp[#i]/#a))-#w*cos(#ps))*SIN(#n*#pi*#z[#i]/#a)
#Ax[#i]=#xp[#i]
#Ay[#i]=#yp[#i]
#Az[#i]=#zp[#i]
#Cx[#i]=#xpp[#i]
#Cy[#i]=#ypp[#i]
#Cz[#i]=#zpp[#i]
#Apz[#i]=#Cz[#i]+#ddz
#Apx[#i]=(#a*SIN(ARCCOS(#zp[#i]/#a))-#w/2*COS(#ps)+#t[#i]*COS(#ps))*COS(#n*#pi*#z[#i]/#a)
#Apy[#i]=(#a*SIN(ARCCOS(#zp[#i]/#a))-#w/2*COS(#ps)+#t[#i]*COS(#ps))*SIN(#n*#pi*#z[#i]/#a)
#Bpz[#i]=#Cz[#i]-#ddz
#Bpx[#i]=(#a*SIN(ARCCOS(#zp[#i]/#a))-#w/2*COS(#ps)-#t[#i]*COS(#ps))*COS(#n*#pi*#z[#i]/#a)
#Bpy[#i]=(#a*SIN(ARCCOS(#zp[#i]/#a))-#w/2*COS(#ps)-#t[#i]*COS(#ps))*SIN(#n*#pi*#z[#i]/#a)
!!next
**now building the triangular plates

!!for #i = 1 to #plates step 1
DP   S12#i              #Bpx[#i]  #Bpy[#i]  #Bpz[#i]
DP   S22#i              #Bpx[#i-1]#Bpy[#i-1]#Bpz[#i-1]
DP   S32#i              #Apx[#i]  #Apy[#i]  #Apz[#i]
DP   S31#i              #Apx[#i-1]#Apy[#i-1]#Apz[#i-1]
** Upper Triangle
BT   S12#iS22#iS32#i
!!next
!!for #i = 1 to #plates step 1
** Lower Triangle
BT   S32#iS22#iS31#i
!!next
*********************************************
***Now defining the feeding section***
**Long side wire
DP: Feed0p :  :  :  : #Apx[0] : #Apy[0] : #Apz[0]-3
DP: Feed1p :  :  :  : #Apx[0] : #Apy[0] : #Apz[0]
BL: Feed0p : Feed1p
** small side wire
DP   Feed0              #Apx[0]   #Apy[0]   #Apz[0]-5
DP   Feed1              #Apx[0]   #Apy[0]   #Apz[0]-3
LA   wire1
BL   Feed0Feed1
** shifting the whole geometry to make a space for the feeding wire
TG       -1   -1       0                                    5-#Apz[0]
EG   1    0    0       0                                              1 1
```

A.2.3: 4.5-turn non-conformal hemispherical helical antenna with a strip of tapered width and a side fed nonlinearly tapered matching section

```
***Defining the feeding section***
*** The MAtching Section ****
** Tapered Wire feeding (exponential tapering)
#divm= 30
#ap=#Apx[0]-(#Apx[0]-#Bpx[0])/2
#L_cap= #ap*3*#pi/8 ** The arc length
#c= 4/(exp(#L_cap)-1) ** the exponential correction coefficient

** Calculating the points
!!for #i = 0 to #divm step 1
#X[#i]=(#i/#divm)*(#ap-#ap*sin(#pi/8))+#ap*sin(#pi/8)
#Y[#i]=-sqrt((#ap)^2-(#X[#i])^2)
#Z[#i]=#c* (exp(#i*(#L_cap/#divm))-1)
#tp[#i]=sin((5*#pi/6)*(1/#L_cap)*(#i*#L_cap/#divm))
#psip[#i]=#i*((3*#pi/8)/#divm)+#pi/8
#tp[0]=0 ** Forcing the first thickness to be zero
#Fpux[#i]=#X[#i]-#tp[#i]*sin(#psip[#i])
#Fpuy[#i]=#Y[#i]+#tp[#i]*cos(#psip[#i]) **#Y[#i] here is alredy negative
#Fpuz[#i]=#Z[#i]
#Fpdx[#i]=#X[#i]+#tp[#i]*sin(#psip[#i])
#Fpdy[#i]=#Y[#i]-#tp[#i]*cos(#psip[#i]) **#Y[#i] here is alredy positive
#Fpdz[#i]=#Z[#i]
!!next
** First small triangle
DP   Sp11              #Fpdx[1]  #Fpdy[1]  #Fpdz[1]
DP   Sp21              #Fpux[0]  #Fpuy[0]  #Fpuz[0]
DP   Sp31              #Fpux[1]  #Fpuy[1]  #Fpuz[1]
BT   Sp11 Sp21 Sp31
** the other triangles
!!for #i = 2 to #divm
DP: Sp12#i : : : : : #Fpdx[#i] : #Fpdy[#i] : #Fpdz[#i]
DP: Sp22#i : : : : : #Fpux[#i-1] : #Fpuy[#i-1] : #Fpuz[#i-1]
DP: Sp32#i : : : : : #Fpdx[#i-1] : #Fpdy[#i-1] : #Fpdz[#i-1]
DP: Sp13#i : : : : : #Fpux[#i] : #Fpuy[#i] : #Fpuz[#i]
BT: Sp12#i : Sp22#i : Sp32#i
BT: Sp13#i : Sp22#i : Sp12#i
!!next
** small side wire
DP: Feed0 : : : : : #ap*sin(#pi/8) : -#ap*cos(#pi/8) : -1
DP: Feed1 : : : : : #ap*sin(#pi/8) : -#ap*cos(#pi/8) : 0
LA   wire1
BL   Feed0Feed1
** shifting the whole geometry to make a space for the feeding wire
TG       -1   -1       0                                    1
EG   1    0    0       0                                              1 1
```

A.2.4: Collapsed two-dimensional geometry of a 4.5-turn non-conformal hemispherical helical antenna with a strip of tapered width and a side fed tapered matching section MATLAB code

```
%%% 2D_turns
close all;
clear all;
format long eng
 a=20;
n=9; %no. of turns on a full sphere
w= 3; %strip width
thetap=(w/2)/a; %since the strip width is constant thetap is constant too
ps=0;  %angle of strip slope
plates=200; % same as no. of Z-divisions, 2*#plates = #triangluar plates
dz=a/plates;
%List of matrices
x=[];
y=[];
z=[];
xp=[];
yp=[];
zp=[];
t=[];
xpp=[];
ypp=[];
zpp=[];
Ax=[];
Ay=[];
Az=[];
Cx=[];
Cy=[];
Cz=[];
Apx=[];
Apy=[];
Apz=[];
Bpx=[];
Bpy=[];
Bpz=[];
%Defining the Central Line
z(1)=0;
theta(1)=acos(z(1)/a);
x(1)=a;
y(1)=0;
zp(1)=a*cos(theta(1)-thetap);
xp(1)=a*sin(acos(zp(1)/a))*cos(n*pi*z(1)/a);
yp(1)=a*sin(acos(zp(1)/a))*sin(n*pi*z(1)/a);
%Increased thickness as going to the top
t(1)=(w/2-0.5)/a*(z(1))+0.5;
zpp(1)=zp(1);
xpp(1)=(a*sin(acos(zp(1)/a))-w/2*cos(ps))*cos(n*pi*z(1)/a);
ypp(1)=(a*sin(acos(zp(1)/a))-w/2*cos(ps))*sin(n*pi*z(1)/a);
%Defining the intial points
Ax(1)=xp(1);
Ay(1)=yp(1);
```

```
Az(1)=zp(1);
Cx(1)=xpp(1);
Cy(1)=ypp(1);
Cz(1)=zpp(1);
Apz(1)=Cz(1);
Apx(1)=(a*sin(acos(zp(1)/a))-w/2*cos(ps)+t(1)*cos(ps))*cos(n*pi*z(1)/a);
Apy(1)=(a*sin(acos(zp(1)/a))-w/2*cos(ps)+t(1)*cos(ps))*sin(n*pi*z(1)/a);
Bpz(1)=Cz(1);
Bpx(1)=(a*sin(acos(zp(1)/a))-w/2*cos(ps)-t(1)*cos(ps))*cos(n*pi*z(1)/a);
Bpy(1)=(a*sin(acos(zp(1)/a))-w/2*cos(ps)-t(1)*cos(ps))*sin(n*pi*z(1)/a);
for in=2:1:plates-8+1
i=in-1;
%Defining the Central Line
z(in)=i*dz;
theta(in)=acos(z(in)/a);
x(in)=a*sin(acos(z(in)/a))*cos(n*pi*z(in)/a);
y(in)=a*sin(acos(z(in)/a))*sin(n*pi*z(in)/a);
zp(in)=a*cos(theta(in)-thetap);
xp(in)=a*sin(acos(zp(in)/a))*cos(n*pi*z(in)/a);
yp(in)=a*sin(acos(zp(in)/a))*sin(n*pi*z(in)/a);
%Increased thickness as going to the top
t(in)= (w/2-0.5)/a* (z(in))+0.5;
zpp(in)=zp(in);
xpp(in)=(a*sin(acos(zp(in)/a))-w/2*cos(ps))*cos(n*pi*z(in)/a);
ypp(in)=(a*sin(acos(zp(in)/a))-w/2*cos(ps))*sin(n*pi*z(in)/a);
%Defining the intial points
Ax(in)=xp(in);
Ay(in)=yp(in);
Az(in)=zp(in);
Cx(in)=xpp(in);
Cy(in)=ypp(in);
Cz(in)=zpp(in);
Apz(in)=Cz(in);
Apx(in)=(a*sin(acos(zp(in)/a))-w/2*cos(ps)+t(in)*cos(ps))*cos(n*pi*z(in)/a);
Apy(in)=(a*sin(acos(zp(in)/a))-w/2*cos(ps)+t(in)*cos(ps))*sin(n*pi*z(in)/a);
Bpz(in)=Cz(in);
Bpx(in)=(a*sin(acos(zp(in)/a))-w/2*cos(ps)-t(in)*cos(ps))*cos(n*pi*z(in)/a);
Bpy(in)=(a*sin(acos(zp(in)/a))-w/2*cos(ps)-t(in)*cos(ps))*sin(n*pi*z(in)/a);
end
%%%%%%%%%%%%%%%%%%%%%%%%%%%%%%%%%%%%%%%%%%%%
%%% Drawing the Individual turns in 2D %%%
%%%%%%%%%%%%%%%%%%%%%%%%%%%%%%%%%%%%%%%%%%%%
%List of matrices
Appx=[];
Appy=[];
Appz=[];
Bppx=[];
Bppy=[];
Bppz=[];
Appx(1)=Apx(1);
Appy(1)=Apy(1);
Appz(1)=0;
Bppx(1)=Bpx(1);
Bppy(1)=Bpy(1);
Bppz(1)=0;
```

```
% radii correction on the x-y plane Keeping the same angle phi
dpA=[];
phipA=[];
dA=[];
dpB=[];
phipB=[];
dB=[];
for in=2:plates-8+1
dpA(in)= sqrt((Apx(in-1)-Apx(in))^2+(Apy(in-1)-Apy(in))^2+(Apz(in-1)-Apz(in))^2);
phipA(in)= (atan((Apx(in)-Apx(in-1))/(Apy(in)-Apy(in-1))));
dA(in)= sqrt((Apx(in-1)-Apx(in))^2+(Apy(in-1)-Apy(in))^2);

Appx(in)=Apx(in)-(dpA(in)-dA(in))*sin(phipA(in));
Appy(in)=Apy(in)+(dpA(in)-dA(in))*cos(phipA(in));
Appz(in)=0;

dpB(in)= sqrt((Bpx(in-1)-Bpx(in))^2+(Bpy(in-1)-Bpy(in))^2+(Bpz(in-1)-Bpz(in))^2);
phipB(in)= (atan((Bpx(in)-Bpx(in-1))/(Bpy(in)-Bpy(in-1))));
dB(in)= sqrt((Bpx(in-1)-Bpx(in))^2+(Bpy(in-1)-Bpy(in))^2);

Bppx(in)=Bpx(in)-(dpB(in)-dB(in))*sin(phipB(in));
Bppy(in)=Bpy(in)+(dpB(in)-dB(in))*cos(phipB(in));
Bppz(in)=0;
end
```

Appendix B: Conformal and Non-Conformal Hemispherical Helices Simulated Radiation Characteristics and VSWR

Section B.1 provides various radiation properties for the conformal hemispherical helix with a strip radiating element of constant width. In subsection B.1.1, the impact of number of turns on axial ratio and VSWR of the conformal design fed by a vertical short wire is shown. Also, the radiation patterns of the 4.5-turn design are given at several frequencies within its bandwidth. In subsection B.1.2, axial ratio and VSWR for the conformal helix, fed by a 1 mm short wire at the center and with a tapered matching section, are presented; the radiation pattern of the 4.5-turn design are also shown at several frequencies. In subsection B.2.1, simulated axial ratio and VSWR results for non-conformal hemispherical helix with a constant strip width and side fed by a vertical short wire are displayed. Finally, simulated radiation patterns at different frequencies for the final design, a 4.5-turn non-conformal hemispherical helix with a tapered radiating element and side fed by a tapered matching section, are presented in subsection B.2.2.

B.1: Conformal Helix

B.1.1: Conformal hemispherical helix fed by a side stub wire

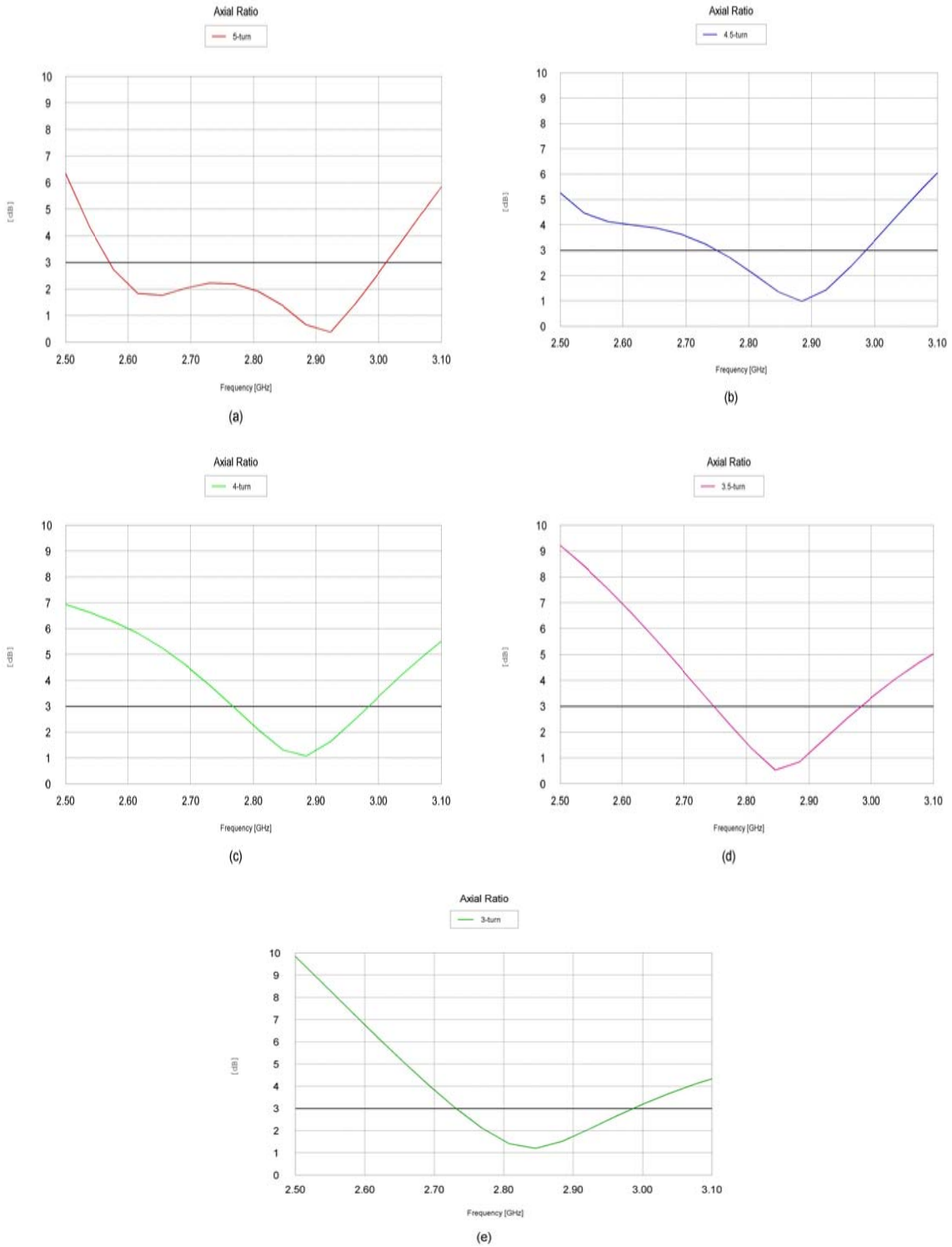

Figure B. 1: Axial ratio versus frequency for conformal hemispherical helix with 5 mm short wire feed and 2 mm wide strip with (a) 5 turns, (b) 4.5 turns, (c) 4 turns, (d) 3.5 turns, (e) 3 turns

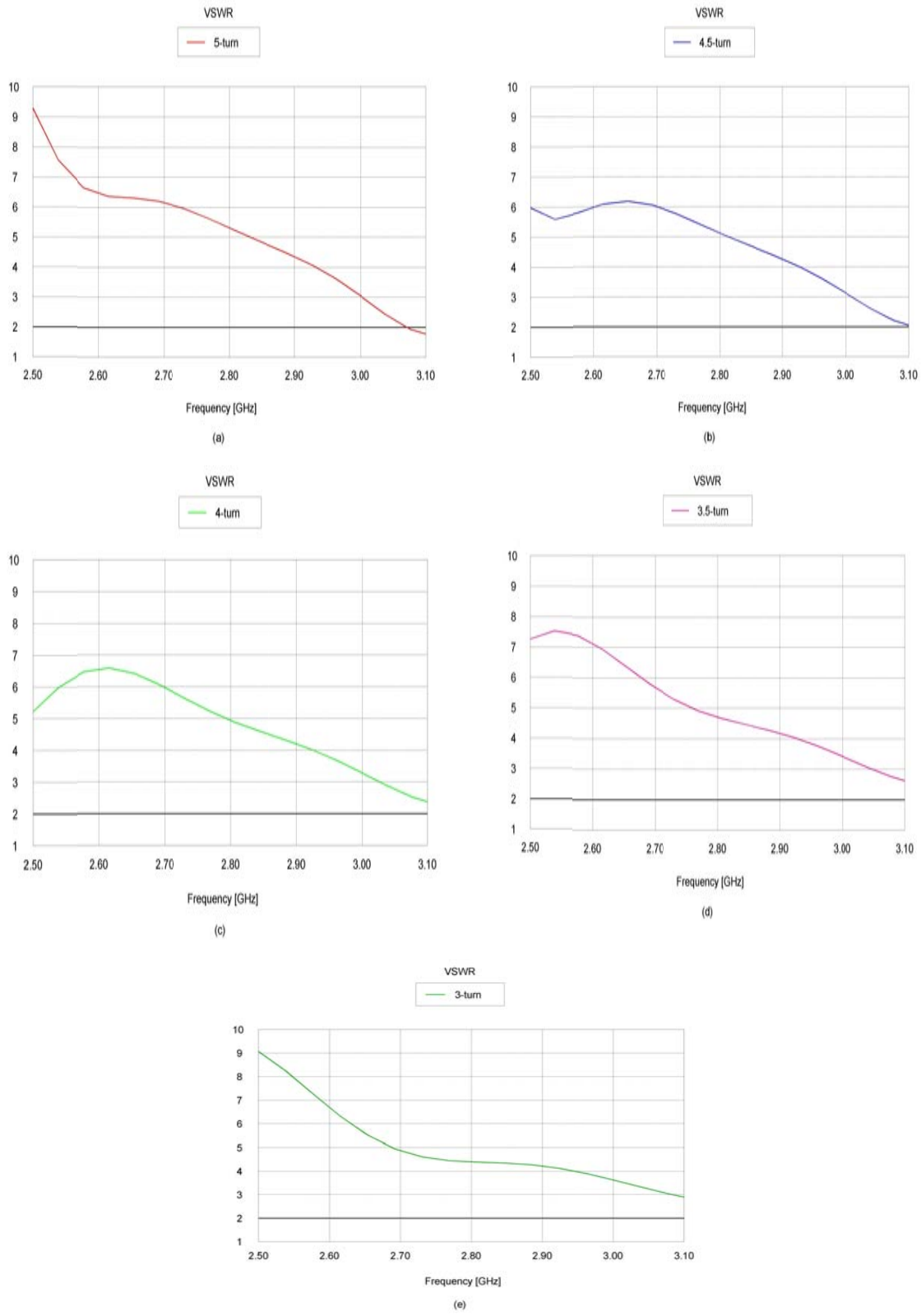

Figure B. 2: VSWR versus frequency for conformal hemispherical helix of Fig. B.1with (a) 5 turns, (b) 4.5 turns, (c) 4 turns, (d) 3.5 turns, (e) 3 turns

B.1.2: Conformal hemispherical helix with a tapered matching section

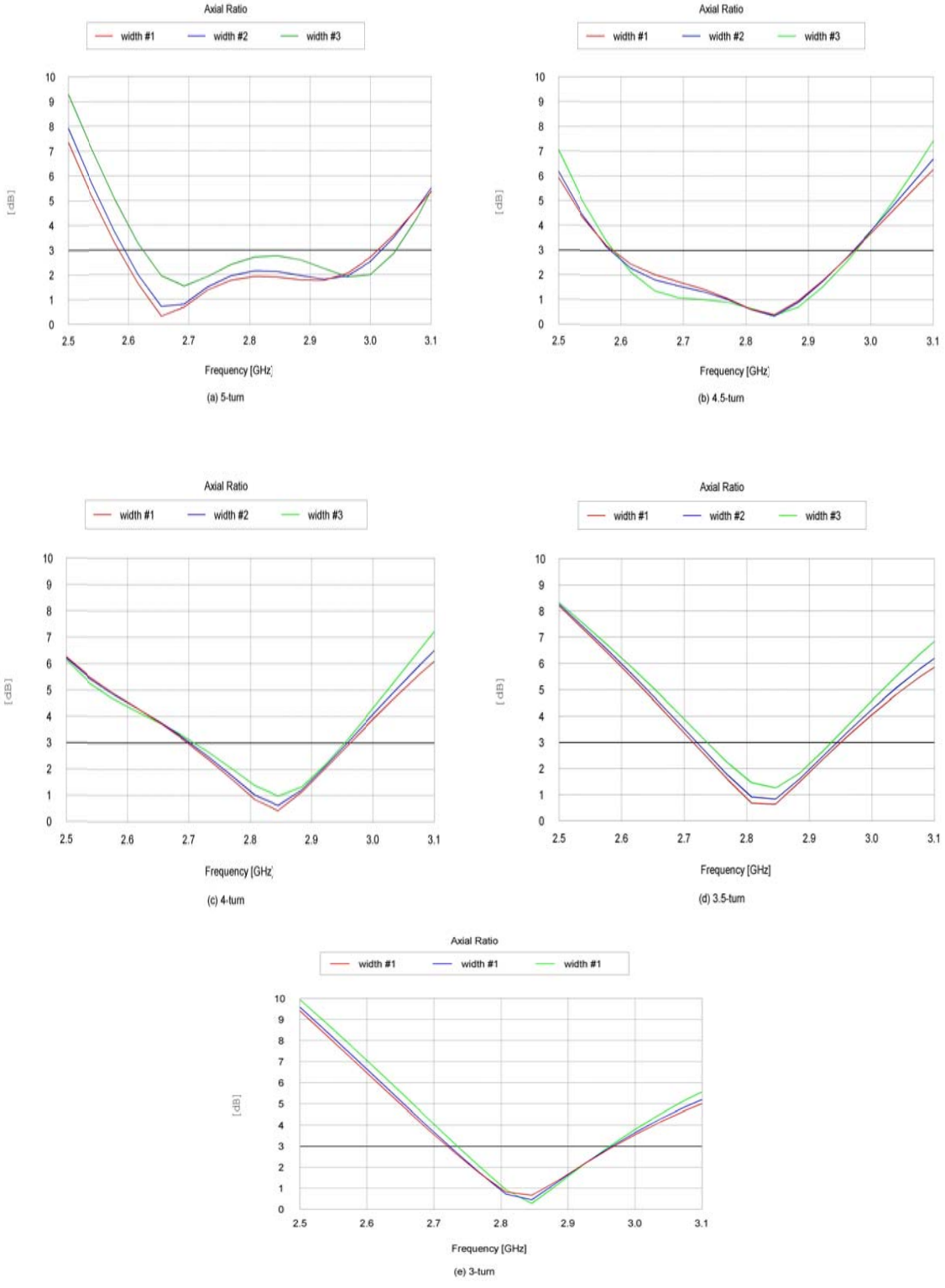

Figure B. 3: Variations of axial ratio versus frequency for antenna of Fig. B.1 with 1 mm short wire feed at center, tapered matching element, and (a) 5 turns, (b) 4.5 turns, (c) 4 turns, (d) 3.5 turns, (e) 3 turns

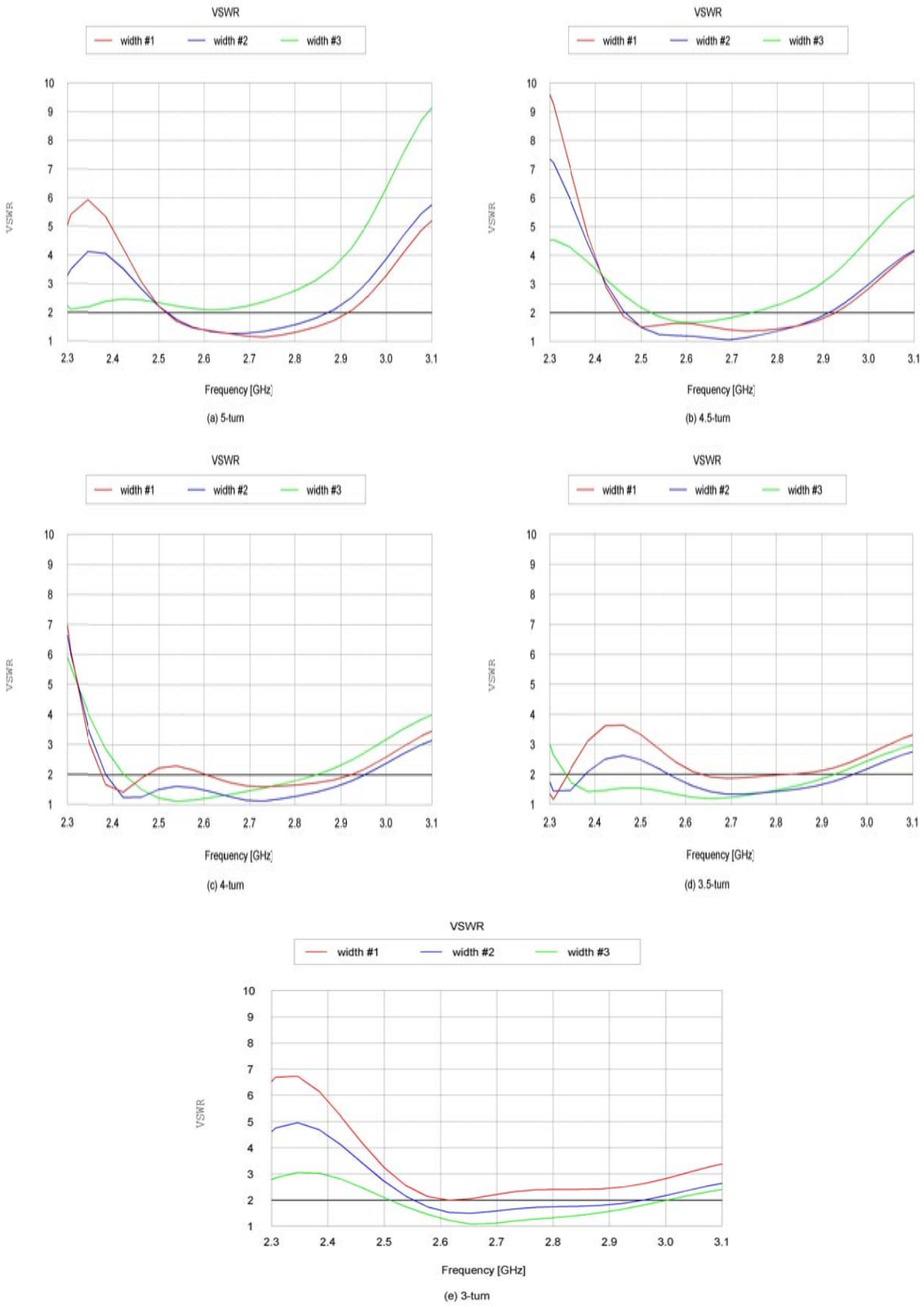

Figure B. 4: Variations of VSWR versus frequency for antenna of Fig. B.1 with 1 mm short wire feed at center, tapered matching element, and (a) 5 turns, (b) 4.5 turns, (c) 4 turns, (d) 3.5 turns, (e) 3 turns

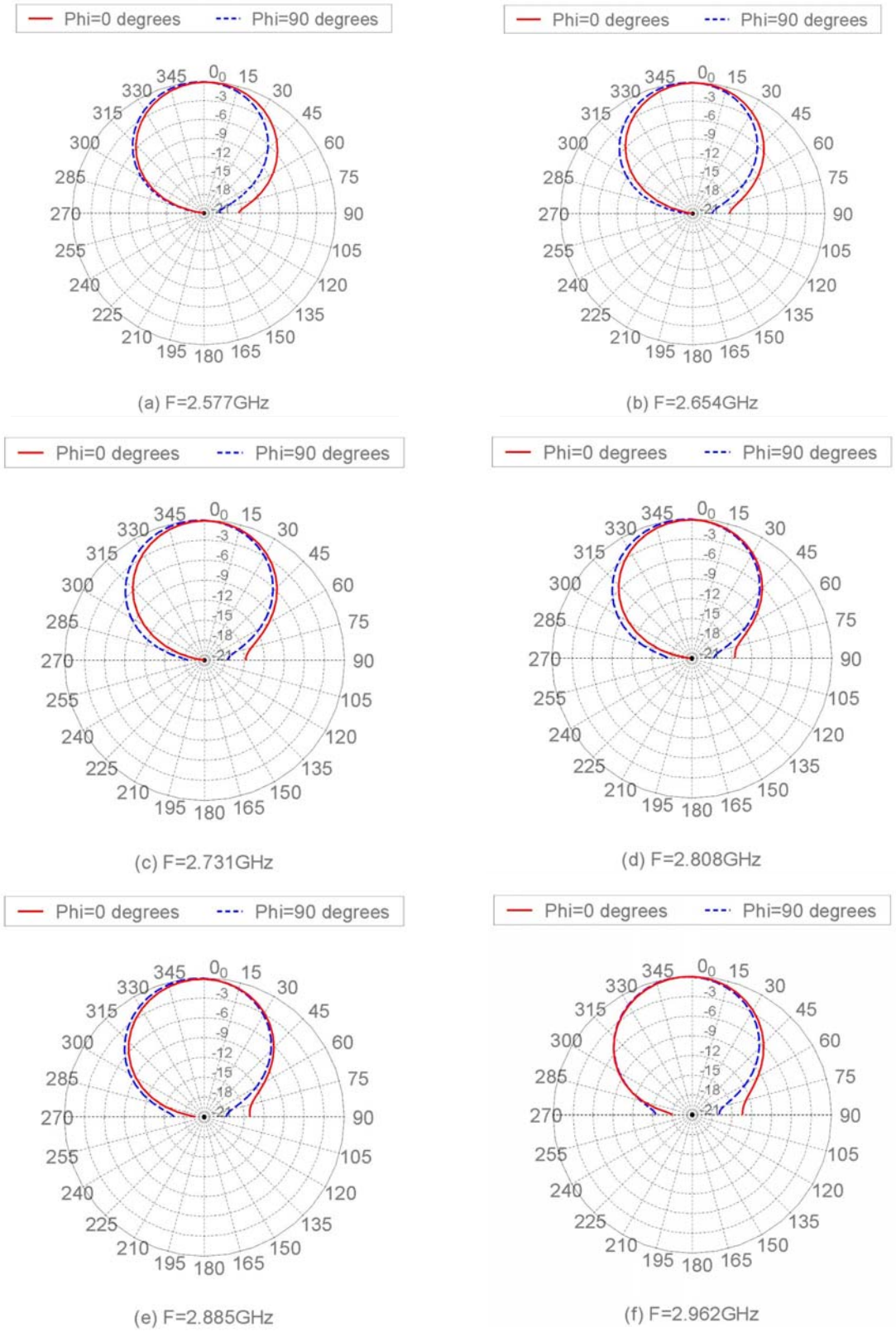

Figure B. 5: Radiation patterns in dB scale of 4.5-turn conformal hemispherical helix with tapered matching element (width 2) at several frequencies; (solid) $\phi = 0^\circ$, (dashed) $\phi = 90^\circ$

B.2: Non-Conformal Helix

B.2.1: Non-Conformal hemispherical helix of constant strip width and vertical wire feed

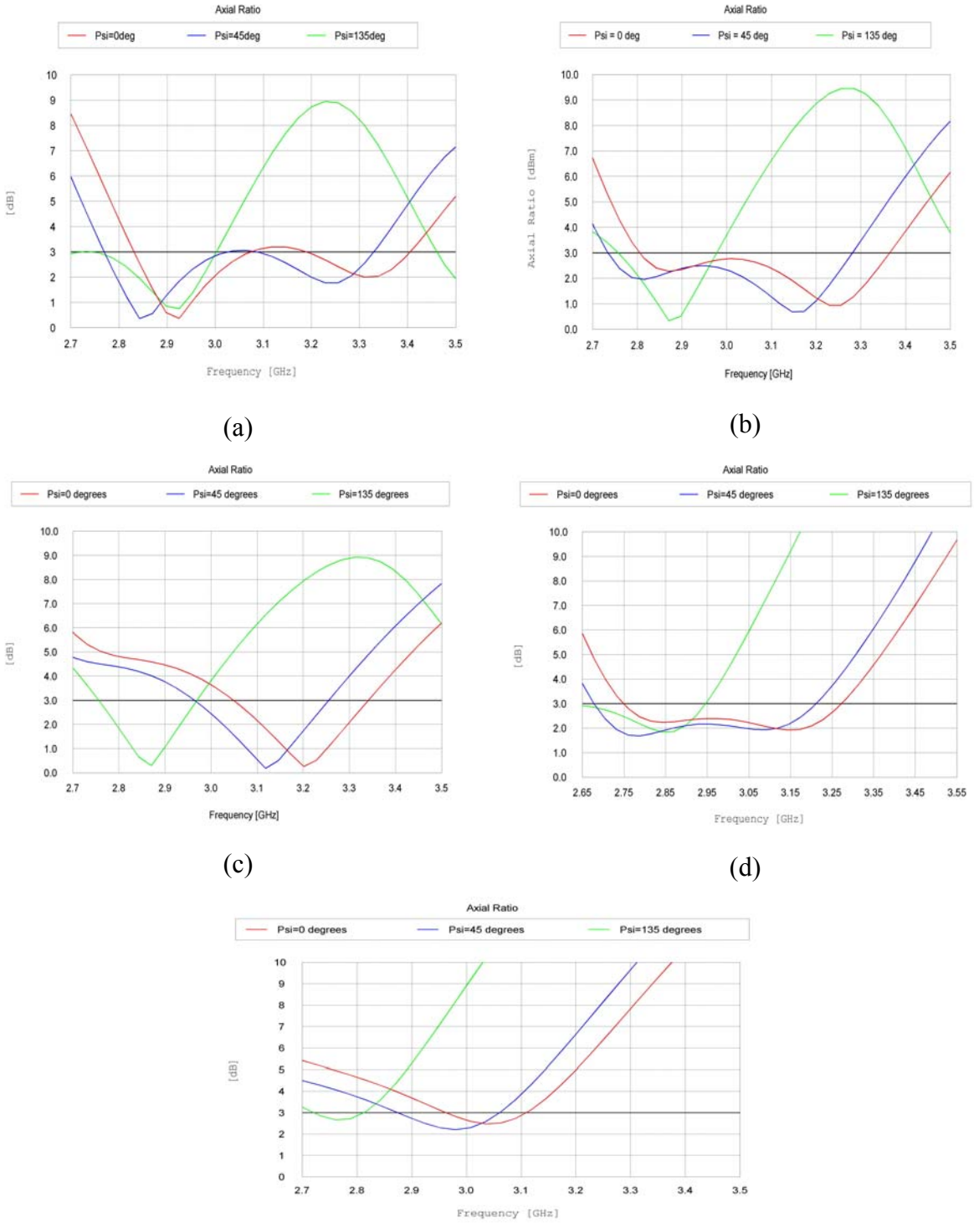

Figure B. 6: Axial Ratio of the Non-conformal helix with a stub wire feed and constant width strip (a) 5 turns (b) 4.5 turns (c) 4 turns (d) 3.5 turns (e) 3 turns

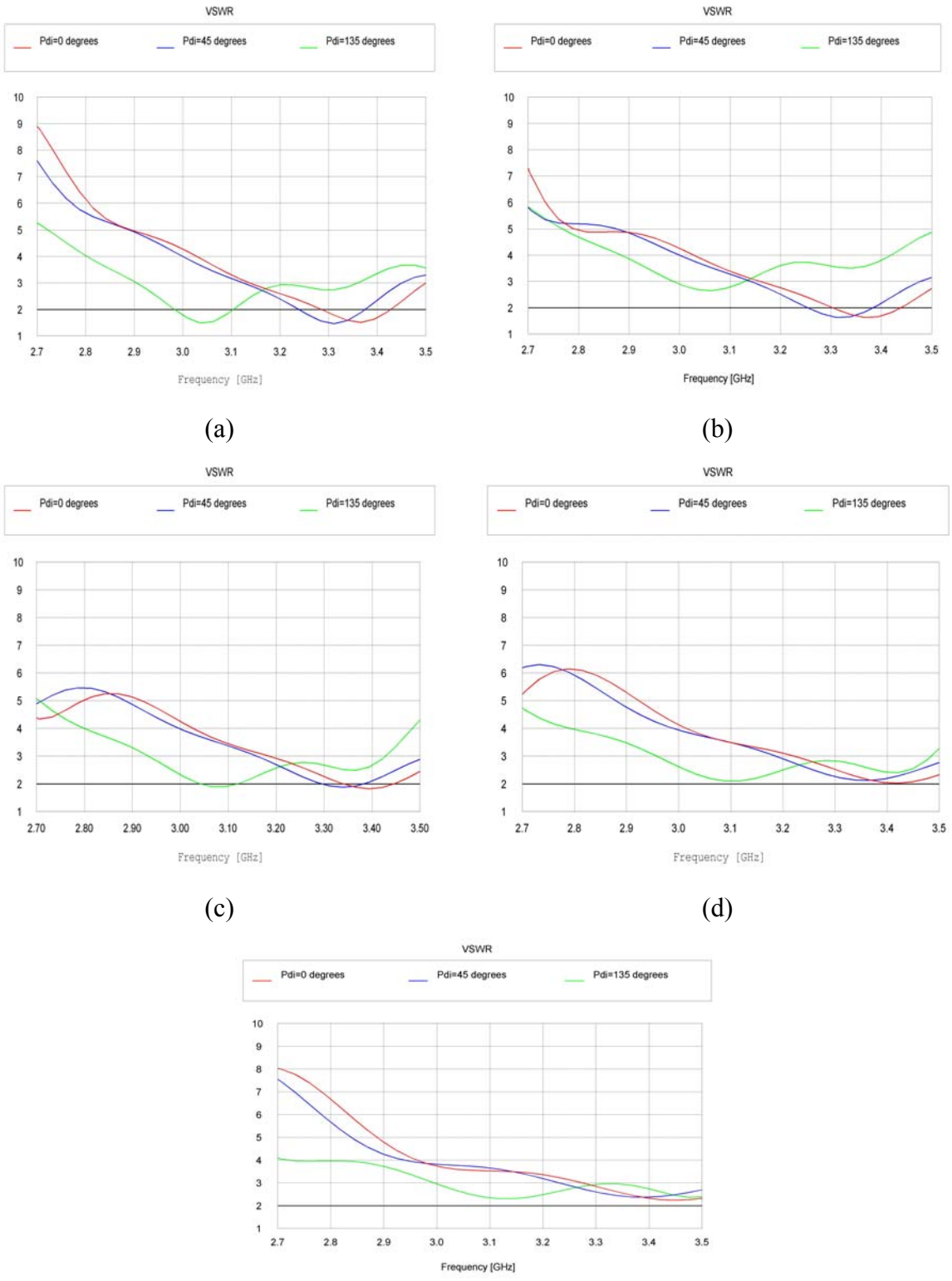

Figure B. 7: VSWR of the Non-conformal helix with a stub wire feed and constant width strip (a) 5 turns (b) 4.5 turns (c) 4 turns (d) 3.5 turns (e) 3 turns

B.2.2: Non-Conformal hemispherical helix of tapered strip and side tapered matching section over finite ground plane

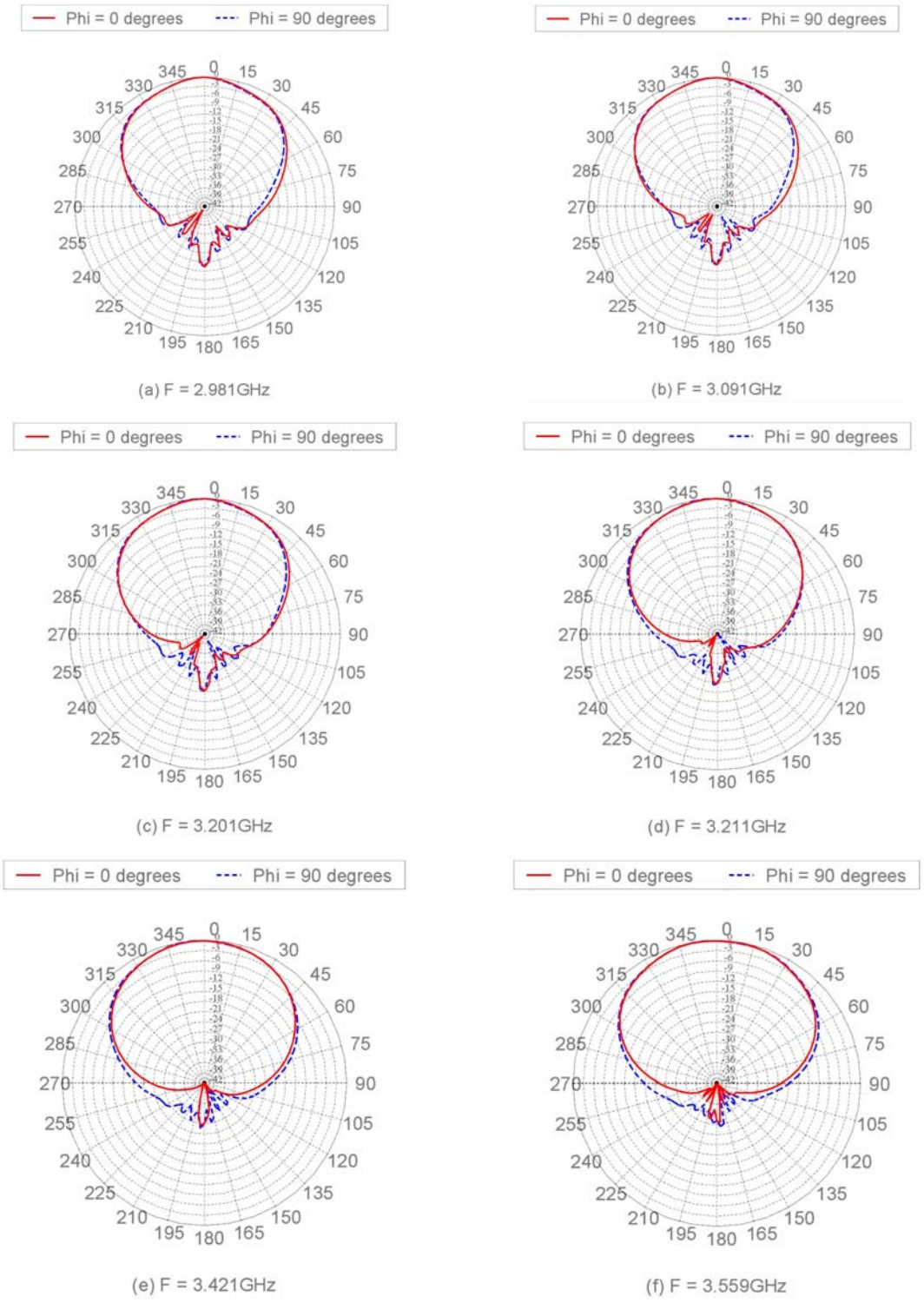

Figure B. 8: Radiation patterns in dB scale of 4.5-turn non-conformal hemispherical helix with side tapered matching section and 0 degree tilt angle on finite ground plane; (solid) $\phi = 0^{\circ}$, (dashed) $\phi = 90^{\circ}$

Appendix C: Measured Directivity Pattern and Axial Ratio of a 4.5-turn Non-conformal Hemispherical Helical Antenna with tapered strip and tapered side fed matching section

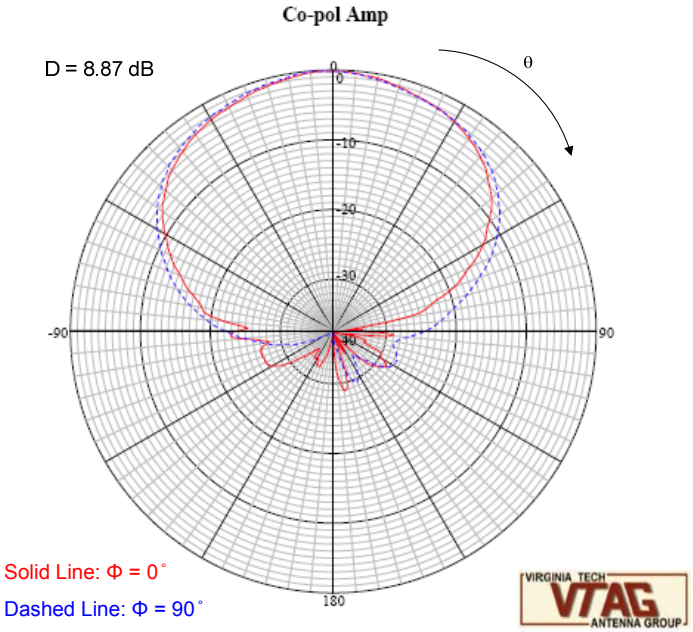

(a)

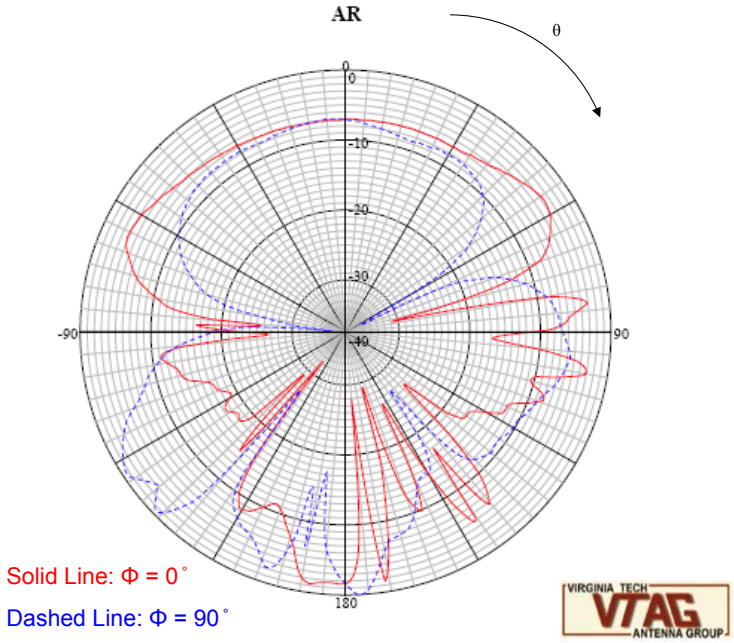

(b)

Figure C. 1: F= 2.80GHz (a) Directivity pattern (b) Axial ratio

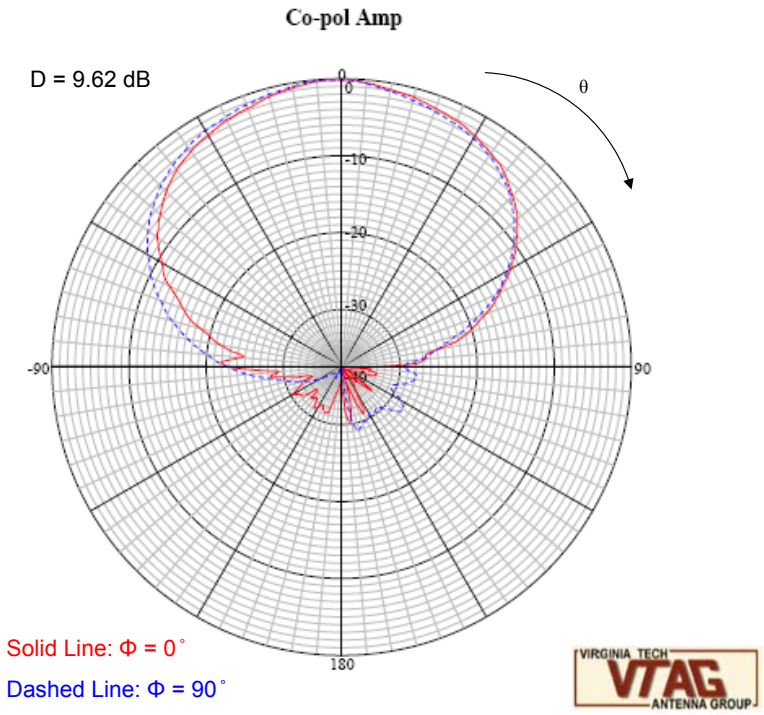

(a)

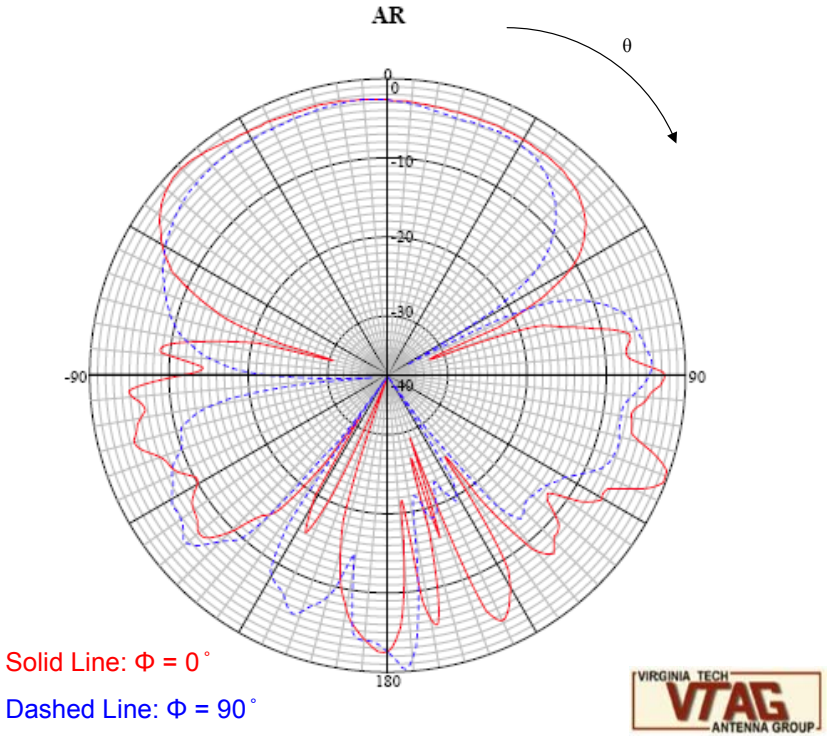

(b)

Figure C. 2: F= 2.95GHz (a) Directivity pattern (b) Axial ratio

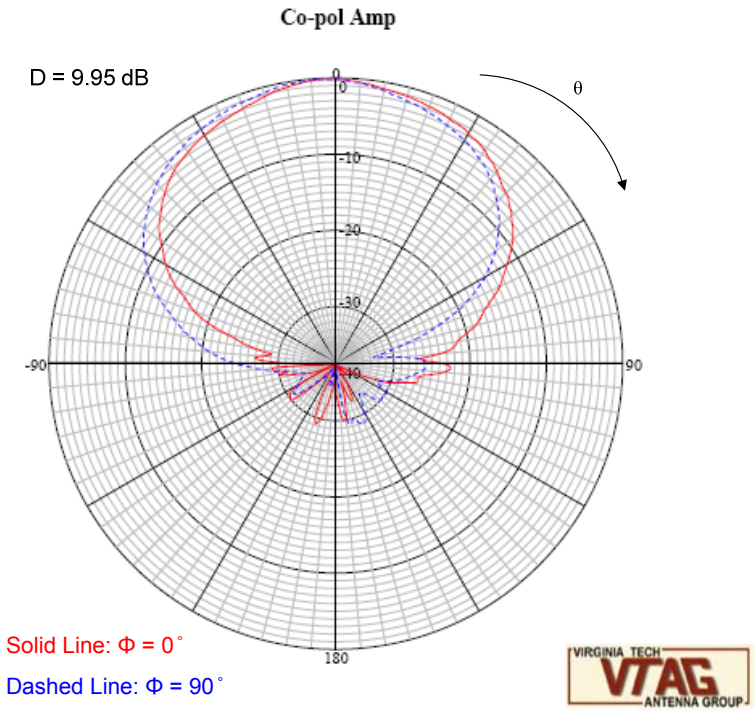

(a)

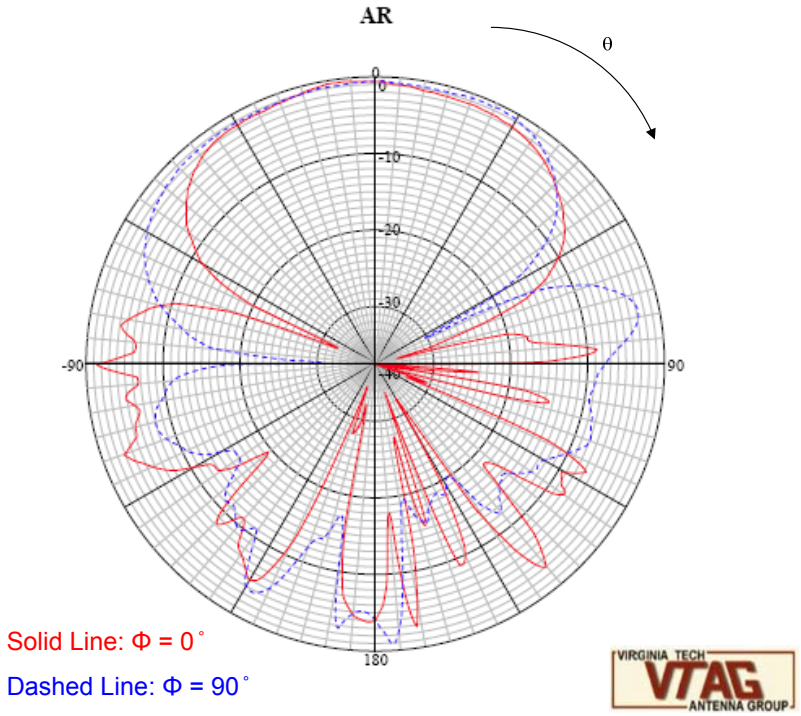

(b)

Figure C. 3: F= 3.10GHz (a) Directivity pattern (b) Axial ratio

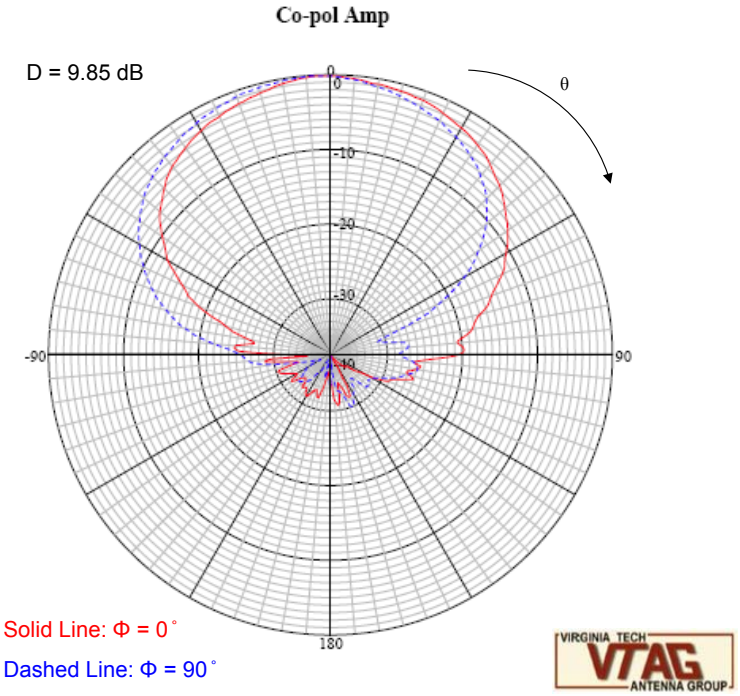

(a)

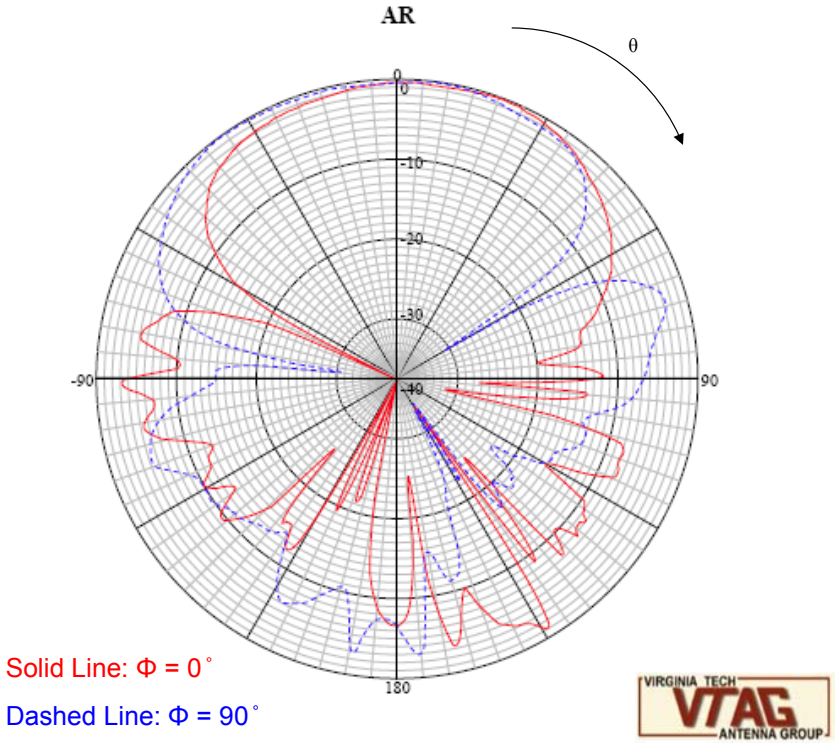

(b)

Figure C. 4: F= 3.25GHz (a) Directivity pattern (b) Axial ratio

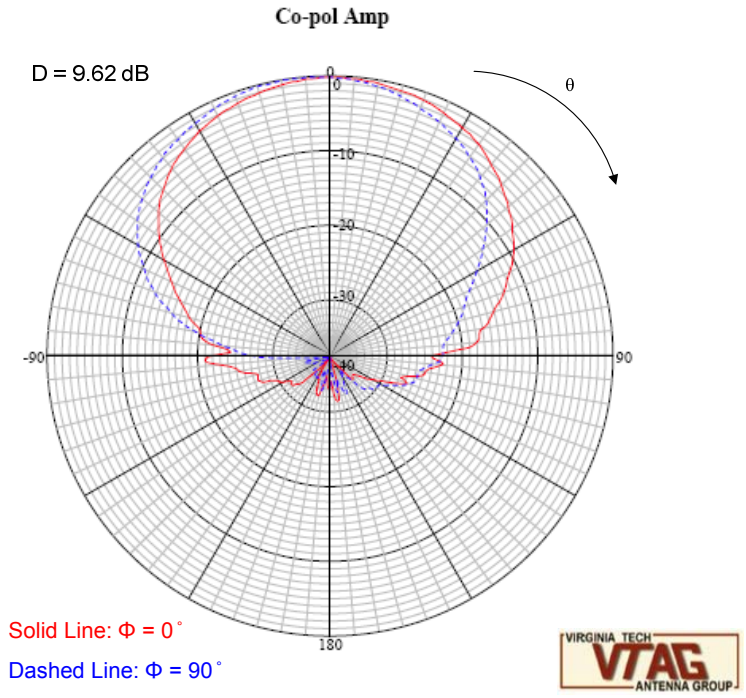

(a)

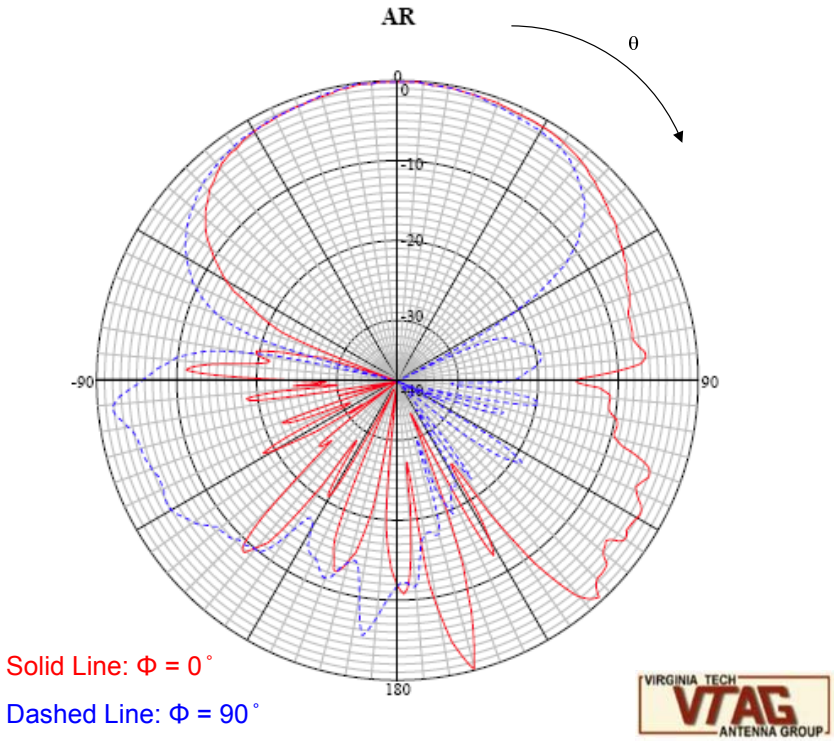

(b)

Figure C. 5: F= 3.40GHz (a) Directivity pattern (b) Axial ratio

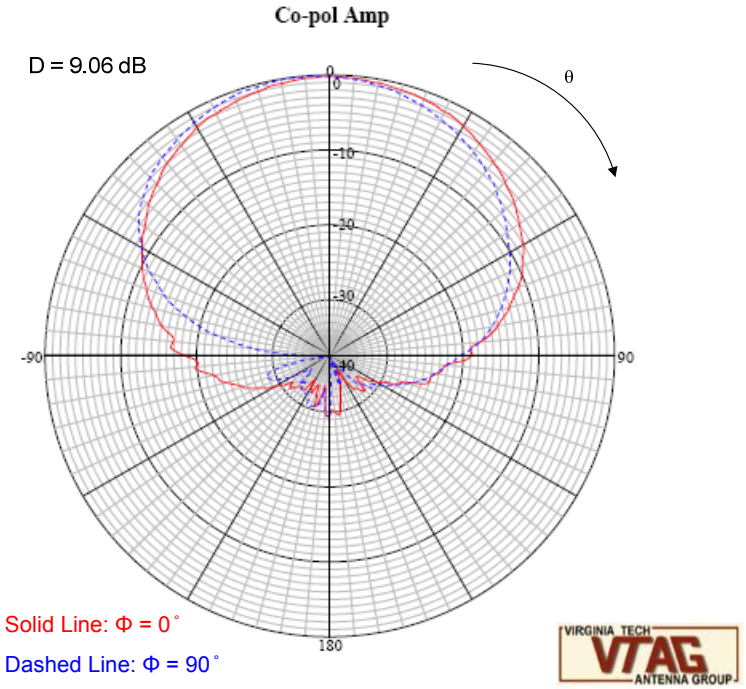

(a)

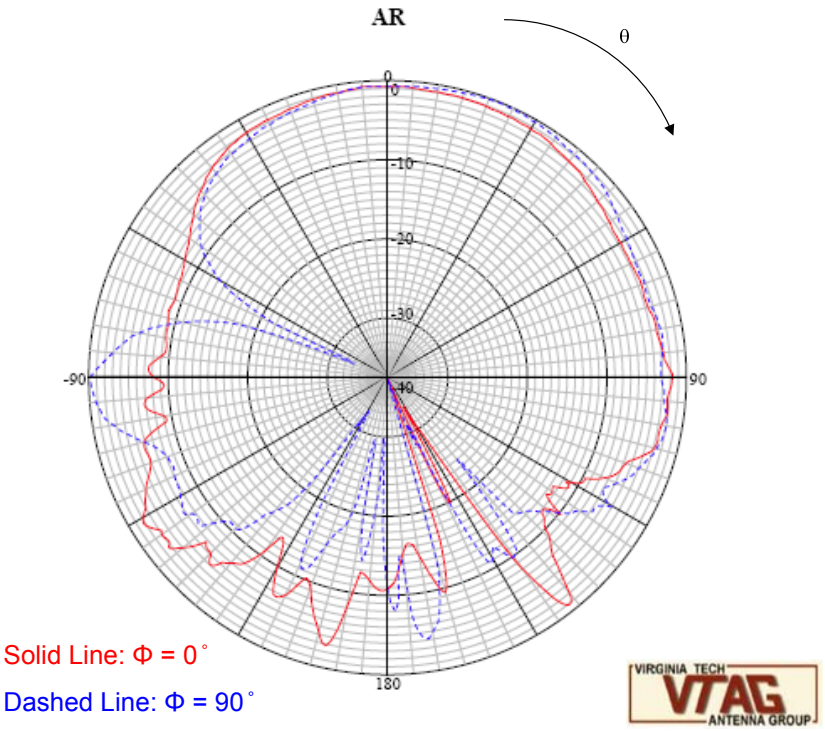

(b)

Figure C. 6: F= 3.55GHz (a) Directivity pattern (b) Axial ratio

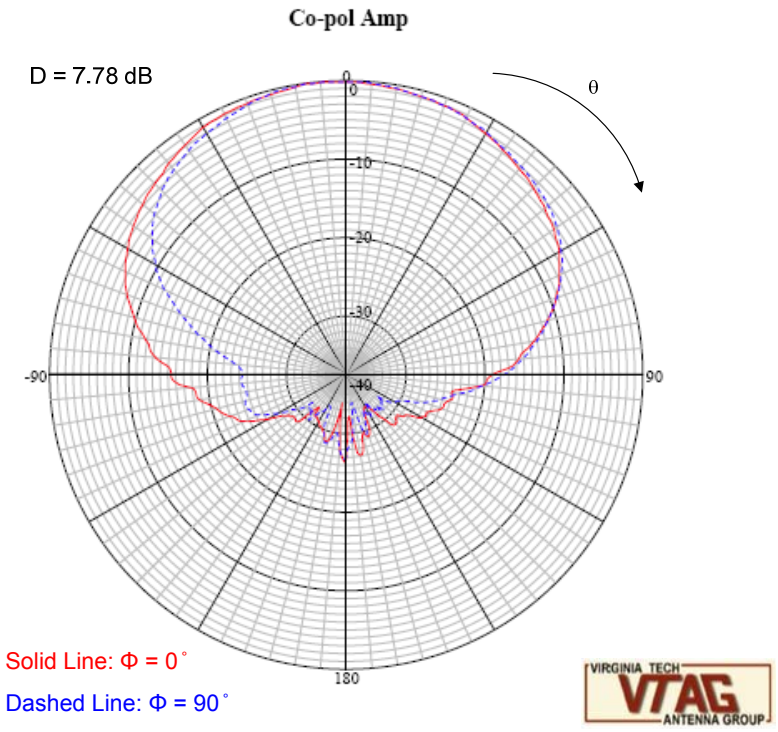

(a)

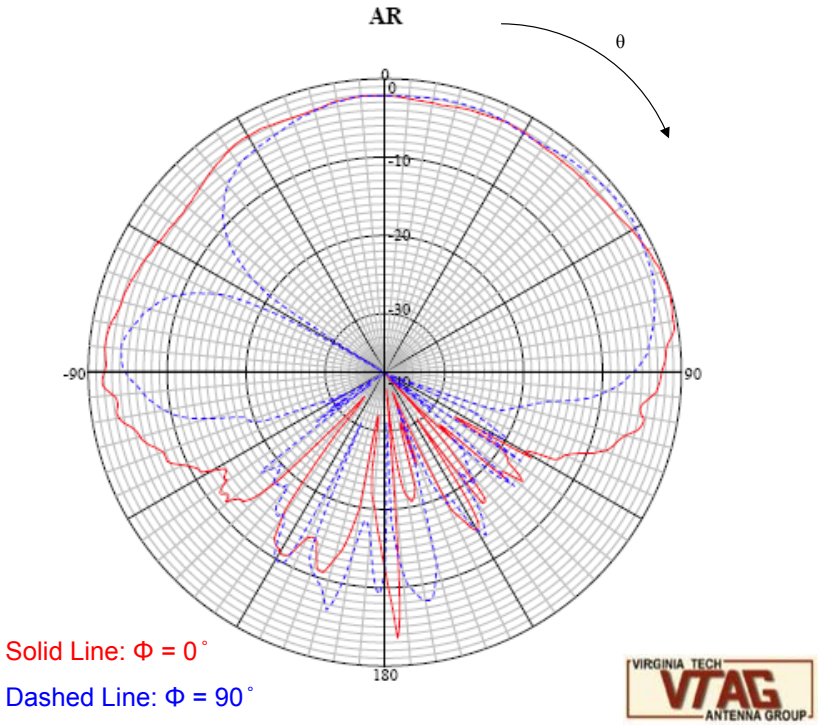

(b)

Figure C. 7: F= 3.70GHz (a) Directivity pattern (b) Axial ratio

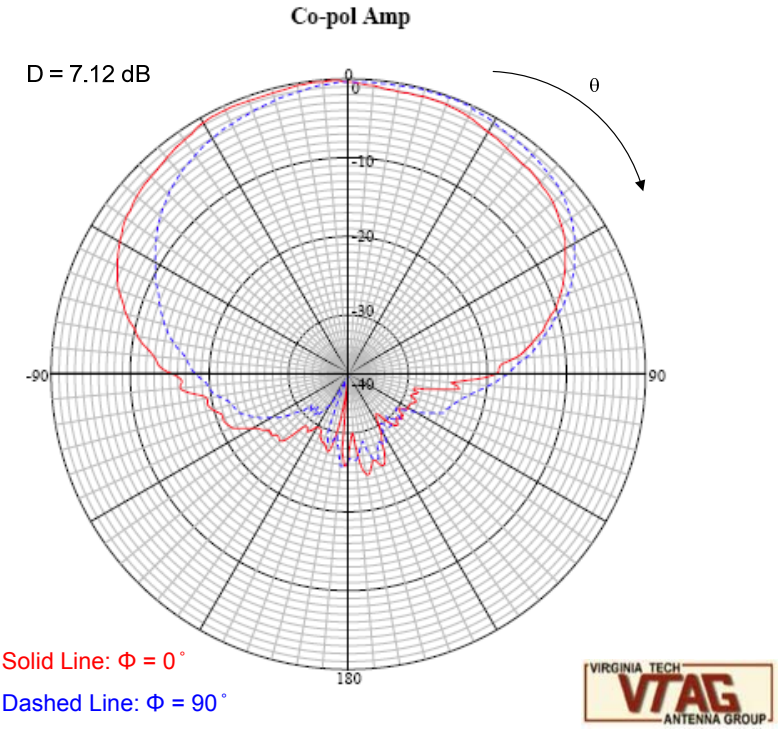

(a)

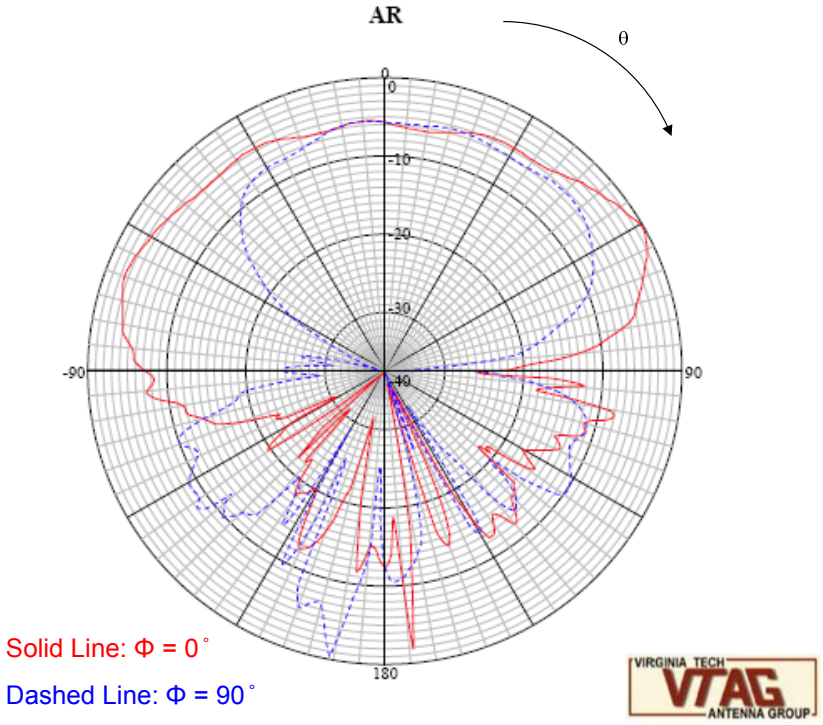

(b)

Figure C. 8: F= 3.85GHz (a) Directivity pattern (b) Axial ratio